Magnetic properties of rare Earth transition metal compounds

Slanicka, Martin

MAGNETIC PROPERTIES OF RARE EARTH TRANSITION METAL COMPOUNDS

by

Martin Slanicka

Presented in candidature for the degree of Master of Science

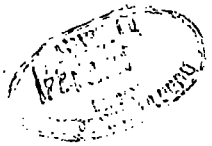

September 1970.

ABSTRACT

The structural and magnetic properties of pseudo-binary compounds formed between the heavy rare earth metals and the transitional metals iron, cobalt or nickel have been investigated.

The present work is a continuation of the investigation of the physical properties of the pseudo-binary compounds named above. The magnetic measurements were carried out on a vibrating sample magnetometer in applied magnetic fields of up to 10KOe. The range of temperatures used was from liquid helium (4.2°K) to about 800°K.

Further evidence has been found that the room temperature lattice spacing anomaly observed in (Gd, Y) Co_2, (Gd, Er) Co_2 systems are due to a transition from the ferromagnetic to the non-ferromagnetic state, with decreasing Gd concentration.

Transition metal moment collapse has been observed in series Ho $(Co, Ni)_2$ and Er $(Co, Ni)_2$. The value of additional 3d - electrons at which the moment collapsed increases going from yttrium to gadolinium compounds.

CONTENTS

LIST OF FIGURES

LIST OF TABLES

CHAPTER I

1.1 Ionic magnetic moment.

The magnetic dipole moment of an orbiting electron in a circular path of radius r and angular frequency w is

$$\mu_{or} = - er^2 w / 2c \qquad \text{(Eqn. 1.1)}$$

The relationship between w and r for an electron in motion about an atom is constrained by the quantum limitation that the orbital angular momentum must be a multiple of $\hbar$. This requires that the magnetic moment associated with orbital motion must be a multiple of eh/2mc. This quantity is known as the Bohr magneton and has a value of 9.27×10^{-21} erg/gauss.

The angular momentum associated with the spin of an electron can be characterized by a spin quantum number $s = \pm \frac{1}{2}$. This spinning motion has an associated magnetic moment, which is customarily written

$$\mu sp = gs\mu_B \qquad \text{(Eqn. 1.2)}$$

where g is a quantity called the spectroscopic splitting factor. Since g = 2.0023 for a free electron, the magnetic moment of a spinning electron is almost exactly one Bohr magneton. If we assume that the total angular momentum is given by Russel - Saunders coupling of spin and orbital motion and employ the terminology of Lande' then the total magnetic moment of an atom or ion is

$$\mu = g_J \mu_B J \qquad \text{(Eqn. 1.3)}$$

Here $g_J = 1 + \frac{J(J+1) + S(S+1) - L(L+1)}{2J(J+1)}$ (Eqn. 1.4)

is the Lande g - factor.

According to quantum mechanics, the total angular momentum vector of an atom has a magnitude $\hbar [J(J+1)]^{\frac{1}{2}}$, but the component which can be aligned with the axis of a magnetic field must be one of the set $\hbar m_J$, where the aximuthal quantum number m_J is a member of the set J, (J - 1), (J - 2),....., (1 - J), -J. For each value of m_J, the total magnetic moment μ of Eqn. 1.3 has a component $g_J m_B m_J$ aligned with the field axis.

Such a component acquires a potential energy

$$U_{J,m} = - g\mu_B m_J H \qquad \text{(Eqn. 1.5)}$$

in a magnetic field of intensity H, and it is this set of possible energies which must be considered with respect to the Boltzmann energy $k_o T$ in determining the gross magnetization for a given H and given T. Thus the magnetic moment per unit volume is

$$M = N\left[\frac{\sum_{-J}^{J} (g\mu_B m_J) \exp (g\mu_B m_J H/k_o T)}{\sum_{-J}^{J} \exp (g\mu_B m_J H/k_o T)}\right] \qquad \text{(Eqn. 1.6)}$$

and after substitution $M = Ng\mu_B JB_J(y)$

where $y \equiv (g\mu_B JH/k_o T)$

and $B_J(y)$ is the Brillouin function, which after some manipulations of the sums in Equation 1.6 has the form

$$B_J(y) = \frac{2J+1}{2J} \coth \frac{(2J+1)(y)}{2J} - \frac{1}{2J} \coth \frac{y}{2J} \qquad \text{(Eqn. 1.7)}$$

The Brillouin function varies from zero when the applied field is zero to unity for infinite field. Thus the saturation magnetization of a paramagnetic solid is $M(0) = Ng\mu_B J$. Under weak field conditions, the Brillouin function is asymptotic to $B_J(y) \approx y(J+1)3J$, $y \ll 1$ and for these conditions the paramagnetic susceptibility has a Curie law behaviour :

$$x_m = \frac{M}{H} = \frac{Ng^2\mu_B^2 J(J+1)}{3k_oT} = \frac{C}{T} \qquad \text{(Eqn. 1.8)}$$

and each magnetic atom has an effective dipole moment

$$\mu_{eff} = g\mu_B [J(J+1)]^{\frac{1}{2}} \qquad \text{(Eqn. 1.9)}$$

For ferromagnetic ordering Weiss (Ref. 1.1) described the interaction of a magnetic atom with the crystal by a molecular field, whose magnitude H_m was proportional to the magnetic moment per unit volume; that is

$$H_m = \gamma M \qquad \text{(Eqn. 1.10)}$$

where γ is called the molecular field constant. The idea of a molecular field leads directly to the Curie - Weiss law for susceptibility above the Curie point T_c

$$x_m = \frac{C}{T - T_c} \qquad T > T_c = \gamma C \qquad \text{(Eqn. 1.11)}$$

For a given value of J, the plot $M(T)/M(0)$ versus T/T_c yields a universal curve. The best agreement with experimental data is for $J = \frac{1}{2}$.

For an antiferromagnetic solid at low temperatures the total energy of the crystal in the absence of an external magnetic field is lowest when dipoles of opposing magnetic moments alternate. This arrangement is very stable at low temperatures and the susceptibility in an applied field is small. When the temperature rises the efficiency of this dipole - dipole interaction decreases and the susceptibility increases until at the Neél temperature T_N the spins become "free" to respond to a field. For still higher temperatures the behaviour is paramagnetic, and the susceptibility follows a modified Curie law

$$x_m = \frac{C}{T + \theta} \qquad \text{(Eqn. 1.12)}$$

The low temperature ordering in a ferromagnetic material is similar to that of an antiferromagnetic material, but the two opposing spin systems have magnetic moments of unequal magnitude and a net spontaneous magnetization results as the lowest energy state of the system. This magnetization decreases to zero magnitude when the solid is warmed to the Curie point T_c and the behaviour is once again paramagnetic at higher temperatures.

If the temperature variation of the magnetization M_A and M_B of two sublattices is different, the resultant magnetization $M = M_A + M_B$ is either a) always of one sign as shown in Fig. 1.1a) or reverses sign at some temperature T_k Fig 1.1b) for which $|M_A| = |M_B|$ This temperature is called the compensation point.

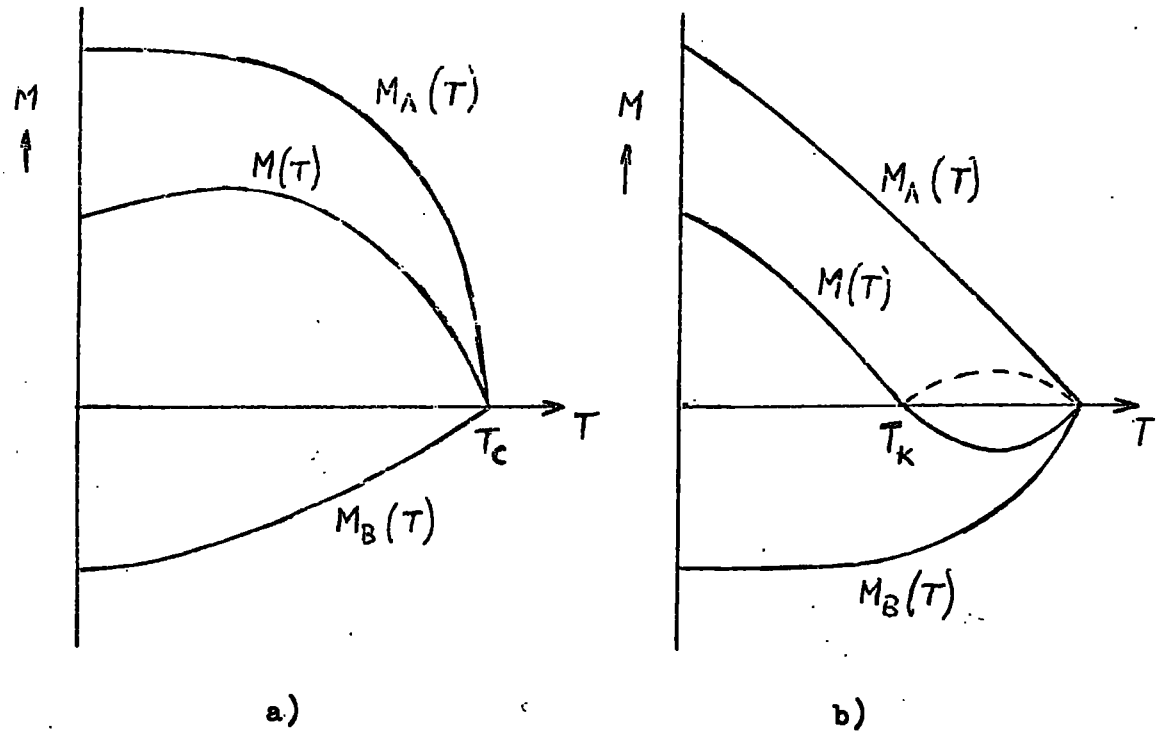

Fig. 1.1 Ferrimagnetic Magnetization/Temperature Curves.

1.2 Itinerant electron model.

The original treatments of ferromagnetism assume that the magnetic electrons are fixed on a particular ion. This is the localized spin model. The nearest approach to this in a ferromagnetic metal is in the rare-earth group elements in which the magnetic moment of each ion arises from the partially filled 4f shell which is well inside the ion and can therefore be considered to be localized; but even here, we should still take account of the effect of the non-magnetic outer conduction electrons. In the iron group elements, however, the magnetic moment of each ion arises from the electrons in the partially filled 3d shell. Since the 3d shell is at the outside of the ion, the wave functions of the 3d electrons of neighbouring ions overlap and a fairly narrow band of states is formed. This means that the "magnetic" electrons can move from one ion to another (this is sometimes called the itinerant model) and so the localized spin picture is no longer applicable. It is also clear that the localized spin model cannot be strictly valid because, if it was, the saturation magnetization of a ferromagnet, when all elementary moments are aligned, should correspond to an integral number of Bohr magnetons, whereas nonintegral values are actually found (Ni = 0.6, Fe = 2.2 and Co = 1.7 Bohr magnetons respectively).

The problem of itinerant versus localized spin models has been reviewed by Herring (Ref. 1.2) and from it we recall that

the itinerant model is favoured by the fractional saturation moments (Ref. 1.3) in the ferromagnetic state, by the electronic specific heat and by band calculations and Fermi surface measurements. The localized model however, appears to be more appropriate for the description of neutron scattering form factors, the magnetic entropy and the behaviour of dilute alloys. (Ref. 1.4).

1.3 Localization in the Band Model.

Friedel (Ref. 1.5) has shown qualitatively that localized magnetic moments are not incompatible with the band approximation.

Such moments can originate from a local piling up of electronic charge with one spin, compensated electrostatically by an equal local repulsion of electrons with the opposite spin. The displacements of charge can take place within the band, and can result in fractional numbers of electronic charges. This is so since each electron in the band contributes only an infinitesimal amount of the total polarization.

The extension of Stoner's band model which Friedel proposed is quite similar to the extension from the Zener (Ref. 1.6) to the Yoshida (Ref. 1.7) model for superexchange of d (or f) shells via conduction electrons. The difference is that Friedel's model involves a coupling via the same (d) band within which the localized moments occur. In this treatment the possible role of the conduction band was neglected. Localized

moments should occur only if the band is sufficiently narrow and weak coupling occurs from one atom to the next only if the band is neither too empty nor too full.

This coupling may be ferromagnetic or antiferromagnetic, depending on the exact structure and filling of the band, and should give rise at high temperatures to a Langevin type of paramagnetism. On the other hand, for a nearly empty or nearly full band, they should be strongly coupled ferromagnetically and give rise, at high temperatures, to a Pauli type of paramagnetism.

In the same year a quantitative theory of the one spin problem was worked out by Anderson (Ref. 1.8) and the model has become known by the author's name. It was first presented in connection with the problem of dilute alloys, but has been extended to pure metals. The case for many spins has been presented by Liu (Ref. 1.9) treating a ferromagnetic metal as a lattice of overlapping Anderson - type localized moments.

1.4 Theory of Magnetism in Rare Earth Metals and Alloys.

1.4.1 The Heavy Rare Earth Metals.

In nature the oxides of the rare earth metals occur in mixed ores such as monasite and lastnaesite. Scandium and yttrium resemble the rare earth elements very closely in chemical and physical properties and are present in rare earth-containing ores.

Our interest will be directed towards what are

commonly called the heavy rare earth metals, i.e. those with a more than half filled 4f - shell. As stated previously, the main carriers of the highly localized magnetic moment in these metals are the unpaired electrons in the 4f shell. The paramagnetic moment is accurately given by the application of Hund's rules, which state that 1) the spin arrangement should have the maximum total spin angular momentum (S), and 2) the orbital arrangement should have the maximum orbital angular momentum (L) within the restriction of rule (1) and of the Pauli exclusion principle. Then the total angular moment becomes $J = L + S$ for heavy rare earths, as shown in Table 1. The radius of the 4f shell is small and the shell lies inside the closed 5s and 5p shells. These outer shells contribute significantly to the shielding of the 4f electrons and influence the electronic and magnetic properties. The valence electrons come from the 5d, 6s and 6p shells.

In general, most of the rare earth metals are trivalent except europium and ytterbium, in which the stable configurations are $4f^7$ and $4f^{14}$, hence those are divalent.

The total magnetic moment of rare earth metals in the ferromagnetic state at absolute zero (Table 1.1) is given by the sum of the 4f moment and a moment arising from conduction electrons spin polarization. Except for 6d, however, the 4f magnetic moment may be reduced from the value of the free atom due to the crystal field.

Neutron diffraction results indicate that the radius of the 4f shell is about 0.1 of the interatomic distance in the metals and about 0.3 of the atomic radius, and no evidence has yet been found for the existence of a 4f band.

Systematic differences from element to element in the heavy rare earths may be attributed to the so-called lanthanide contraction. The origin of this decrease in lattice parameter lies in the fact that with increasing atomic number the increase in the charge of the 4f electrons is insufficient to completely screen the extra nuclear charge. Consequently the increased electrostatic attraction causes the radii of the outer shells to decrease. The crystal structures of the heavy rare earth metals, except Yb, are hexagonal close packed (hcp). For the ideal packing of spheres in an hcp structure $c/a = 1.633$, but for the heavy rare earth c/a varies from 1.59 for Gd and 1.58 for Tb to approximately 1.57 for the remaining elements. One possible explanation for the differences in c/a is found in the changes of the symmetry of charge distributions with increasing occupation of the 4f shell electrons. In these shells the orbital angular momentum is zero for Gd (Table 1.1), indicating a more spherical charge distribution, whereas in Ho and Er the angular momentum reaches a max. value of $L = 6$ and the 4f charge density is highly anisotropic.

Metal	2S	L	J	T_N(°K)	T_c(°K)	Theoret. Value gJ	Exper. moment (μB)
Gd	7	0	3.5	-	293.2	7.0	7.55
Tb	6	3	6	229	221	9.0	9.34
Dy	5	5	7.5	178.5	85	10.0	10.6
Ho	4	6	8	132	20	10.0	10.34
Er	3	6	7.5	85	19.6	9.0	9.0
Tm	2	5	6	56	22	7.0	7.14
Yb	1	3	3.5	Does not order		4.0	-

Table 1.1 The magnetically ordered states for heavy rare earth metals.

1.4.2 Magnetic Contributions to the Rare Earths.

The different types of magnetic structure that occur throughout the heavy rare earth metals (Ref. 1.10) can be considered as the natural consequence of a single Hamiltonian for the 4f localized moment system.

In this theory we deal with three types of energy for the spin system corresponding to the localized ions.

$$\mathcal{H} = \mathcal{H}_{ex} + \mathcal{H}_{ef} + \mathcal{H}_{ms} \qquad \text{(Eqn. 1.13)}$$

The first contribution is a long range oscillatory exchange interaction first derived by Ruderman and Kittel for nmr studies, extended by Kasuya and Yosida for rare earth ferromagnetics.

This has the form

$$\mathcal{H}_{ex} = -\Gamma(Si, Se) \qquad \text{(Eqn. 1.14)}$$

and is the dominant coupling term and will be discussed in detail later.

The second contribution is the anisotropy energy of the unstrained lattice resulting from interaction of the crystalline electric field caused by the charged rare earth ions in the hcp lattice. Although the point charge model is inadequate for calculating magnitudes of the crystal field, the crystal field does exhibit the symmetry of the ionic lattice. The crystal field interaction consists of a large axial and smaller planar anisotropy and its role in determining the magnetic structures has been discussed by Elliott (Ref. 1.11).

The last contribution to $\mathcal{H}$ comes from magnetostriction effects. These effects arise from the modification of the crystal field splittings by the strain.

$$\mathcal{H}_{ms} = \mathcal{H}_e + \mathcal{H}_m$$

Here $\mathcal{H}_e$ is the elastic energy associated with the homogeneous strain components, and $\mathcal{H}_m$ is the magnetoelastic interaction, coupling the spin system to the strains.

It can be shown that the Hamiltonian of (Eqn. 1.13) leads to the various types of magnetic structures (Ref. 1.12). Evenson and Liu (Ref. 1.13) have given a general proof of the theory that the first order transition from the helical state to the ferromagnetic or conical ferromagnetic state in Tb, Dy,

Ho and Er can be explained by the magneto - elastic effect for a general ordered spin state.

The crystal field effects are relatively small, due to the paired electrons in 5s and 5p states, and they are normally introduced as a perturbation on the spin - orbit coupling between L and S. The situation is different for the transition metals, in which the crystal field effects are very important, as indicated in Table 1.2

Ions	Coulomb Energy Differences	Crystal Field Energies	Spin-Orbit Energies
Fe group	$10 - 40 \times 10^3 cm^{-1}$	$10 - 20 \times 10^3 cm^{-1}$	$100 - 800 cm^{-1}$
Rare Earth	$5 - 40 \times 10^3 cm^{-1}$	$\sim 200 cm^{-1}$	$600 - 3000 cm^{-1}$

Table 1.2 The contribution of energy for the spin system corresponding to the localized ions.

The first column represents the ranges covered by the difference in energy between the ground term and the first excited term, the absolute magnitudes of the Coulomb binding energies for the transition shell electrons are of the order $10^5 cm^{-1}$.

1.4.3 Exchange Interactions in the Rare Earths.

Returning to the determination of $\mathcal{H}_{ex}$ (Eqn. 1.14), the interaction between rare earth atomic moments must be an indirect one, since overlap of the 4f wave functions, particularly for the heavy elements, is exceedingly small. The most satisfactory theory for this interaction is the Ruderman-Kittel-

Kasuya-Yosida (RKKY) theory (Ref. 1.14, 15, 16). This assumes that an exchange interaction exists between the spin Si of a single ion and spin Se of a conduction electron of the type $\mathcal{H}_{ex} = -\Gamma(Si, Se)$ where Γ is the exchange energy and uses a delta function to represent the ionic potential. The conduction electrons which are assumed to be free are scattered under the influence of this interaction.

This scattering leads to a polarisation of the electrons in the vicinity of the ion (i) given in Ref. 1.17 by

$$Pi(r) = \frac{9\pi Z^2 \Gamma}{4V^2 E_F} S_i F(2k_f r) \qquad \text{(Eqn. 1.15)}$$

where $F(x) = \dfrac{x \cos x - \sin x}{x^4}$ $\qquad x = 2k_f r$

Z is the atomic density of conduction electrons, V the atomic volume, E_F the Fermi energy, k_f the wave vector of the electrons at the Fermi surface and r is the distance from the ion. The function F(x), and hence the polarisation, is long range and oscillatory, decaying as $\cos x/x^3$ at large distances. This polarisation interacts with a second ion with spin S_j at position r_j and has the form $-\Gamma S_j P_i(r_j)$ and in the absence of spin-orbit interactions is equivalent to a coupling

$$\mathcal{H}_{ij} = -I_{ij} S_i S_j \qquad \text{(Eqn. 1.16)}$$

where $$I_{ij} = \frac{9\pi Z^2 \Gamma^2}{4V^2 E_F} F(2k_f r_j) \qquad \text{(Eqn. 1.17)}$$

Thus the exchange interaction which exists between two spins has a similar oscillatory form to the conduction electron polarization. In order to include the effect of the spin-orbit coupling on the spins S_i, S_j we have to use the projection of S on J in these interactions. De Gennes has shown that for $E_{LS} \gg kT$ where E_{LS} is the spin-orbit coupling energy, this projection has the form $S = (g - 1) J$.

Applying the interaction $\mathcal{H}_{ij}$ in a molecular field approximation to determine the paramagnetic Curie point leads to an expression (1.10). Neglecting direct coupling between f shells it follows that

$$k\theta = \frac{3\pi Z^2}{4} \Gamma^2 (g-1)^2 J(J+1) \sum_{i \neq j} F(2k_f r_{ij}) \quad \text{(Eqn. 1.18)}$$

Experimental results are in good agreement with RKKY theory for many of the properties of the rare earth metals. (Ref. 1.17, 18, 19).

Especially remarkable agreement may be seen from the variation of the observed Curie temperature with the de Gennes factor: $(g - 1)^2 J (J + 1)$ (Ref. 1.12). On the other hand, however, band structure calculations and Fermi surface determinations for the rare earth metals (Ref. 1.20) show that these are quite different from the almost free electron picture. A clear indication is given of the transition - metal like behaviour to be expected for the conduction electrons. The changes of the Fermi surface will affect the electronic behaviour and have been used to interpret some of the magnetic properties of the metals (Ref. 1.13).

Further experiments to explore the Fermi surface and energy bands are necessary before a full understanding of this behaviour is possible. These will require purer materials than are presently available.

1.4.4 Origin of exchange parameter Γ.

Recalling the Equation $\mathcal{H}_{SE} = -\Gamma \mathbf{S}\mathbf{E}$ for the s-f interaction, the experimental value and sign of Γ is still somewhat indefinite. Theoretical work (Ref. 1.21) shows that in addition to the obvious constributions to Γ due to the positive exchange integral $\mathcal{J}$ between the 4f shell and the conduction electrons, there is a negative interband mixing between the conduction electrons and local moment electron orbitals.

The implications of interband mixing on electron states near the Fermi surface were recognized in the 1930's, but only recently have Anderson and Clogston (Ref. 1.22, 8) confirmed the importance of this mechanism. The interband mixing contributions to Γ are very sensitive to the conduction - electron character; also Γ varies significantly with the conduction electron k direction. This can cause severe anisotropies in the RKKY conduction - electron spin density distribution.

A simple example of interband mixing is as follows (Fig. 1.2). Consider the mixing of two functions, an unoccupied conduction - electron state of spin $\uparrow$ which lies just above the Fermi surface and an occupied 4f $\downarrow$ level.

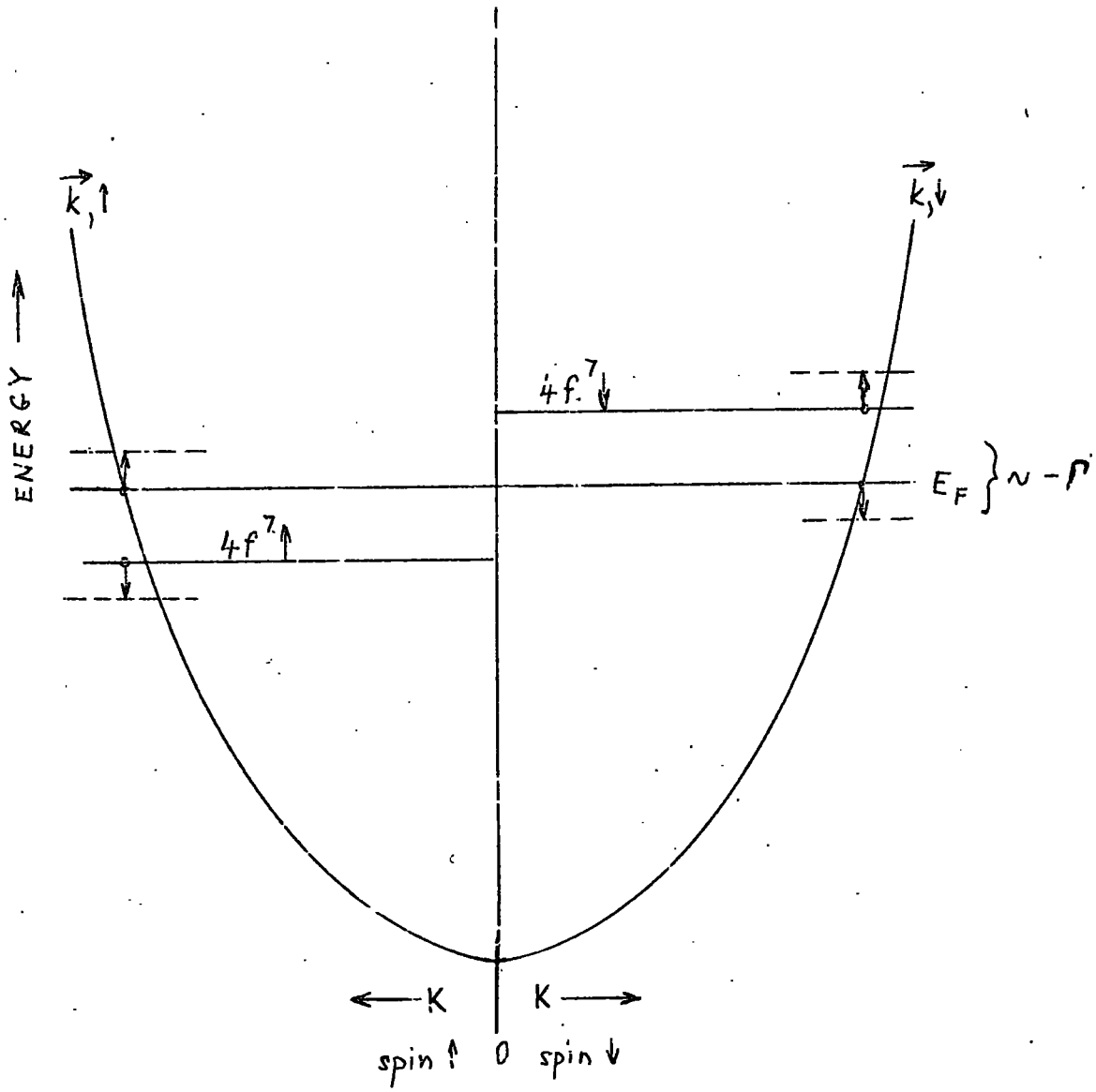

Figure 1.2 A schematic representation of interband mixing for Gd and its contribution to a $\Gamma(0)$ defined for the Fermi - surface electrons.

Then this mixing will raise the energy of the state at the Fermi surface. This is termed an "emission" process since an occupied 4f state has conduction - electron character part of the time. There is also a similar "absorption" process which involves the 4f ↓ virtual states (above the Fermi surface) and an occupied ↓ conduction - electron orbital.

The combined effect of these processes is to lower the minority spin ↓ conduction - electron energies and increase the energies of the majority spin ↑ electrons, so resulting in a negative polarisation.

1.5 Rare - Earth - Transition Metal Compounds.

The intermetallic compounds of the 3d - transition metals with the rare earth metals belong to two groups:

1. The compounds with a high transition metal content such as A_2B_{17}, AB_5, A_2B_7, AB_3 and AB_2 where A is a rare earth element or yttrium and B is Fe, Co or Ni, and

2. The compounds with high rare earth metal content as A_3B, A_7Ni_3, A_4Co_3 and ANi.

The compounds of the first group have crystal structures derived from the fundamental $CaCu_5$ (Ref. 1.23) and $CaZn_5$ (Ref. 1.24) types by ordered substitutions of the atoms.

As the pseudo-binary compounds investigated in the present work were formed from intermetallic compounds of the type AB_2, we shall now describe some properties of these.

They belong to the large class of intermetallics crystallizing into the structures known as Laves phases. All of them are cubic with a $MgCu_2$ structure (Fig. 1.3) (Strukturbericht Type C15), which has 24 atoms/unit cell. Two other types of Laves phases exist, the $MgZn_2$ hexagonal structure (C14 type) with 12 atoms/unit cell and the $MgNi_2$ hexagonal structure (C36 type) with 24 atoms/unit cell. These have been reported in some rare earth manganese compounds (Ref. 1.25) and as impurity phases in some pseudo-binary compounds (Ref. 1.26).

The Laves phases represent a very efficient method of filling space and, with atomic size ration $R_A/R_B = 1.225$, the average number of nearest neighbours in the structures is $13\frac{1}{3}$. It appears that the $MgCu_2$ structure cannot develop unless the radius ratio of components falls within certain limits, and it was originally thought that these structures are size stabilized so that a size ratio close to an ideal value of 1.225 is required for the phases to form. However the ideal ratio is the same for all three phases and there does not appear to be any discrimination between the types on this basis, so that other factors appear to be involved.

Laves and Witte (Ref. 1.27) have stressed the importance of an additional requirement, namely that the number of electrons per atom in the conduction band should be within a certain range. This "valence" electron per atom concentration (VEC) dependence has subsequently been confirmed on compounds with transition metals (Ref. 1.28) and has been related to the density of states variation

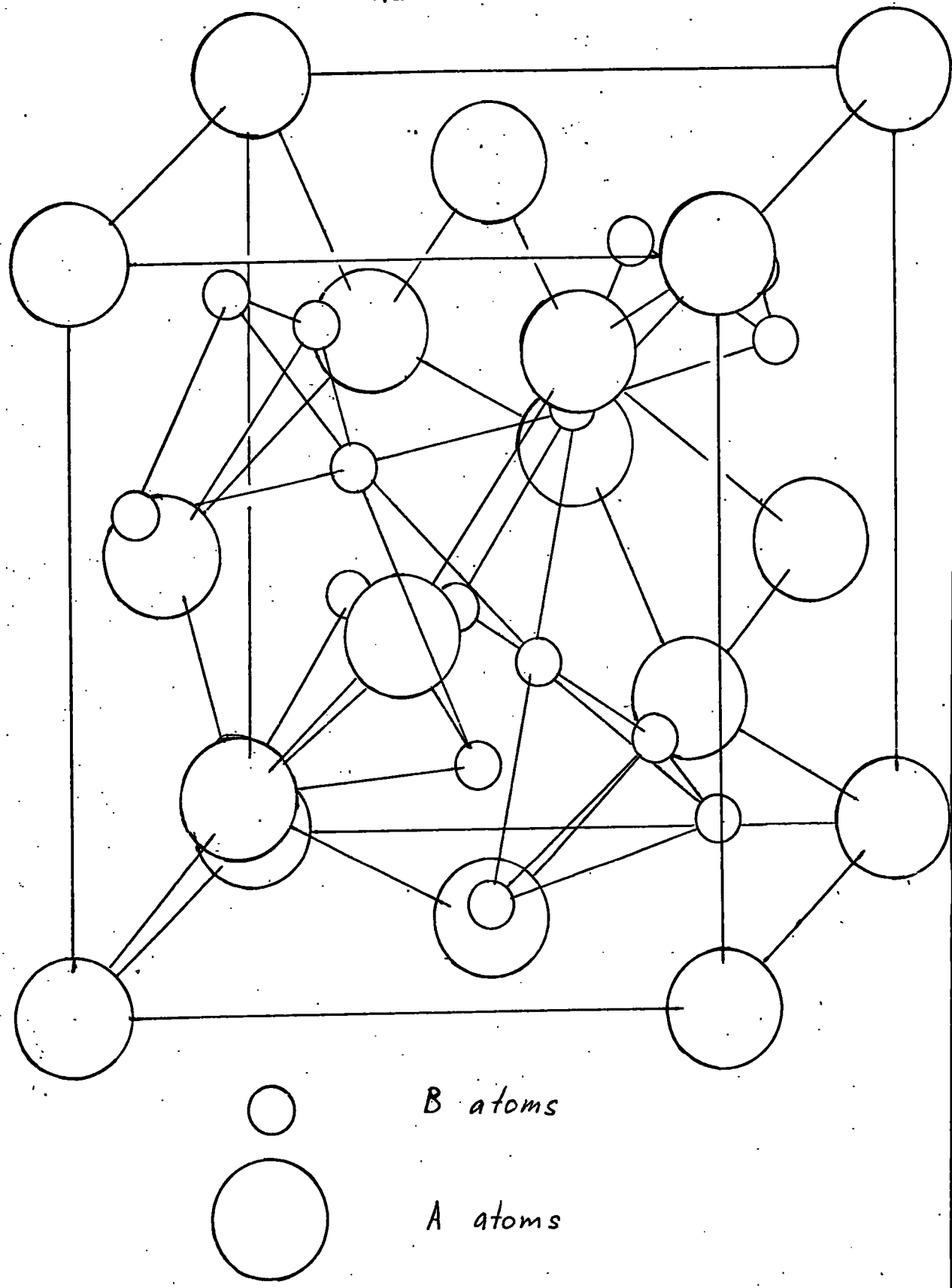

Figure 1.3 Structure of $MgCu_2$

obtained from hydrogen solubility, susceptibility and electronic specific heat measurements (Ref. 1.29). This dependence is interpreted in terms of the interaction between the band structure and the Fermi surface. In the solid state, there is a tendency for any material to adopt a strcture in which the Fermi surface is near a Brillouin zone boundary, where the density of states is high, since the energy of the Fermi surface will then be lower.

Previous recent studies determined that the cubic C15 type is stable for vec 1.33 to 1.72 and the hexagonal C14 for vec 1.8 to 2.32. At higher vec the cubic type is again stable and the intermediate ranges are usually twophase.

There must, however, be other, as yet unknown, factors governing the stability of the Laves phases, since many systems which satisfy the requirements of size ration and vec do not form in these structures. Among these are the compounds of copper with rare earths and the scandium group metals, of which not one forms in a Laves phase.

Summary of magnetic properties of AB_2

The magnetic properties of these materials are complex and varied, and at present we cannot give a satisfactory unified explanation of their behaviour. In the following the essential features of the published work will be summarized. (Table 1.3).

Almost all AB_2 are magnetically ordered. The magnetic moments correspond to ferrimagnetic ordering with the moment of

Rare Earths	Fe		Co		Ni	
	Tc	μ_B	Tc	μ_B	Tc	μ_B
Y	550	2.91			Pauli param.	
Ce	221	2.4	Param.		Pauli param.	
Pr	-	-	50	3.2	(a)	0.86
Nd	-	-	116	3.8	16	1.8
Sm	700	2.5	259	2.0	21	0.25
Gd	813	3.6	400	4.9	85	7.1
Tb	696	3.9	256	6.7	45	7.8
Dy	750	5.4	159	7.6	30	9.2
Ho	600	5.2	95	7.8	22	8.4
Er	450	4.7	36	7.0	21	6.8
Tm	610	2.52	18	4.7	(a)	3.2
Ln	610	2.97	Pauli Par.		Pauli Par.	

a) Magnetic state uncertain.

Table (1.3) Magnetic Moments and Curie Temperatures of AB_2

the Fe, Co ions reduced from the free ion value of $2.2\mu_B$ and $1.7\mu_B$ respectively, and zero magnetic moment of Ni.

Neutron diffraction measurements (Ref. 1.25) on $TbNi_2$ confirmed that Ni has zero moment and this has been attributed (Ref. 1.30) to electron transfer from the rare earth components to the Ni 3d shell, putting it into the $3d^{10}$ state. The measured moments of ANi_2 are therefore due to the rare earth components only and it is evident that these are lower than the free tripositive ion values (Table 1.1). The reduced moments have been attributed (Ref. 1.31) to partial quenching of the orbital moment by the crystalline field. Bleaney (Ref. 1.31) estimated the energy level splitting due to the crystalline field in this series.

In ACo_2 the magnetic results, as pointed out by Ross and Crangle (Ref. 1.32) and by Farrel and Wallace (Ref. 1.33) were consistent with the rare earths possessing their free ion moment, aligned opposite to a constant cobalt spin moment.

This picture was further improved by Crangle and Ross (Ref. 1.34), who suggested that the localized A and Co moments were aligned ferromagnetically in the lighter rare earths and antiferromagnetically in heavy rare earths. Neutron diffraction results (Ref. 1.35) indicate a Co moment of $1.0 \pm 0.2\mu_B$ antiparallel to the heavy rare earths moment.

The measured Curie temperatures are consistent

(Ref. 1.33) with the behaviour expected on the basis of a coupling mechanism via the conduction electrons in that they are proportional to the de Gennes function. Since the lattice constants for this series are larger than the corresponding ones in the Ni series, it is to be expected that quenching of the other rare earth moments should be not larger than in the latter.

The Co moment in Gd Co_2 is about 1.1 μ_B but is very small in YCo_2 and in $LuCo_2$ and $CeCo_2$ is zero. These low moments are to be compared with the value of 1.7 μ_B in elemental Co, and have again been attributed (Ref. 1.36) to electron transfer from the rare earth components. Bleaney (Ref. 1.31) suggested that the moment carried by Co in compounds with a magnetic partner is induced and should be proportional to $(g - 1)M/g$, where M is the moment carried by the magnetic partner and g is its Landé factor. A measure of agreement was obtained with the experimental results. Schweizer (Ref. 1.37) has studied $PrCo_2$ by neutron diffraction and finds $\mu_{Co} = 0.5 \pm 0.25 \mu_B$ in this compound. He attributed the variation of cobalt moment to polarization of the 3d electrons by the rare earth spin through the conduction electrons, the magnitude of the resulting moment being thus related to the rare earth spin. This is the same mechanism, presumably, as envisaged by Bleaney.

For the AFe_2 series it is to be expected that the rare earth moments should be less affected by crystal field quenching

than in either of the two former series, because of the lattice dilation. As mentioned earlier iron has a moment of about $2\mu_B$ in the heavy rare earth compounds, while in YFe_2 it is about $1.4\mu_B$. The same explanation has been applied to this moment reduction from $2.2\mu_B$ for elemental iron as for Co, i.e. that of electron transfer (Ref. 1.36). The Fe moments were analysed by Wallace and Skrabek in terms of a permanent moment in all the compounds of $1.45\mu_B$ with an additional induced component proportional to $(g - 1)\, M/g$.

Pseudo-Binary Series.

Two types of pseudo binary rare-earth-transition metal compounds have been investigated in the past. $(A, A^1)\, B_2$ and $A\, (B, B^1)_2$ where A (or A^1) represents a rare-earth element or yttrium, and B (or B^1) represents a transition metal.

For example, series $Gd_x\, Y_{1-x}\, Co_2$ has been interpreted by Taylor et. al. (Ref. 1.38) in terms of a triangular spin configuration and by Lemaire and Schweizer (Ref. 1.39) in terms of a variable Co moment, though no mechanism for this variation was proposed. It has not been possible in this compound to obtain an equilibrium concentration at which both the sublattice magnetizations are equal.

In the series $Dy_x\, Y_{1-x}\, Fe_2$ (Ref. 1.40) the equilibrium concentration at which the iron and dysprosium sublattice moments exactly cancel occurs at $x = 0.28 \pm 0.01$. In addition, the coercivity increases rapidly in this region and has a value in

excess of 10KOe at x = 0.35, T = 4.2°K. In order to account for such results Piercy has suggested that the Fe moment in these compounds varies nonlinearly with x.

Oesterreicher and Wallace (Ref. 1.41) measured the crystallographic and magnetic (susceptibilities and saturation moments) characteristics for the systems Gd Al_2 - Gd Fe_2, Gd Al_2 - Gd Co_2 and Er Al_2 - Er Co_2. The C14 structure was observed in all these series and the stability ranges for this and the C15 terminal phase were measured.

Mansey et. al. (Ref. 1.42) have presented lattice spacings of several A $(B, B^1)_2$ pseudo-binary series. All the series investigated were single phase (C15) and the lattice parameters showed positive deviations from Vegards law (linear interpolation) except for the series involving Ce. The latter exception was explained by the variable valency of Ce.

Piercy and Taylor (Ref. 1.43) examined the magnetic properties of the series Y $(Fe, Co)_2$ and explained the variation of the observed moment throughout the series on the basis of an itinerant moment associated with the transition metal ions.

The magnitude of the 3d - electron moment is extremely dependent on the detailed nature of the compound in which these electrons reside. Indeed in both (Gd, Y) Co_2 and Y $(Fe, Co)_2$, the moment associated with the transitional metal ions has been found to decrease to zero over part of the composition range. In an investigation of the origin of this moment collapse Taylor

(Ref. 1.44) has examined the magnetic properties of Gd (Co, Ni)$_2$ compounds and found a similar transition metal moment variation as a function of composition. He described this behaviour in terms of a rigid band model and has suggested that the nature of this collapse will depend critically on the density of states curve in the vicinity of the Fermi level.

Statement of Problem.

Two basic problems still exist in the interpretation of the properties of the AB_2 compounds. One needs to know the size of the crystal field effect which causes the lowering of the moment carried by the A component and whether there are other reasons for the rare earth moment reduction below the free tripositive ion value.

The magnitude of the effect is uncertain because of the uncertainty in evaluating the component moments and because of the great difficulties of crystal field calculations in these materials, in which the exchange and crystal fields are of comparable magnitude.

Secondly, the transition metal moment is very variable. The explanation in terms of electron transfer into the 3d shell together with induced moments in some cases seems to Piercy (Ref. 1.26) to be untenable as a major cause of the variable moments, since the necessary degree of transfer varies so greatly for the different materials where elements with very

similar electronegativities are involved. He has given the example that in Gd Ni_2, about 0.6 electrons/Ni atom are required while in Gd Fe_2 this is only about 0.2 electrons/Fe atom and, again, the value for YCo_2 and YFe_2 are about 1.7 and 0.8 per atom respectively. His explanation is based on itinerant electron moment associated with transition metal ions and a localized moment at the lanthanide ion.

The present work has been performed in order to obtain further experimental results for a better understanding of these problems. The appearance of the transition metal moment collapse in some series determined which of the pseudo-binary compounds might be most profitably examined, since Taylor (Ref. 1.44) suggested that in going from yttrium to gadolinium compounds the added electrons per atom value at which the moment falls to zero will increase.

The series chosen were Dy $(Co, Ni)_2$, Ho $(Co, Ni)_2$, Er $(Co, Ni)_2$ and the series Gd $(Co, Fe)_2$ and Ho $(Co, Fe)_2$ and gave a coverage of the values of Curie temperatures and magnetizations going from $ANi_2 \rightarrow ACo_2 \rightarrow AFe_2$.

The series (Gd, Er) Co_2 has also been measured to give further evidence that the lattice spacing anomalies observed in system $(GdY)Co_2$ (Ref. 1.45) arise from the transition from the ferromagnetic to the non-ferromagnetic state with decreasing $GdCo_2$ concentration at room temperature.

CHAPTER II

Description of Experimental Method.

2.1 Materials and Arc Melting of Compounds.

The majority of the specimens used in this investigation have been made in our laboratory and the others have been supplied by the University of Birmingham, Department of Physical Metallurgy and Science of Materials.

The rare earth metals used in sample preparation were supplied by Koch-Light Laboratories Ltd., in the form of ingots with stated purities of 3N +.

The transition metals (Fe, Co, Ni) were supplied from the same firm in the form of rods and their stated purities were 4N8 +. The specimens were made in argon arc furnace. Each component was cut, filed and weighed to 0.001 gms in argon in a glove box. The prepared quantities of any given compound varied between 2 and 5 gms. A rotary and a diffusion pump were used to evacuate the furnace chamber to a pressure of less than 0.5 microns Hg. The arc furnace was then flushed with Argon (5N) to atmospheric pressure, pumped out again and filled to the operating pressure of $\sim$ 200mm Hg.

Before the actual melting of the components the furnace was gettered for one minute with molten tantalum. After the components were melted together the resulting ingot was remelted twice after turning it over, for homogenisation. Sometimes

during the second melting the ingot shattered, however by slowing down the process these difficulties were overcome, and at no time was there a loss of weight of the specimen of more than 4%, and usually it was very much less than this. After preparation of the "button" specimens, there was a thin layer of oxide on the surface which was easily removed by filing.

When the specimens were broken with a mortar and pestle all of them were found to be extremely brittle. Small pieces, about 100 mgm, were used as specimens for the magnetometer, and fine powders were ground for X-Ray diffraction measurements.

2.2 Vibrating Sample Magnetometer.

The magnetic measurements were carried out using a vibrating sample magnetometer constructed by H.D. Ellis (Ref. 2.1) and improved electronically by A.R.Piercy (Ref. 1.26) (Fig. 2.1). Further modifications were made during this work to improve measurements at liquid helium temperature.

The first description of this type of magnetometer was published by Foner (Ref. 2.2). In his design the specimen is vibrated perpendicularly to the direction of the applied field at a fixed frequency. The oscillating magnetic field produced by the specimen induces a signal in a multi-turn pick-up coil, the magnitude of this signal providing a measure of the magnetic moment of the specimen. The signal is combined with a reference signal produced by a reference specimen (i.e. small

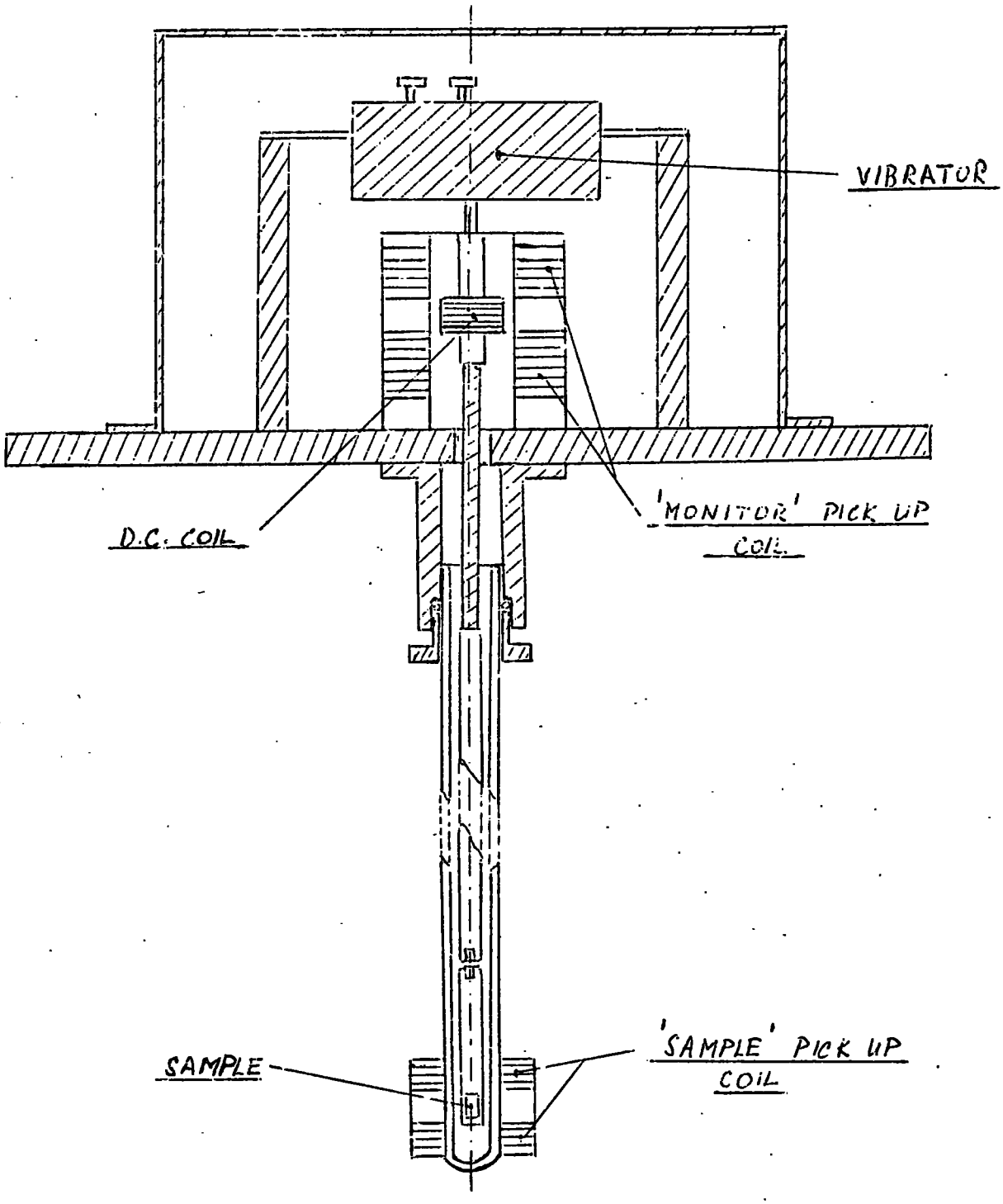

Figure 2.1 Drawing of Magnetometer.

coil carrying a D.C. current) oscillating in a second pick-up coil. The resultant is amplified and passed to a phase sensitive detector (the two signals being 180° out of phase) and in our case is zeroed by altering the current through the D.C. reference coil.

The detection coil system employed in the apparatus used in this work eliminates the effects due to the instability of the power supply driving the magnetic field. This is achieved by constructing the pick-up in the form of two matched coils connected in series opposition. This has the advantage that while "noise" signals are largely balanced out, the signal from the pick up coils is twice that from a simple single coil.

Brief description of the block diagram of the magnetometer shown in Figure 2.2.

The driving oscillator is a Farnell Type LF Solid State Oscillator feeding a 12 - volts sinusoidal signal into a simple 2 - stage power amplifier at 70 c.p.s., which is inductively coupled to the Advance vibrator.

Details of the tuned amplifier (Grubb Parsons TA high gain) and the phase-sensitive detector, have been described by Ellis (Ref. 2.1).

It is worthwhile emphasing two points, however. Firstly the tuned amplifier has band stop filters originally tuned to 10 c.p.s., but subsequently modified to have their stop band at

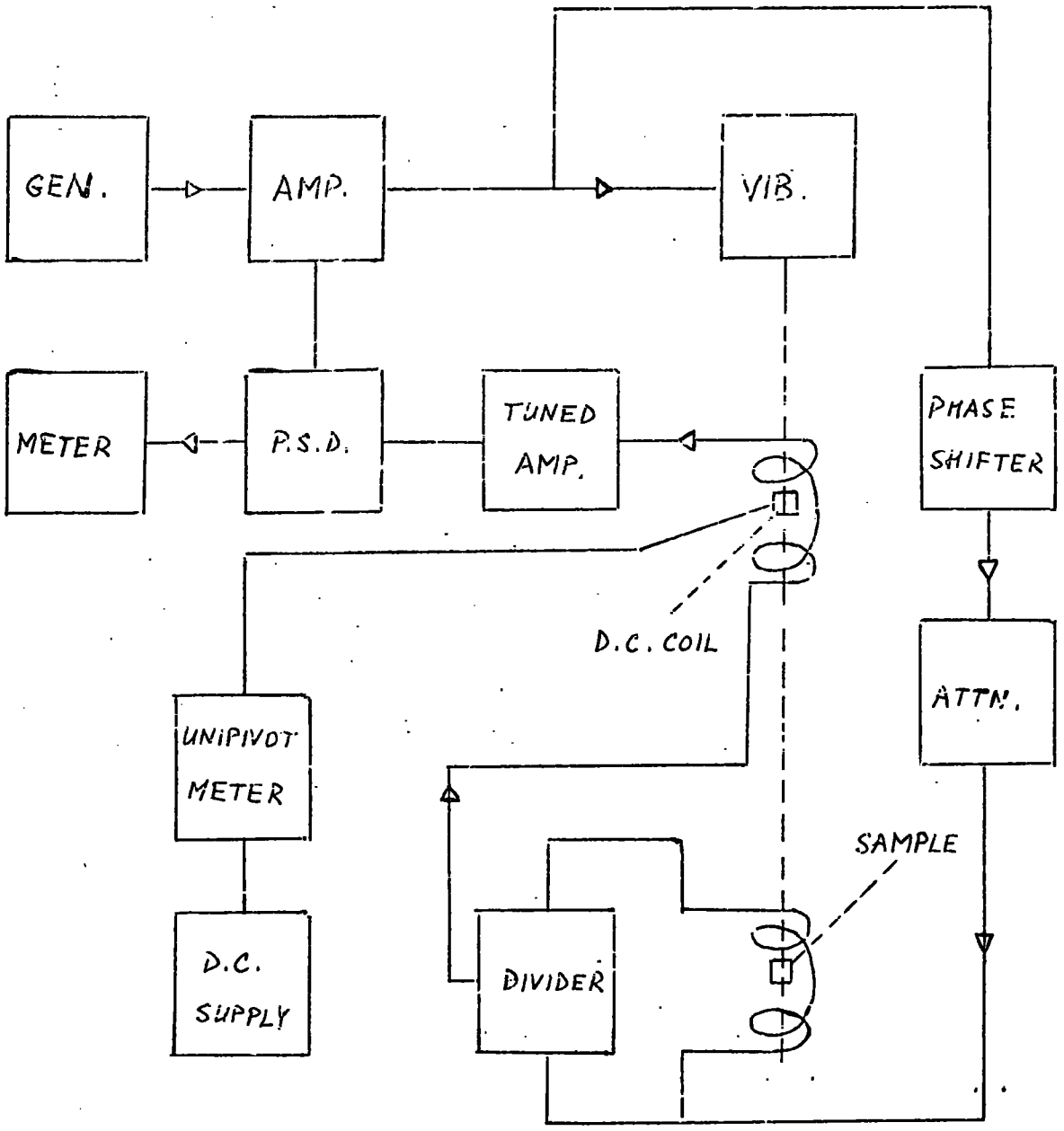

Figure 2.2 Block Diagram of Magnetometer.

70 c.p.s. to avoid interference with the fundamental and harmonics frequency of the main supply voltage and secondly the output from the phase sensitive detector is related to the amplitude of the supplied signal if the phase difference between the signal and reference voltages is kept constant.

The phase shifter and attenuator (Fig. 2.3) were designed by Piercy and are described in his thesis (Ref. 1.26). The D.C. coil (Ref. 2.1) is supplied from a 6 volts 80 ampere-hour accumulator through a variable resistor. The current (0 - 48 mA) is measured with a Cambridge Unipivot Type L milliamperemeter. The potential divider 250kΩ is used to reduce the magnitude of the signal for specimens with large magnetization values.

Two sample pick-up coils have been made, one on a former of PTFE rod for low temperature work and the other one from pyrophyllite for use at high temperatures. Two matched coils were wound on the former, both consisting of 400 turns of 46 SWG enamelled copper wire. The coils are connected in series opposition with a 6 mm gap between them. The coils on the PTFE former are potted in "Durafix" cement, while those on the pyrophyllite former are potted in "Araldite". This potting serves to secure the windings and prevent shorting between the turns.

The vibrating rod is a long drinking straw 4 mm in

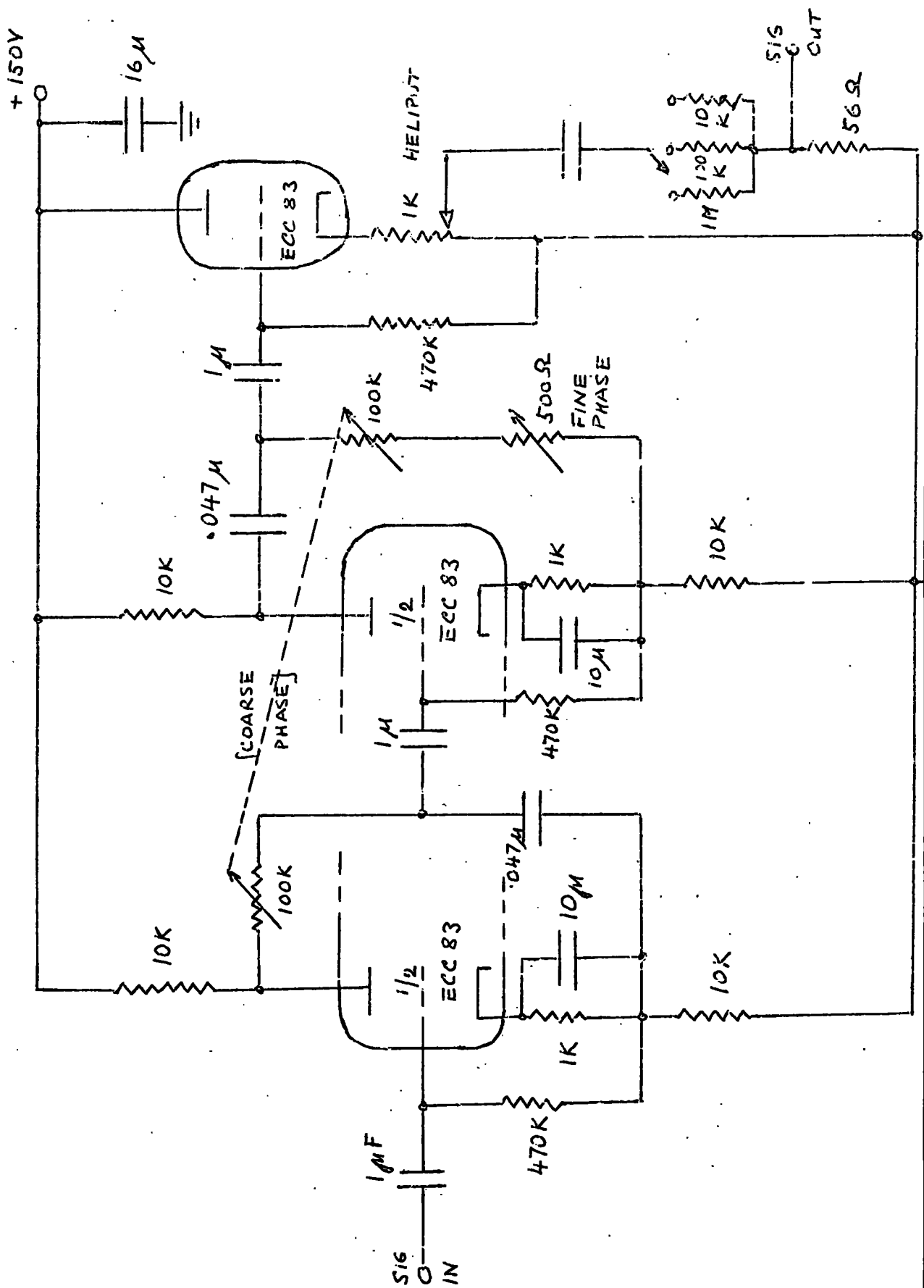

Figure 2.3 Phase Shifter and Attenuator.

diameter. At the end of the rod a fused silica tube is attached with the specimen attached to the bottom. The weight of the sample is usually in the range 20 - 100 mgms and the length kept to less than 4.5 mms as described by Ellis (Ref. 2.1). Before operation the pick up coil is adjusted so that its centre coincides with the centre of the sample itself.

The magnetic field was generated in a water cooled solenoid constructed originally by Hutchinson (Ref. 2.3) but rewound during this work. It consists of nine flat coils of copper strip, in the shape of "pancakes", mounted on a central tufnol tube, with insulating spacers between them. The calibration with a Hall Probe gave a linear dependence of field with current at the rate of 42 Oe/Amp. The solenoid was raised into position on a lifting platform which has also been described previously (Ref. 2.1).

The power supply for the solenoid is a Westinghouse 0 - 200 Volts D.C., 50kW Rectifier, with a continuously variable output control.

2.3 Details of Measurements.

2.3.1 Crystal Structure.

The powered specimens were exposed to CoKx radiation in a Philips Debye-Scherrer powder camera of diameter 11.483 cm and the lattice spacings were derived from the diffraction patterns in the conventional way using the Nelson-Riley

extrapolation. The more usual copper Kx line causes fluorescence of the rare earth components and is therefore unsuitable.

2.3.2 Calibration and Accuracy.

The equation relating the magnetization (σ) to the current in the reference coil (i_σ) is $\sigma = \frac{i_\sigma}{w} \gamma$ (Eqn. 2.1) where w is the mass of the sample and γ is a constant. To obtain this constant the current i_σ was calibrated against the magnetization of a pure iron sample. The absolute magnetization data of Weiss and Forrer (Ref. 2.4) was assumed to hold for this specimen. The function i_σ versus field (up to 8.4 kOe) was measured at room and liquid nitrogen temperatures, the data being extrapolated to the saturation values in each case. From these two sets of measurements an average value of the calibration constant was obtained and gave γ = 0.0627 e.m.u/mA. The equation for specimen magnetization, given in atomic units, for other materials is then:

$$\sigma = \frac{\gamma \, i_\sigma \, W_A}{w \cdot .5586} \qquad \left[\mu_B \text{/molecule}\right] \qquad \text{(Eqn. 2.2)}$$

where w is measured in gms and i_σ in mA. Considering the errors in the separate terms of Eqn. 2.2 an estimate of the total accuracy is made.

The quantities i_σ and w were measured to $\pm$ 1% and γ was measured to within 1.5%, consequently the accuracy is of order $\pm$ 3.5%. For small signals, the error is larger than this, due

to noise which could not be eliminated using the present detection system. The smallest detectable magnetization was $5 \cdot 10^{-3}$ e.m.u. corresponding to 0.1 mA.

2.3.3 The Demagnetising Field.

The internal field Hi, i.e. the field inside the sample body, is different from the applied field H by the demagnetizing field H_D, due to the poles of the sample itself

$$Hi = H - H_D \qquad H_D = N_D M \qquad \text{(Eqn. 2.3)}$$

M is the magnetization and N_D the demagnetizing factor. Unfortunately N_D can only be derived exactly for an isotropic ellipsoid as it is only for this shape that the magnetization is uniform.

In our case it was impracticable to make samples of a definite shape as the compounds studied are both extremely brittle and prone to oxidation. In order to keep the demagnetizing field small, samples were made with their length approximately twice their width. The necessary correction to the applied field H for samples of this shape is then a few percent (Ref. 2.5). This correction is of the same order as the error of measurement determined earlier.

2.3.4 Temperature and Curie Point.

Temperature measurements were carried out over the range from liquid helium (4.2°K) up to 800°K.

A copper-constantan thermocouple was in contact with

the specimen to enable precise measurement of the temperature of the sample. The wires used were "high conductivity" supplied by Lewcos, and "thermocouple telconstant" supplied by Telcon Metals. The junction was melted in a gas flame.

The reference junction was held in liquid nitrogen for temperatures up to room temperature and at 0°C for temperature in excess of this. The thermal emfs were measured with a Pye Portable Potentiometer and the corresponding values of temperature obtained from British Standard Tables (Ref. 2.6). Interpolation between liquid helium and liquid nitrogen temperatures by comparison with standard tables was done for temperatures below - 190°C.

Standard techniques for low temperatures were used. The Helium dewar, which is located inside the nitrogen dewar, is evacuated and filled with helium gas before the liquid is transferred.

The temperature versus magnetization function was taken during the warming up period. The rate of temperature rise was sufficiently low for thermal equilibrium in the specimen to be obtained (Ref. 2.1). A heated oil bath (Lissapol NX) was used to raise the specimen temperature to 200°C. Measurements at higher temperatures are limited by the breakdown of the insulation of the copper wire forming the sample pick up coil. This difficulty has now been overcome by Primavesi on a

new vibrating type magnetometer, which was used to obtain the very high temperature measurements.

The Curie temperatures (T_c) were obtained by extrapolation of the linear portion of a graph of σ^2 versus T. This is possible since on expanding the Brillouin function in Equation $M = Ng\mu_B J B_j(x)$ for small x we get $\sigma_{o,T}^2 \propto (T_c - T)$.

2.3.5 Atomic moment.

The relation between the Bohr magneton number p of a material and the magnetization is given by the equation

$$p = \frac{\sigma_{o,o} \, W_A}{N \mu_B} \qquad \text{(Eqn. 2.4)}$$

The measurement of the absolute saturation magnetization $\sigma_{o,o}$ requires either infinite field or zero temperature. Thus we have to extrapolate from high fields at liquid helium temperatures (the lowest available temperature).

For our region of applied fields of 10^3 to 10^4 Oe we can use the empirical relationship (Ref. 2.7),

$$\sigma_{H,T} = \sigma_{S,T} \left(1 - \frac{a}{H} - \frac{b}{H^2}\right) + cH \qquad \text{(Eqn. 2.5)}$$

which is applicable at low temperatures. Here $a > b \gg c$ are constants and $\sigma_{S,T}$ is termed the saturation magnetization. The difference between $\sigma_{S,T}$ and $\sigma_{o,T}$ is so small in our case that it can be ignored and consequently the saturation magnetization was obtained at 4.2°K from Equation 2.5, by extrapolation of the σ versus 1/H plot to 1/H = 0 and this value was taken to give the atomic moment.

CHAPTER III

Results.

In this chapter are presented the results obtained by using the apparatus and technique described in the previous chapter.

Some of the results of lattice parameters were obtained from the Department of Physical Metallurgy and Science of Materials at the University of Birmingham.

The results of terminal values of compounds were taken from the latest published work.

The lattice parameter values for the series Gd $(Fe, Co)_2$, Ho $(Fe, Co)_2$, Ho $(Co, Ni)_2$, Er $(Co, Ni)_2$, Dy $(Co, Ni)_2$ and (Er, Gd) Co_2 are given in Tables 3.1 to 3.5 and are plotted in Figures 3.1 to 3.3, excluding series Dy $(Co, Ni)_2$ and including series Gd $(Co, Ni)_2$ and Er $(Fe, Co)_2$ to show the overall variation.

The magnetic properties reported here are the saturation moments (σ_s) at 4.2°K, 77°K and room temperature (taken as 290°K), the ferromagnetic Curie Temperatures (T_c) and the magnetization-temperature behaviour. The determinations of the saturation moments and the Curie temperatures are described in Section 2.3d,e.

The σ_s and T_c values are given in Tables 3.6 to 3.10 and are presented in Figures 3.4 to 3.11, excluding the series Dy $(Co, Ni)_2$.

In Figures 3.4, 6, 8 are also plotted the transition metal moments which are obtained if we subtract the pseudo-binary compound saturation moments from rare-earth moments.

The magnetization-temperature behaviour is presented in Figures 3.12 to 3.35.

Composition X	Lattice Parameter (A) ± 0.002A	Atomic Volume ± 0.02A^3
2 (Gd Fe_2)	7.376 *	16.72
1.6	7.383	16.77
1.2	7.361	16.62
0.8	7.327	16.39
0.4	7.292	16.16
0 (Gd Co_2)	7.259 **	15.93

* Ref. 3.1

** Ref. 3.2

Table 3.1 Lattice Parameters for Gd $(Fe, Co)_2$.

Figure 3.1 Lattice spacings in the pseudo-binary series

Gd $(Fe, Co)_2$ and Gd $(Co, Ni)_2$.

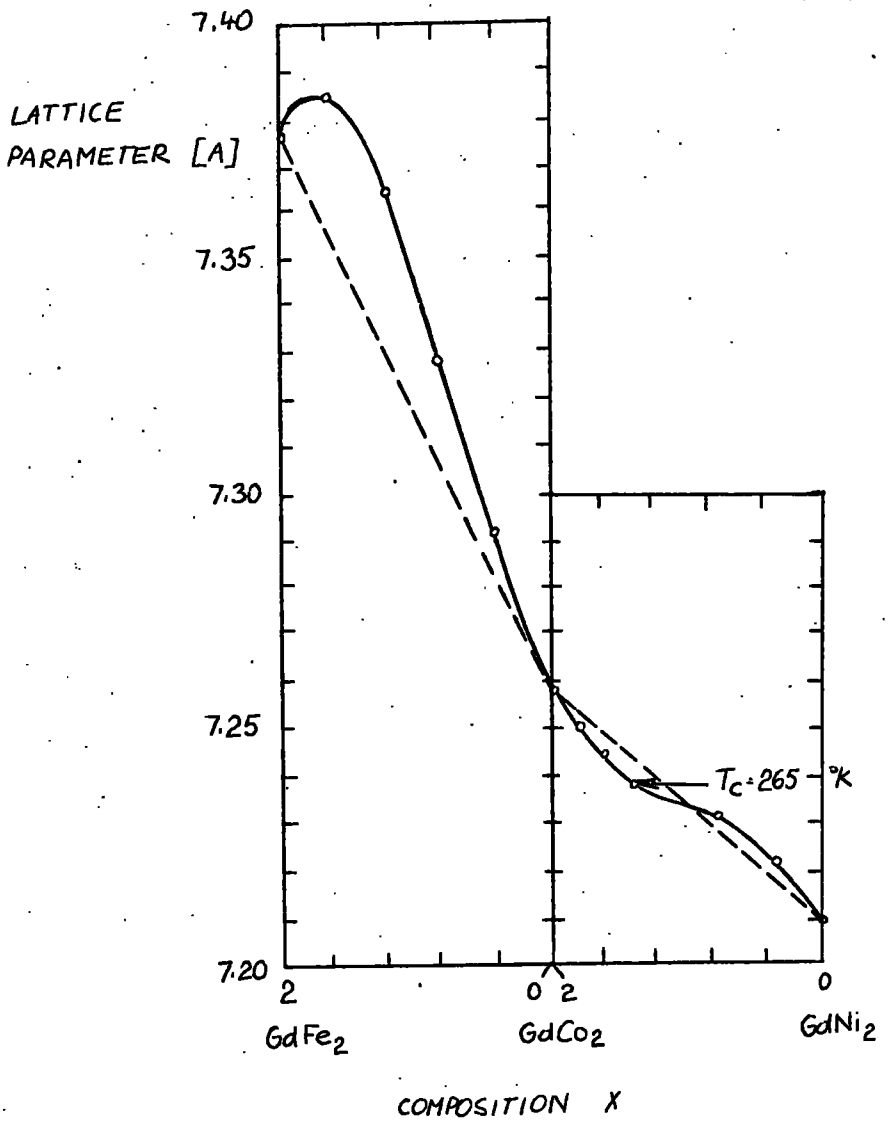

Composition X	Lattice Parameter (Å) ± 0.002A	Atomic Volume ± 0.02A^3
2.0 (Ho Fe_2)	7.299	16.20
1.6	7.301	16.21
1.2	7.274	16.04
0.8	7.247	15.86
0.4	7.211	15.62
0.2	7.186	15.46
0 (Ho Co_2) 2 (Ho Co_2)	7.166	15.33
1.8	7.1695	15.35
1.6	7.163	15.31
1.2	7.156	15.27
0.8	7.150	15.23
0 (Ho Ni_2)	7.1318 *	15.11

* Ref. 3.1

Table 3.2 Lattice Parameters for Ho $(Fe,Co)_2$; Ho $(Co, Ni)_2$.

Figure 3.2 Lattice spacings in the pseudo-binary series Ho $(Fe, Co)_2$ and Ho $(Co, Ni)_2$.

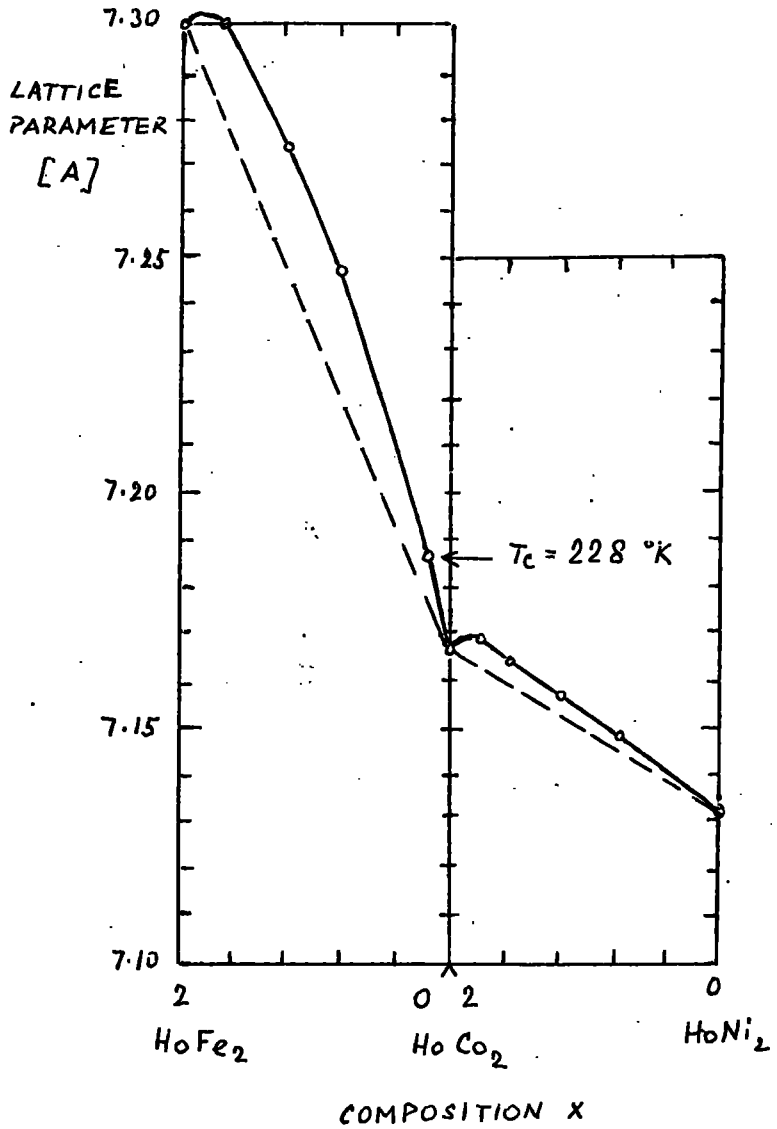

Composition X	Lattice Parameter (A) ± 0.002A	Atomic Volume ± 0.02A^3
2 ($Er Co_2$)	7.1536	15.25
1.667	7.1516	15.24
1.332	7.1489	15.22
1.0	7.1459	15.20
0.668	7.1429	15.18
0.334	7.1380	15.15
0 ($ErNi_2$)	7.1319	15.11

Table 3.3 Lattice Parameters for Er (Co, Ni)$_2$

Composition X	Lattice Parameter (A) ± 0.002A	Atomic Volume ± 0.02A^3
2 ($Dy Co_2$)	7.175 *	15.39
1.5	7.178	15.41
1.0	7.169	15.35
0 ($DyNi_2$)	7.149 **	15.22

* Ref. 3.3

** Ref. 3.1

Table 3.4 Lattice Parameters for Dy (Co, Ni)$_2$.

Figure 3.3 Lattice spacings in the pseudo-binary series $Er(Fe, Co)_2$ and $Er(Co, Ni)_2$.

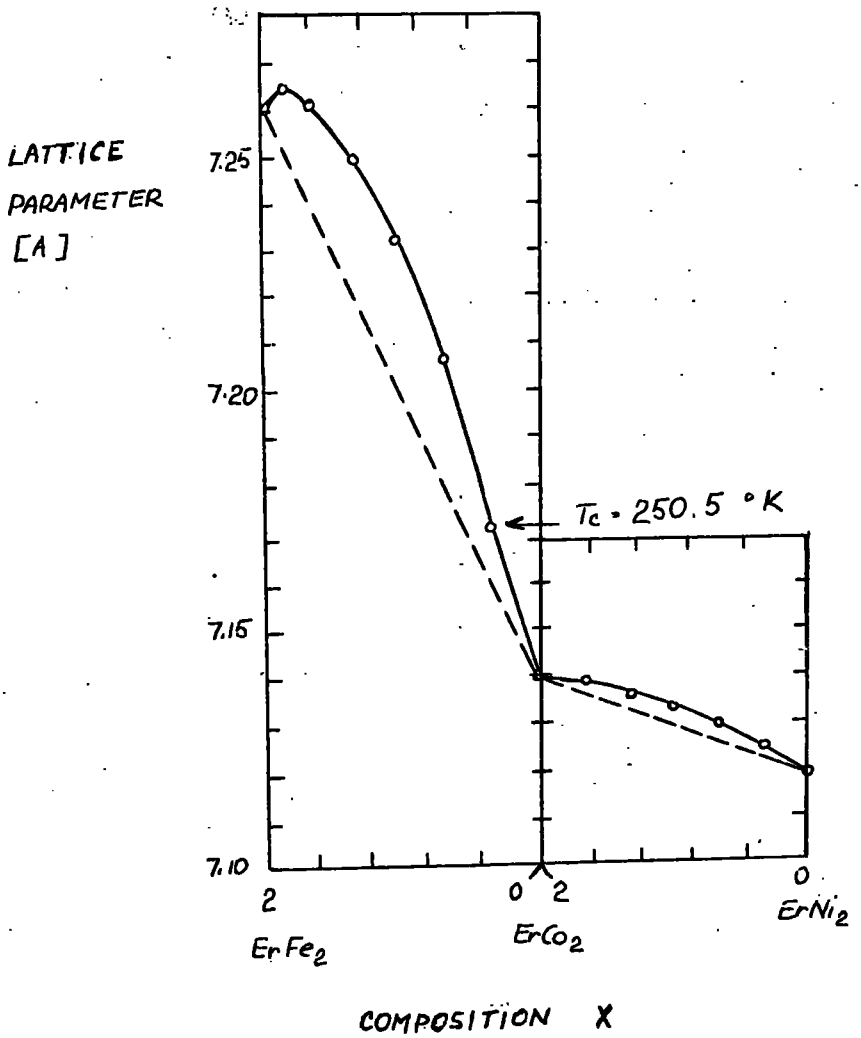

Composition X	Lattice Parameter (A)	Atomic Volume
1.0 ($Er Co_2$)	7.1560 ± 0.0002	15.27
0.83	7.1702 ± 0.0002	15.36
0.67	7.1863 ± 0.0002	15.46
0.50	7.2024 ± 0.0005	15.57
0.33	7.2214 ± 0.001	15.69
0.17	7.2422 ± 0.0005	15.83
0 ($Gd Co_2$)	7.2587 ± 0.0002	15.94

* Ref. 3.2

Table 3.5 Lattice Parameters for (Er, Gd) Co_2 *.

Composition X	Saturation moments (μ_B /MOL) ± 1%			Curie Temperature (°K)
	4.2°K	77°K	290°K	
2.0 ($GdFe_2$)	3.6**			813 **
1.6	3.69	3.11	1.46	861
1.2	4.24	3.82	1.51	815
0.8	4.39	4.04	1.86	739
0.4	4.61	3.75	1.87	619
0 ($GdCo_2$)	4.9 **			400 **

* Ref. 1.34

** Ref. 1.39

Table 3.6 Magnetic Data for Gd (Fe, Co)$_2$

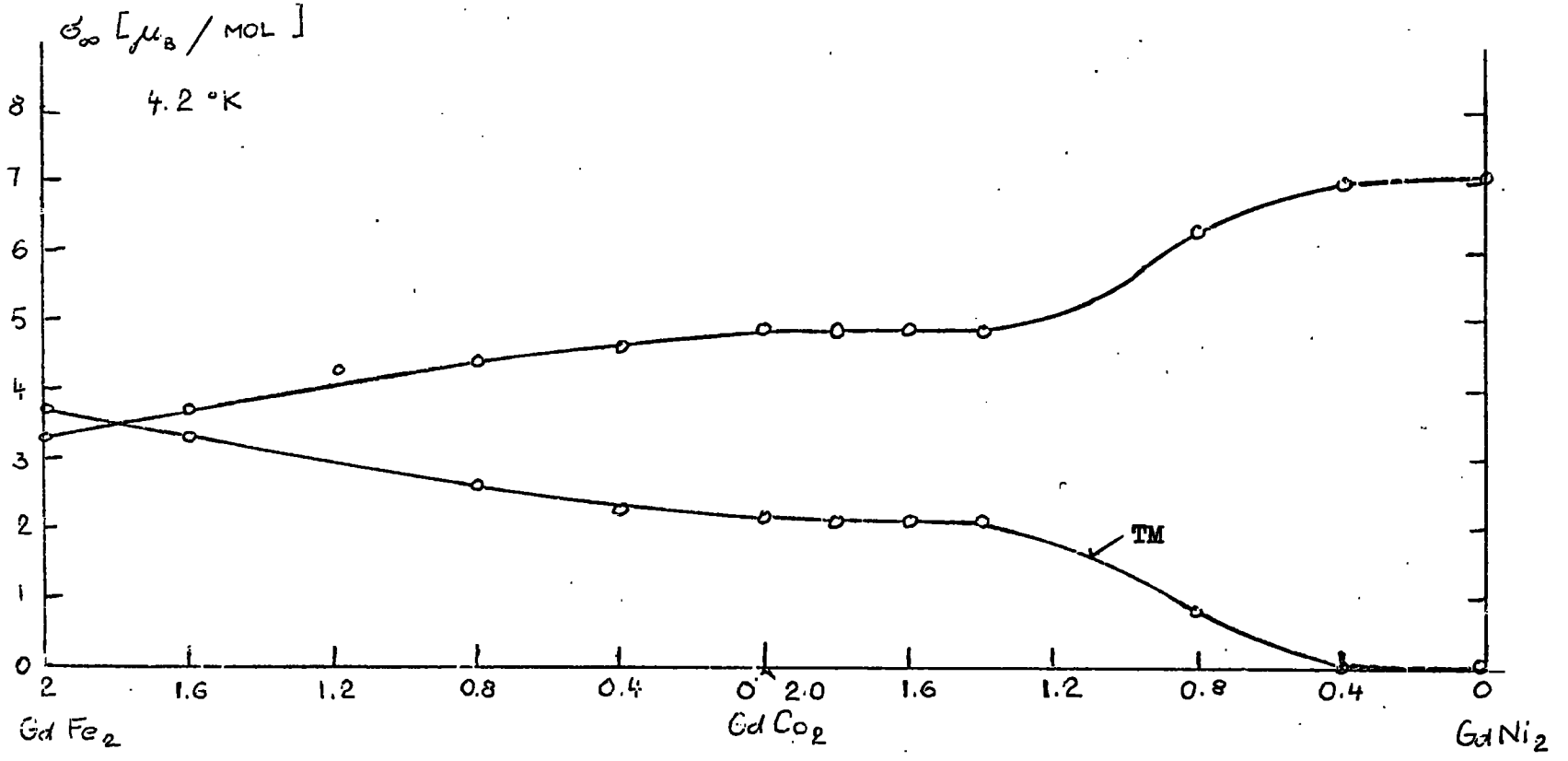

Figure 3.4 Saturation Moments and Transition Metal Moments (TM) for Gd (Fe, Co)$_2$ and Gd (Co, Ni)$_2$.

Figure 3.5 Curie Temperatures for $Gd(Fe,Co)_2$ and $Gd(Co,Ni)_2$ series

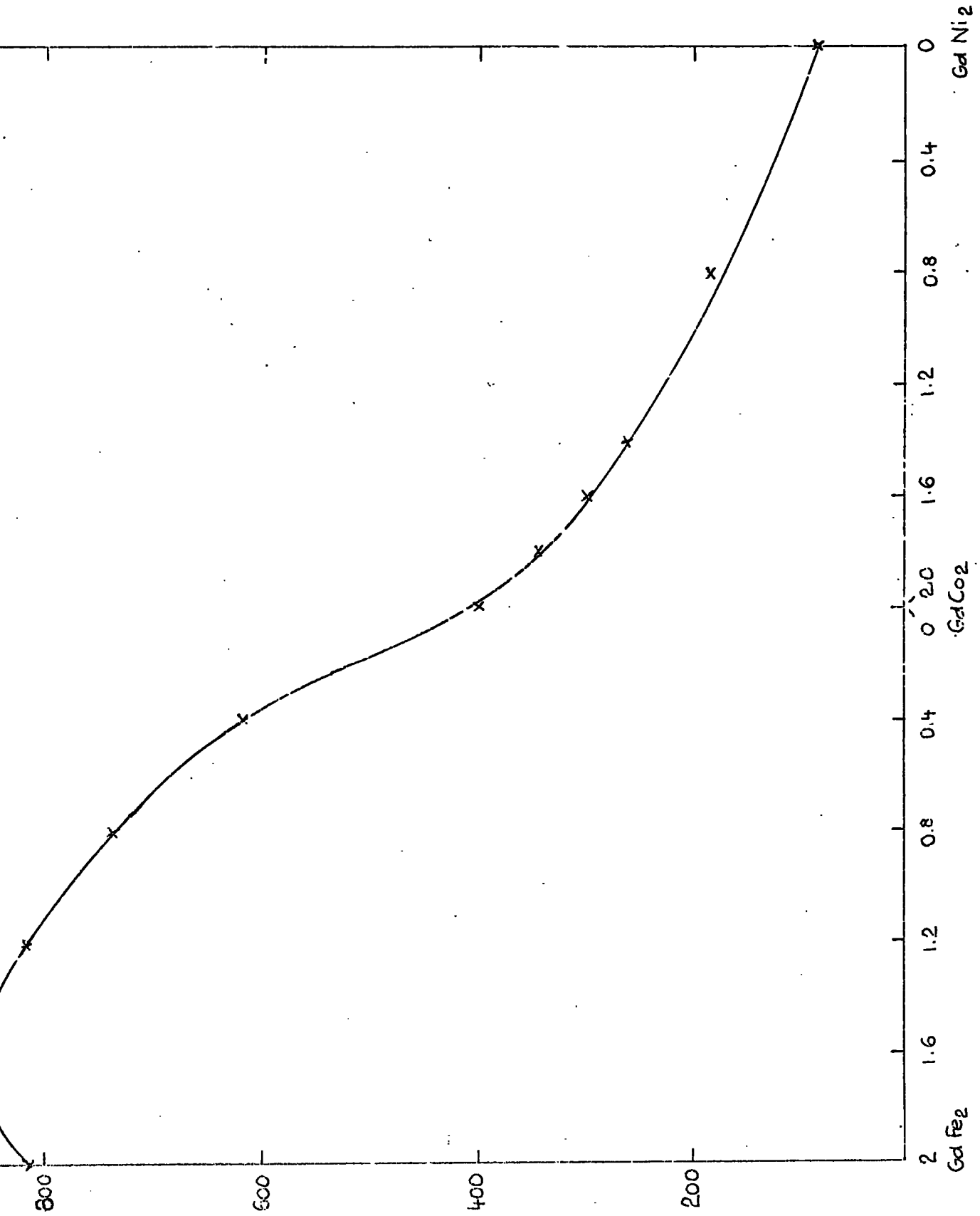

Composition X	Saturation Moments μ_B /MOL			Curie Temperature (°K)
	4.2°K	77°K	290°K	
2.0 (Ho Fe_2)	5.404	5.21	2.89	600 *
1.6	5.66	5.398	3.09	602
1.2	5.56	5.3	2.86	573
0.8	5.458	5.086	2.42	477
0.4	6.61	5.667	1.91	411
0.2	-	-	-	228
0 (Ho Co_2)	7.8 **	-	-	95 **
2 (Ho Co_2)				
1.8	8.93			44
1.6	8.78			45.3
1.2	8.69			45
0.8	8.38			43.7
0 (Ho Ni_2)	8.4 **			22 **

* Ref. 1.34

** Ref. 1.33

Table 3.7 Magnetic Data for Ho $(Fe, Co)_2$, Ho $(Co, Ni)_2$.

Figure 3.6 Saturation Moments and Transition Metal Moments (TM) for Ho $(Fe, Co)_2$ and Ho $(Co, Ni)_2$.

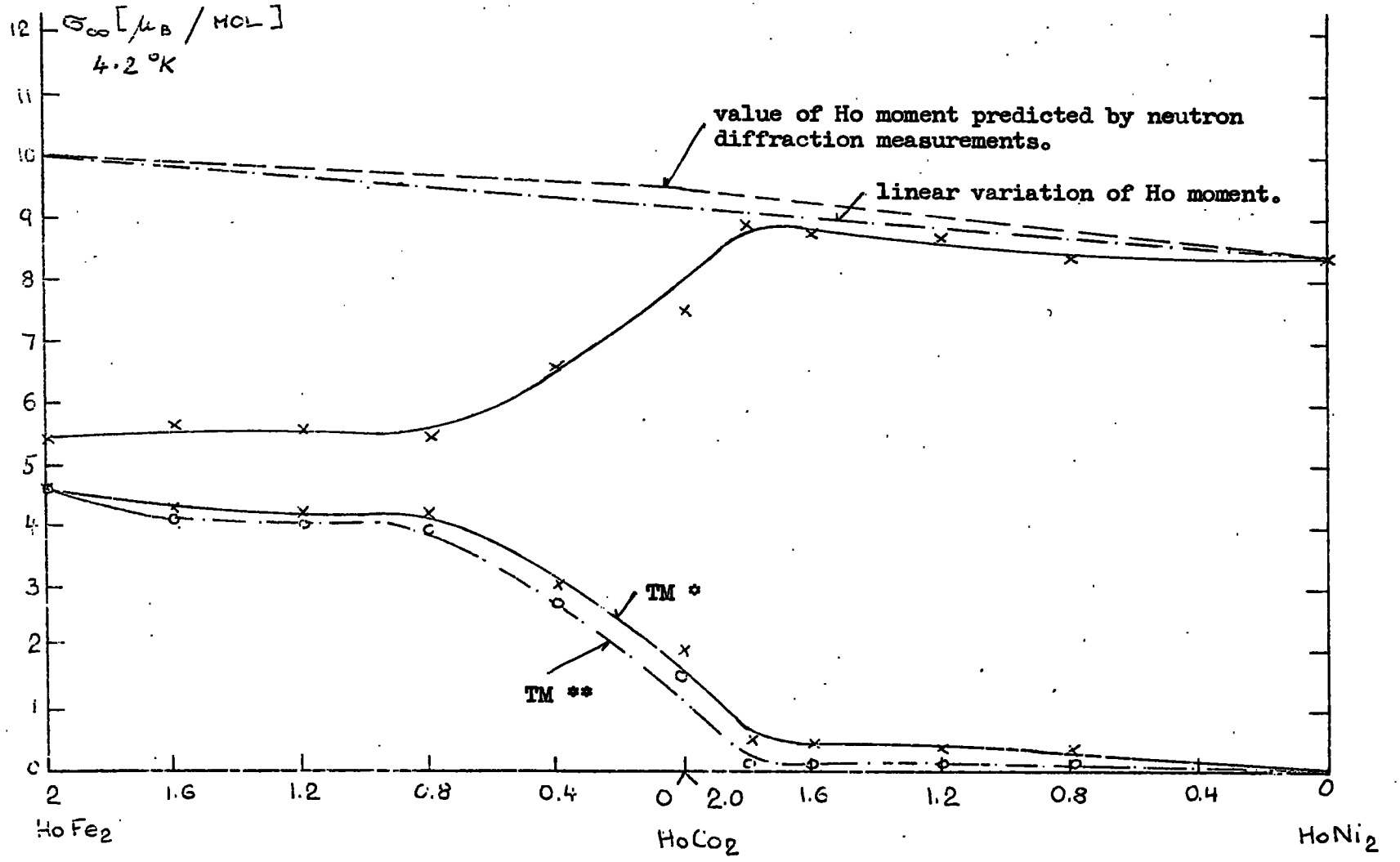

* TM if Ho varies as predicted by neutron diffraction measurements.

** TM if Ho varies linearly.

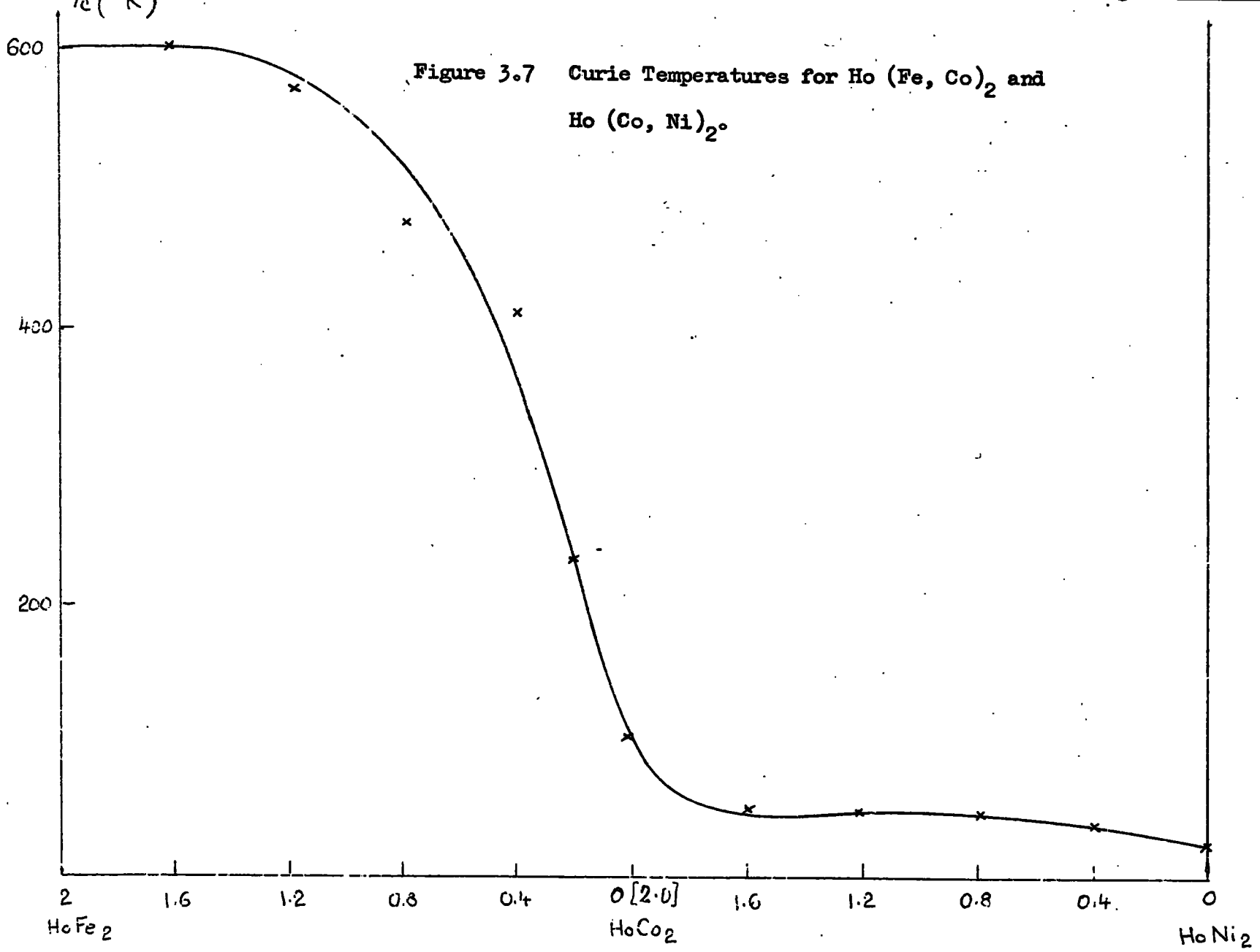

Figure 3.7 Curie Temperatures for Ho $(Fe, Co)_2$ and Ho $(Co, Ni)_2$.

Composition X	Saturation Moments μ_B /MOL ± 3% 4.2°K	Curie Temperature °K
2.0 ($Er Co_2$)	7.0 *	36
1.666	7.2	29
1.332	7.08	29
1.00	6.91	28
0.668		27.7
0.334	7.0	27
0 ($Er Ni_2$)	6.8 *	21 *
$Er Co_{1.6}Fe0.4$	5.33	250.5

* Ref. 1.33

Table 3.8 Magnetic Data for Er $(Co, Ni)_2$; Er $(Co_{1.6}\ Fe_{0.4})$

Figure 3.8 Saturation Moments and Transition Metal Moments (TM) for Er $(Co, Ni)_2$.

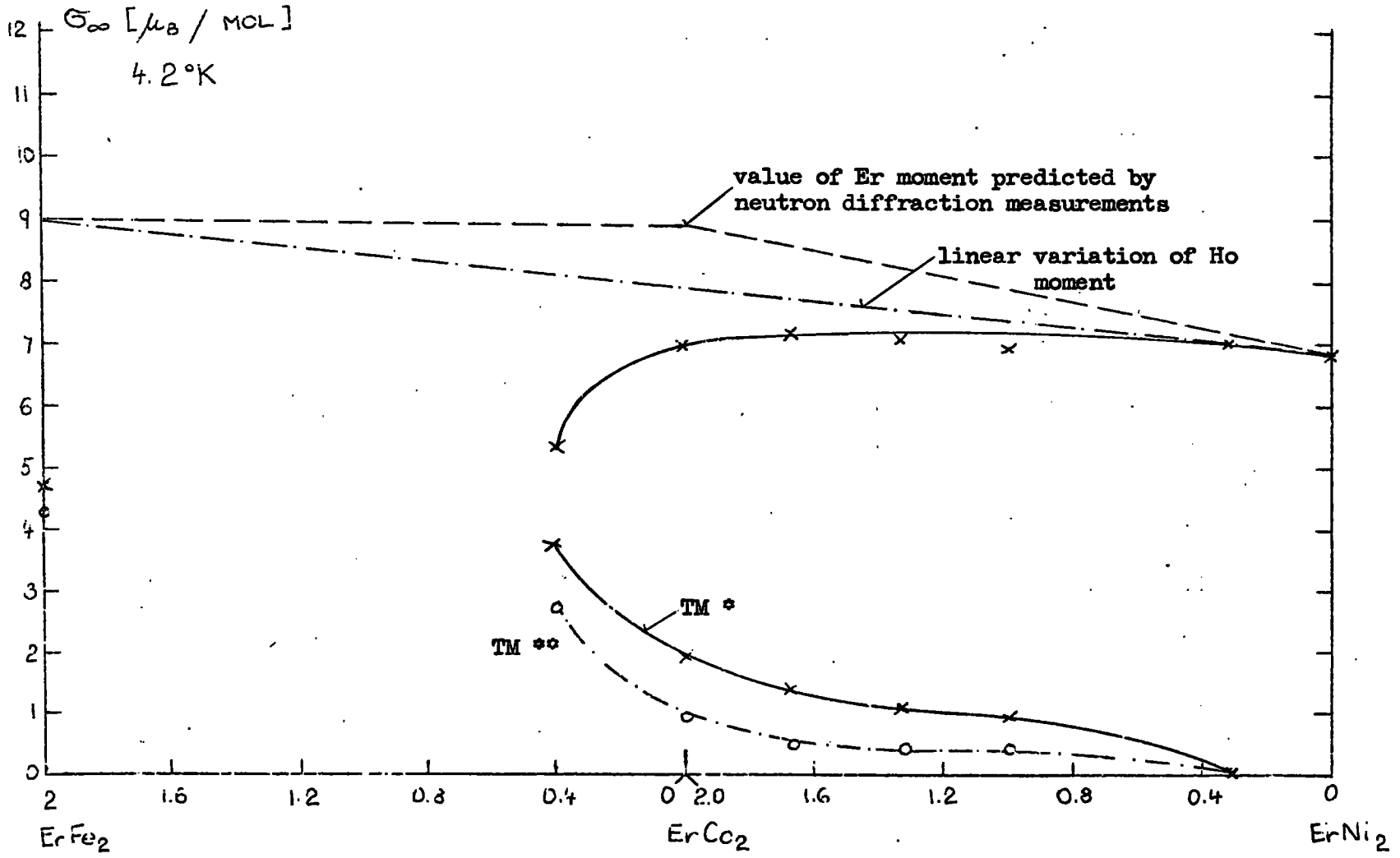

* TM if Er varies as predicted by neutron diffraction measurements.

** TM if Er varies linearly.

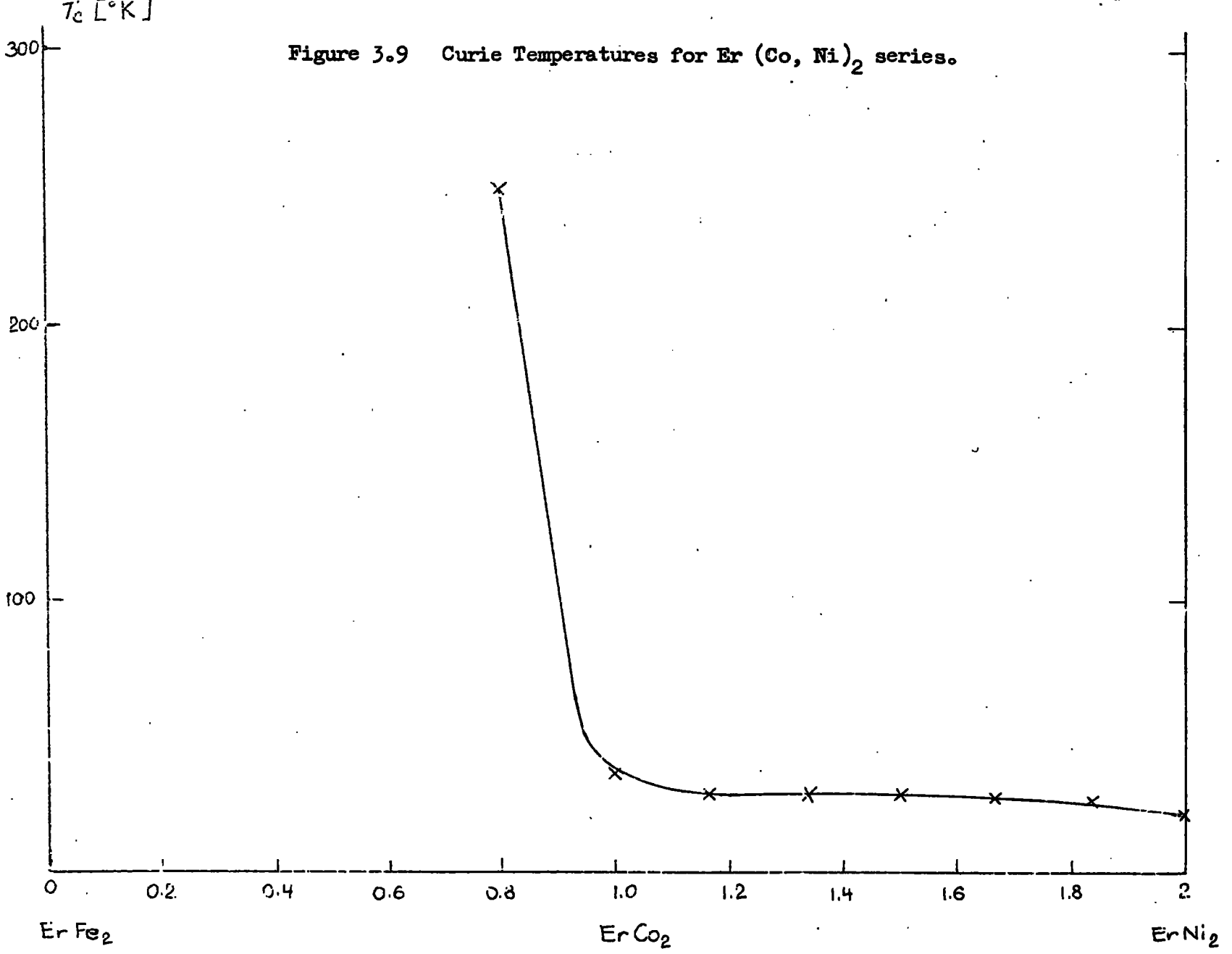

Figure 3.9 Curie Temperatures for Er $(Co, Ni)_2$ series.

Composition X	Saturation moments μ_B /MOL 4.2°K	Curie Temperature (°K)
2.0 ($Dy Co_2$)	7.6 *	159 *
1.5	9.75	142.5
1.0	8.85	131
0 ($Dy Ni_2$)	9.2 *	30*

* Ref. 1.33

Table 3.9 Magnetic Data for Dy $(Co, Ni)_2$.

Composition X	Saturation Moments μ_B /Molecule			Curie Temperature (°K)
	4.2°K	77°K	290°K	± 5
1.0 ($ErCo_2$)	7.0 *			36 *
0.83	6.05	3.61	0.13	138
0.67	5.24	4.23	0.13	226
0.50	5.06	4.5	0.29	270
0.33	5.03	4.4	1.69	330
0.17	4.98	4.84	2.42	378
0 ($GdCo_2$)	4.9 **			400 **

* Ref. 1.33

** Ref. 1.39

Table 3.10 Magnetic Data for (Gd, Er) Co_2.

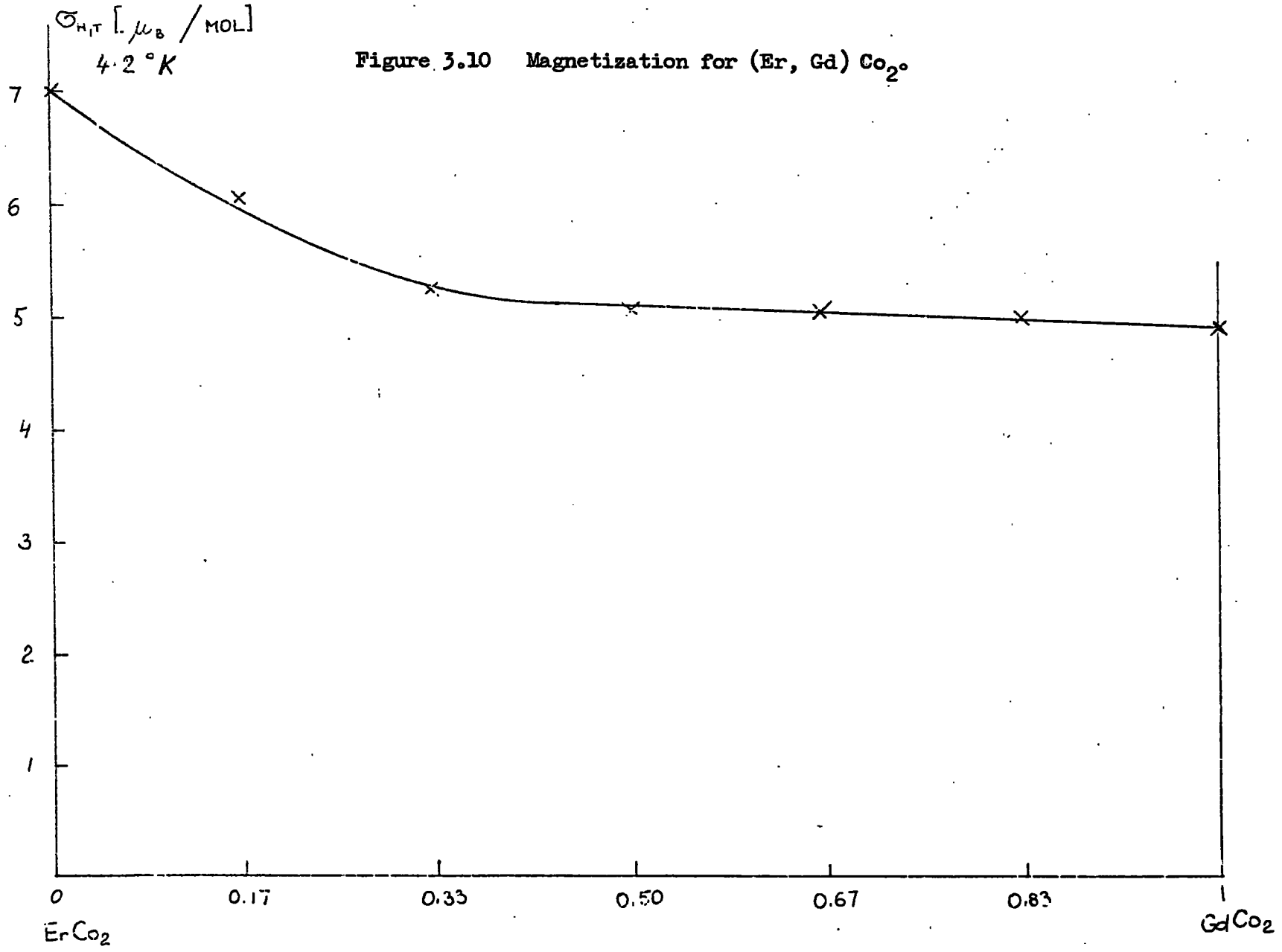

Figure 3.10 Magnetization for (Er, Gd) Co_2.

Figure 3.11 Curie Temperatures for (Er, Gd) Co_2.

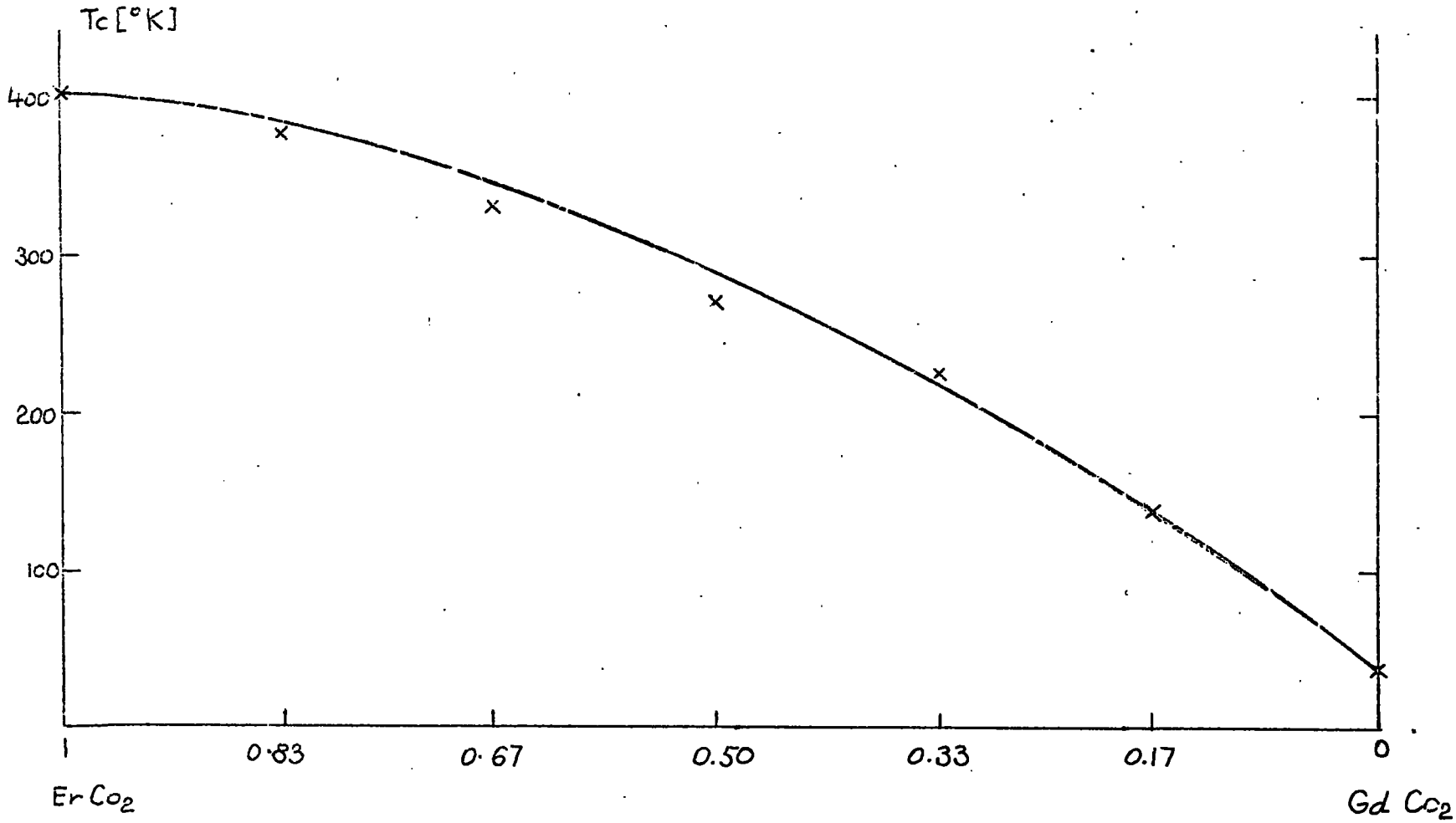

Figure 3.12 σ/T curve for Gd $(Co_{1.6}\ Fe_{0.4})$.

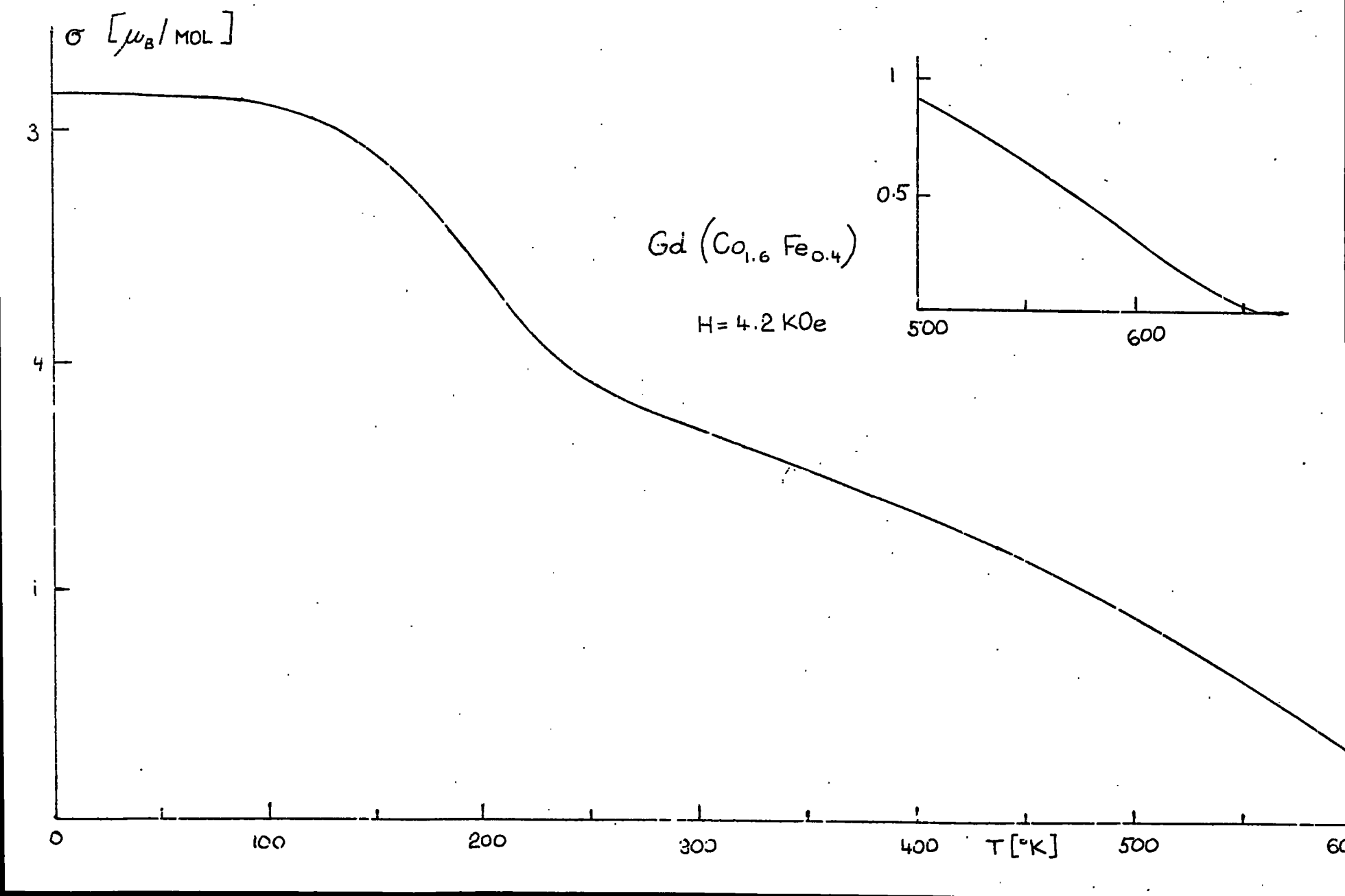

Figure 3.13 σ/T curve for Gd ($Co_{1.2}$ $Fe_{0.8}$)

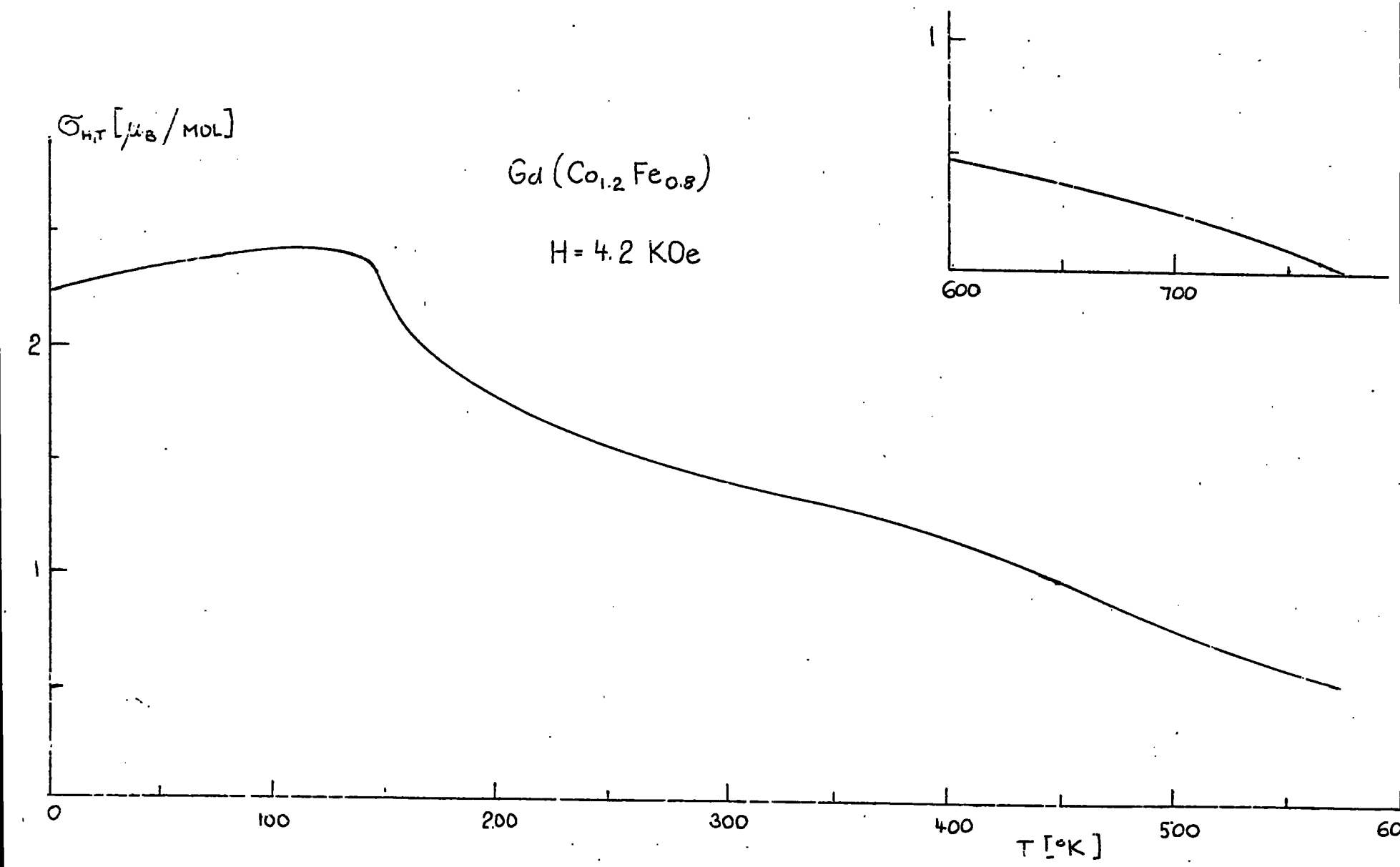

Figure 3.14 σ/T curve for Gd $(Co_{0.8}\ Fe_{1.2})$.

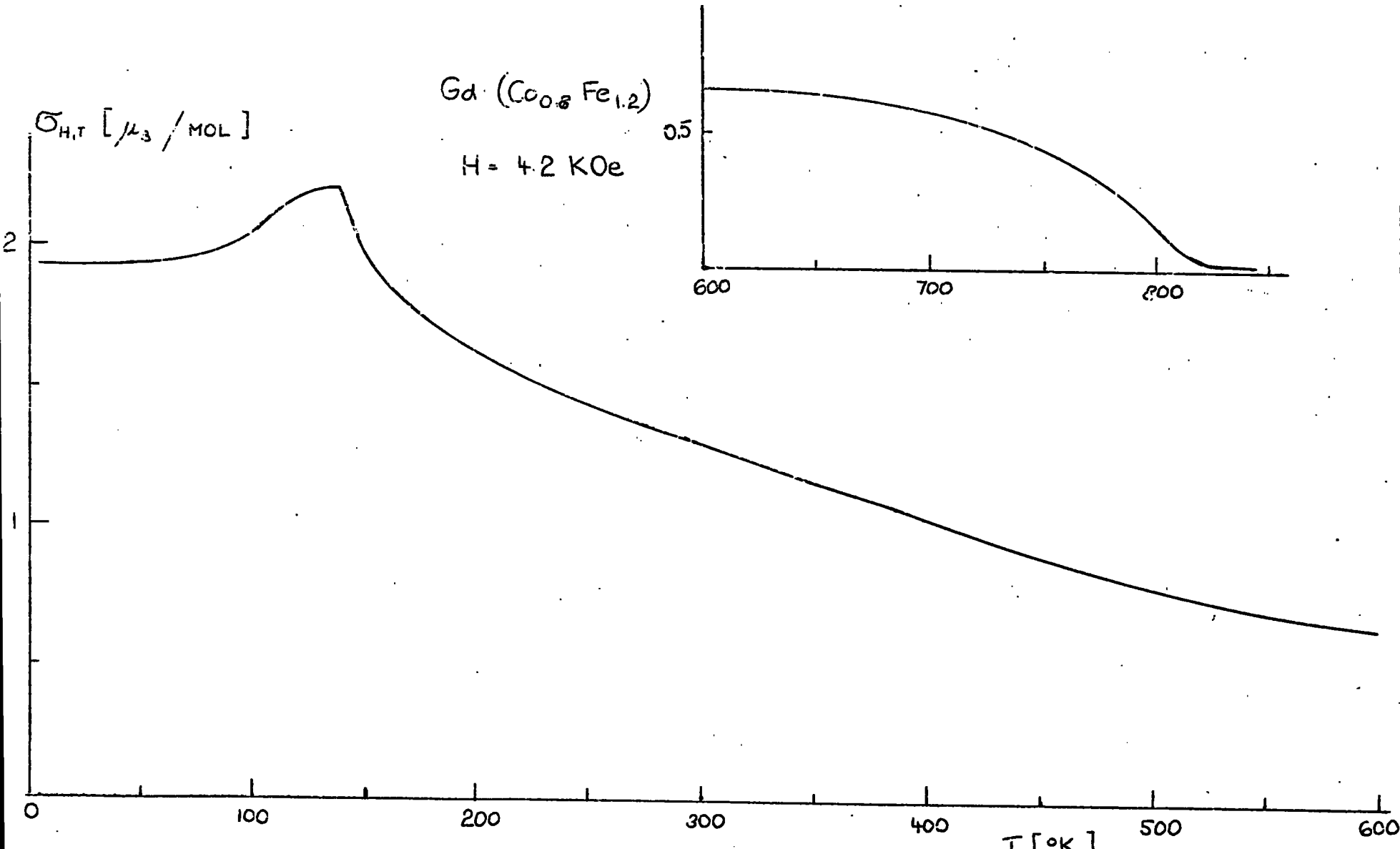

Figure 3.15 σ/T curve for Gd $(Co_{0.4}\ Fe_{1.6})$

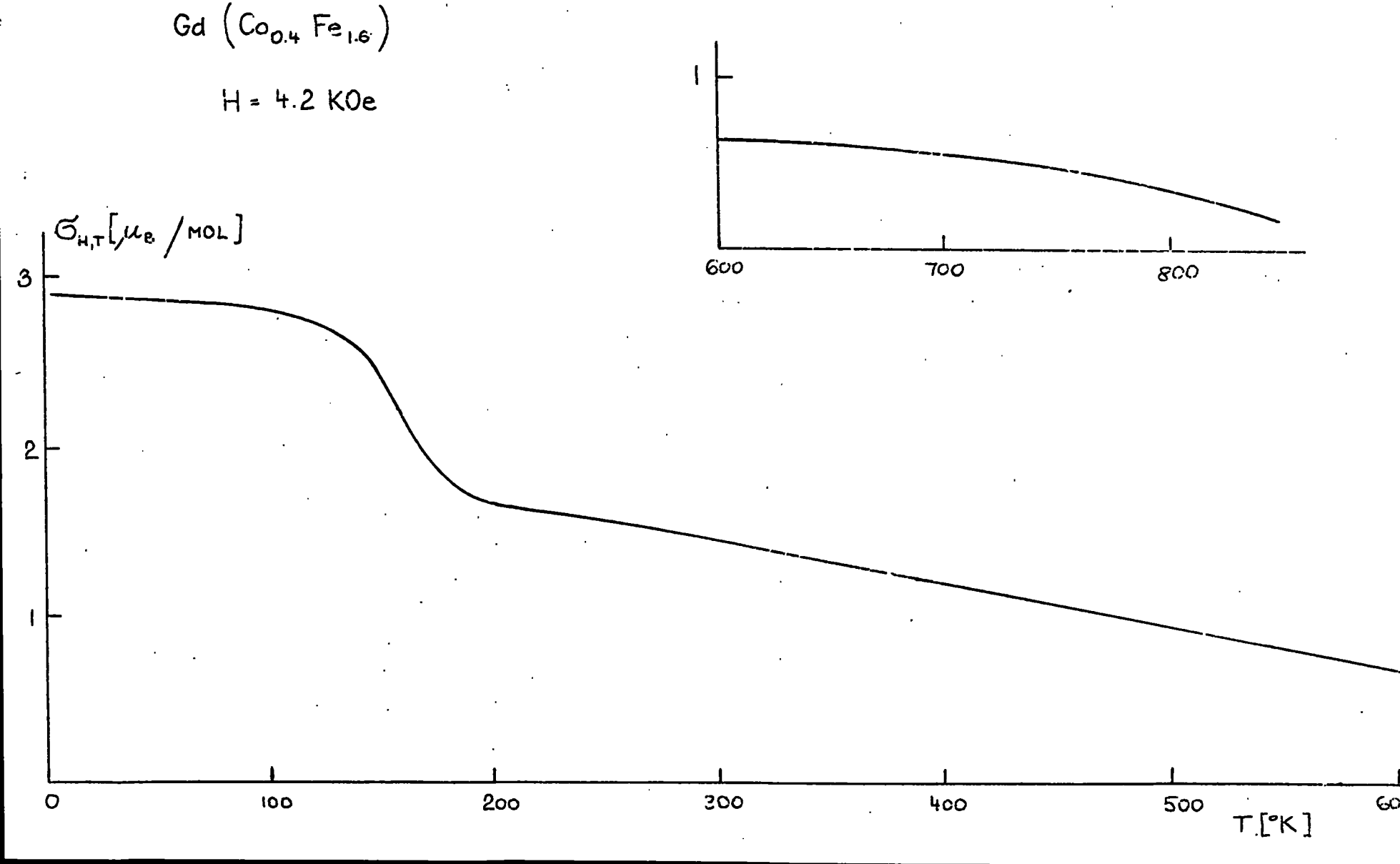

Figure 3.16 σ/T curve for Ho ($Co_{1.8}$ $Fe_{0.2}$)

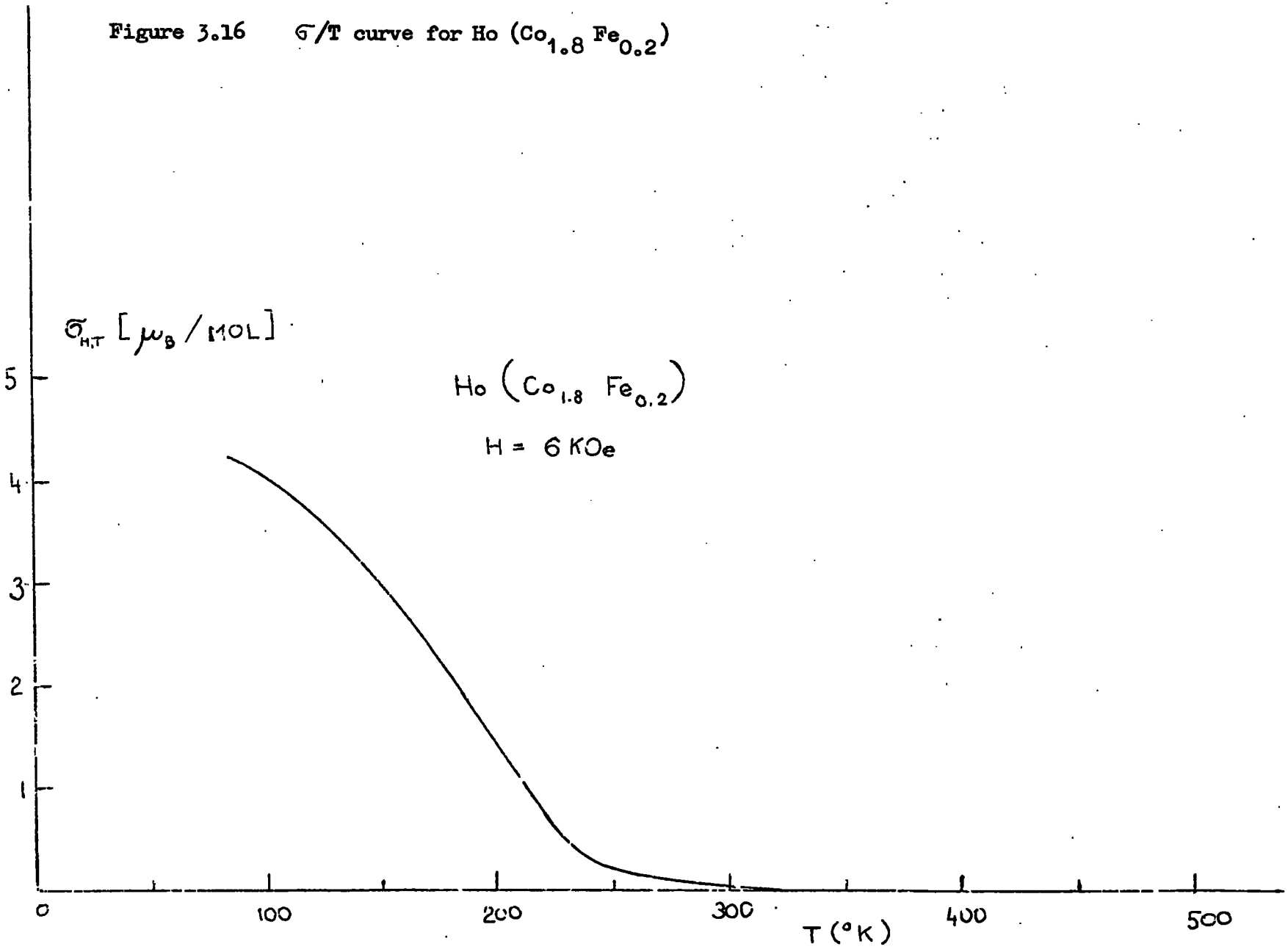

Figure 3.17 σ/T curve for Ho $(Co_{1.6}\ Fe_{0.4})$

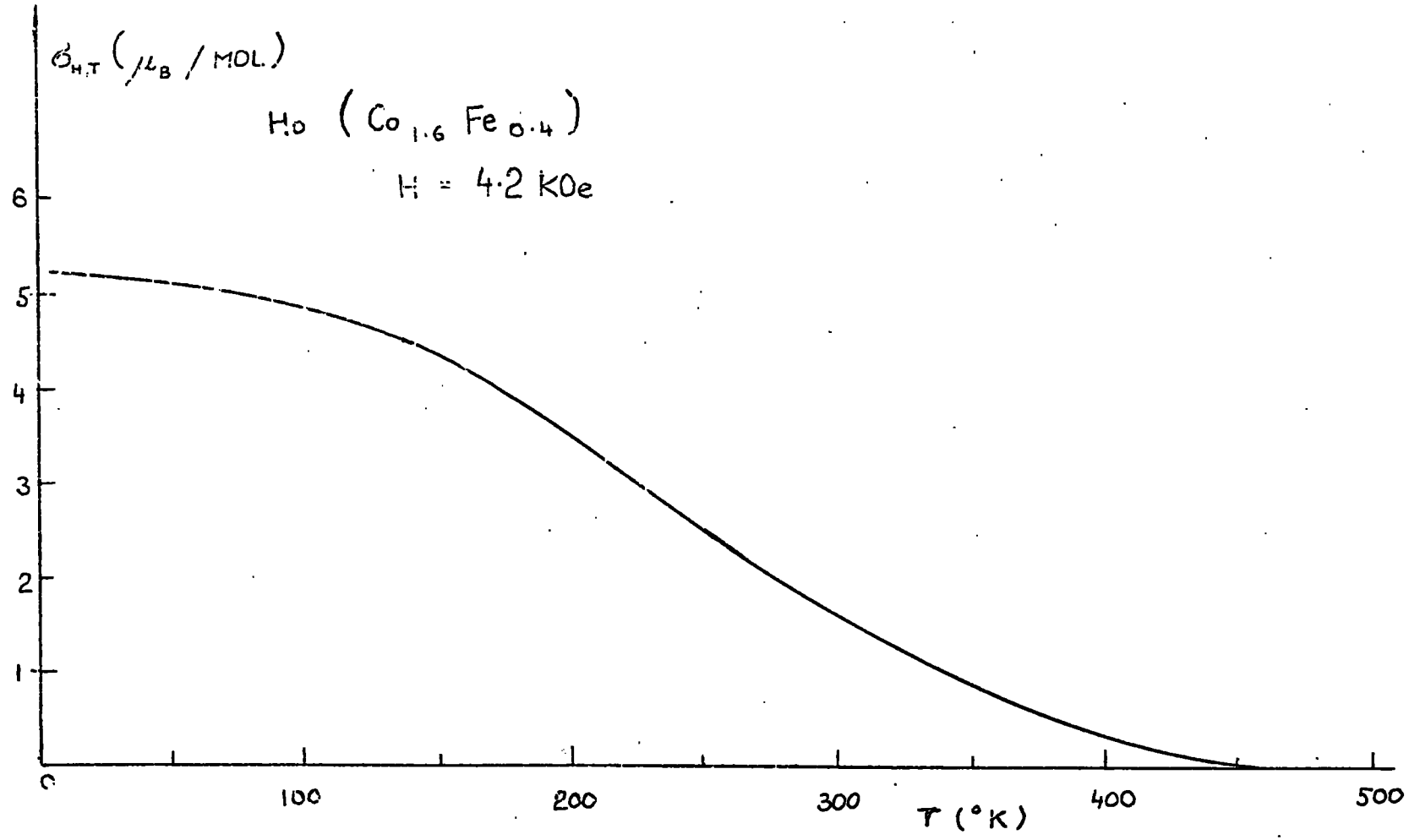

Figure 3.18 σ/T curve for Ho $(Co_{1.2}\ Fe_{0.8})$

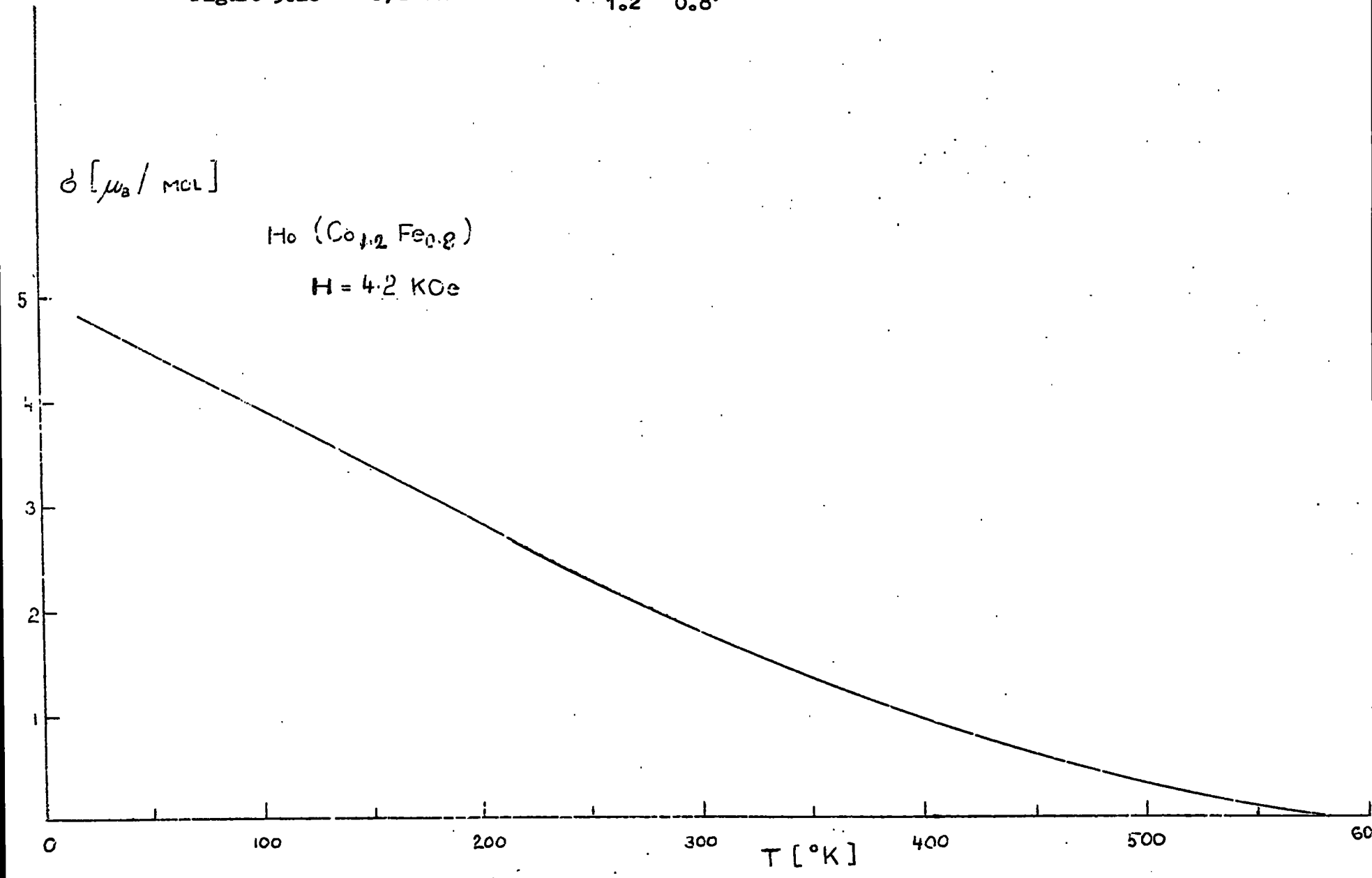

Figure 3.19 $\dot{G}/T$ curve for Ho $(Co_{0.8}\ Fe_{1.2})$

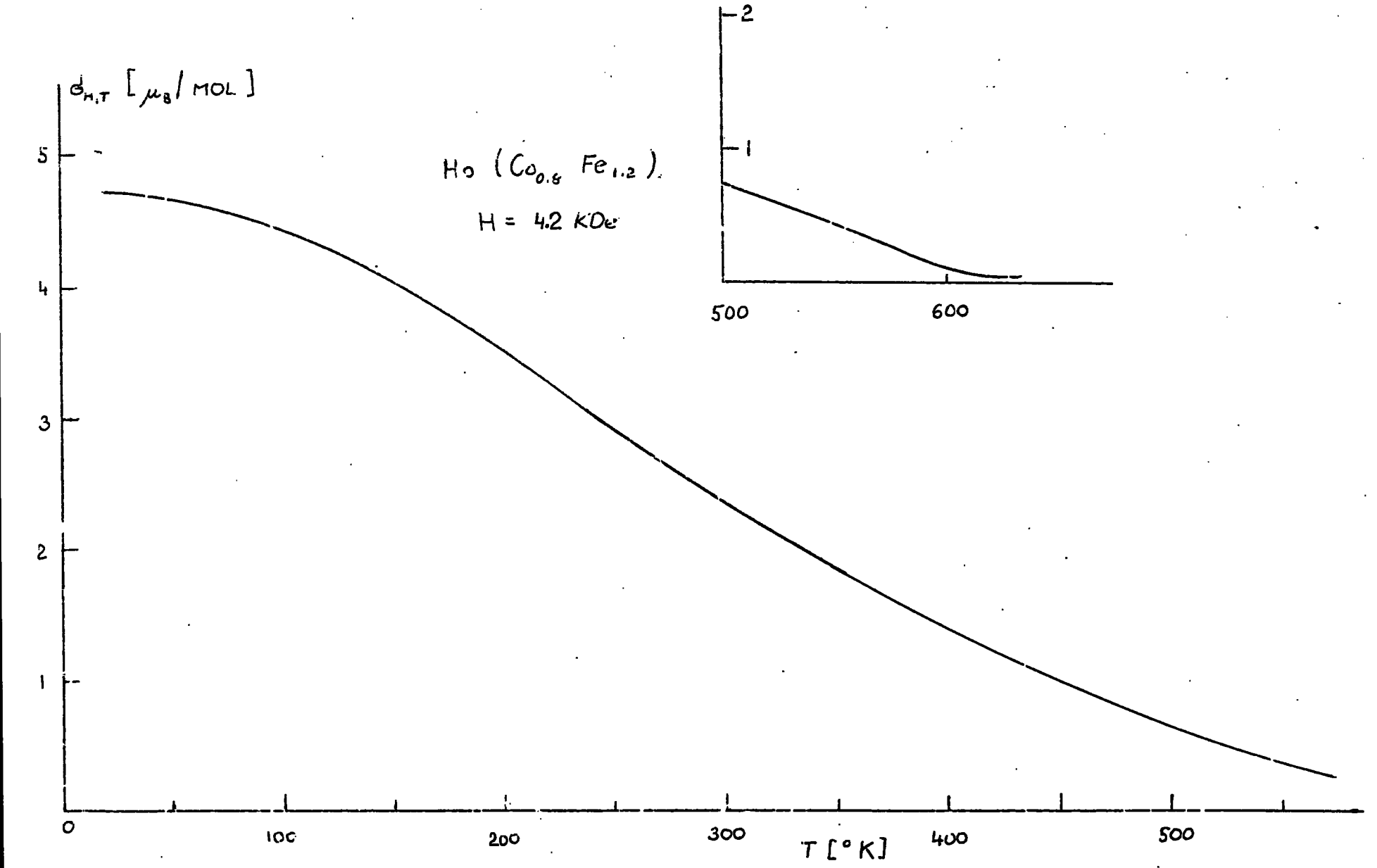

Figure 3.20 σ/T curve for Ho $(Co_{0.4}\ Fe_{1.6})$

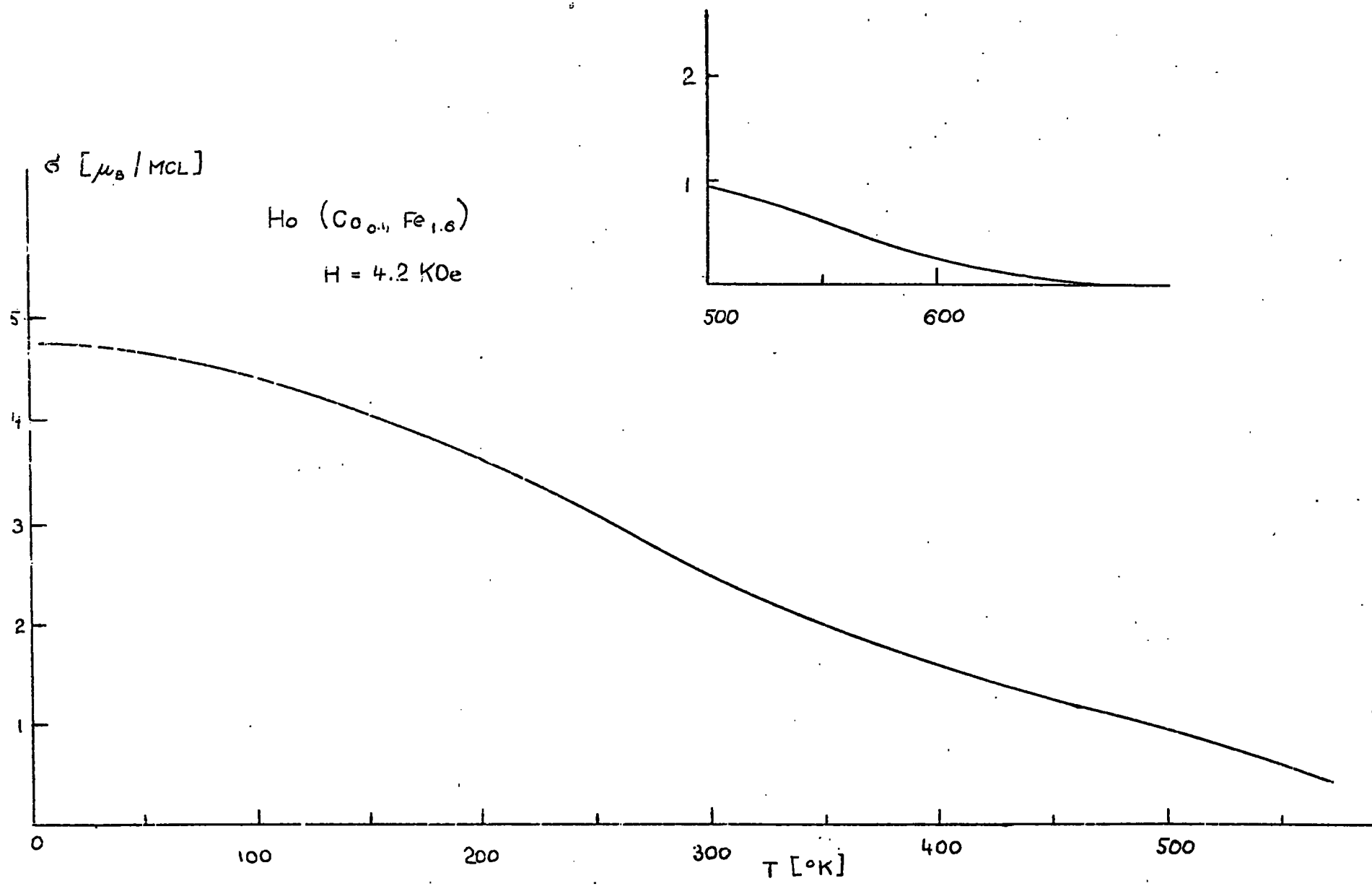

Figure 3.21 σ/T curve for Ho $(Co_{1.8}\ Ni_{0.2})$

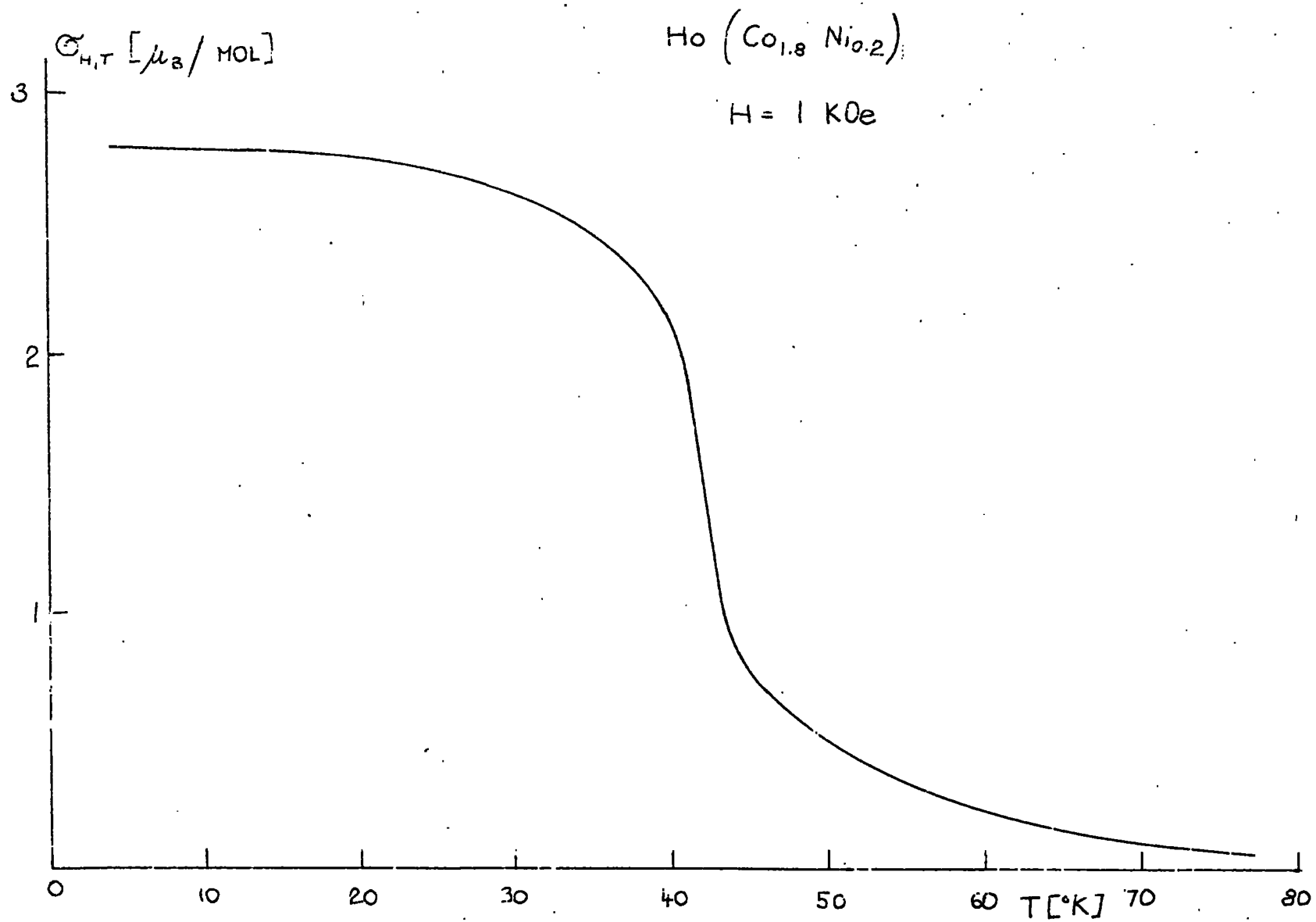

Figure 3.22 σ/T curve for Ho $(Co_{1.6}\ Ni_{0.4})$

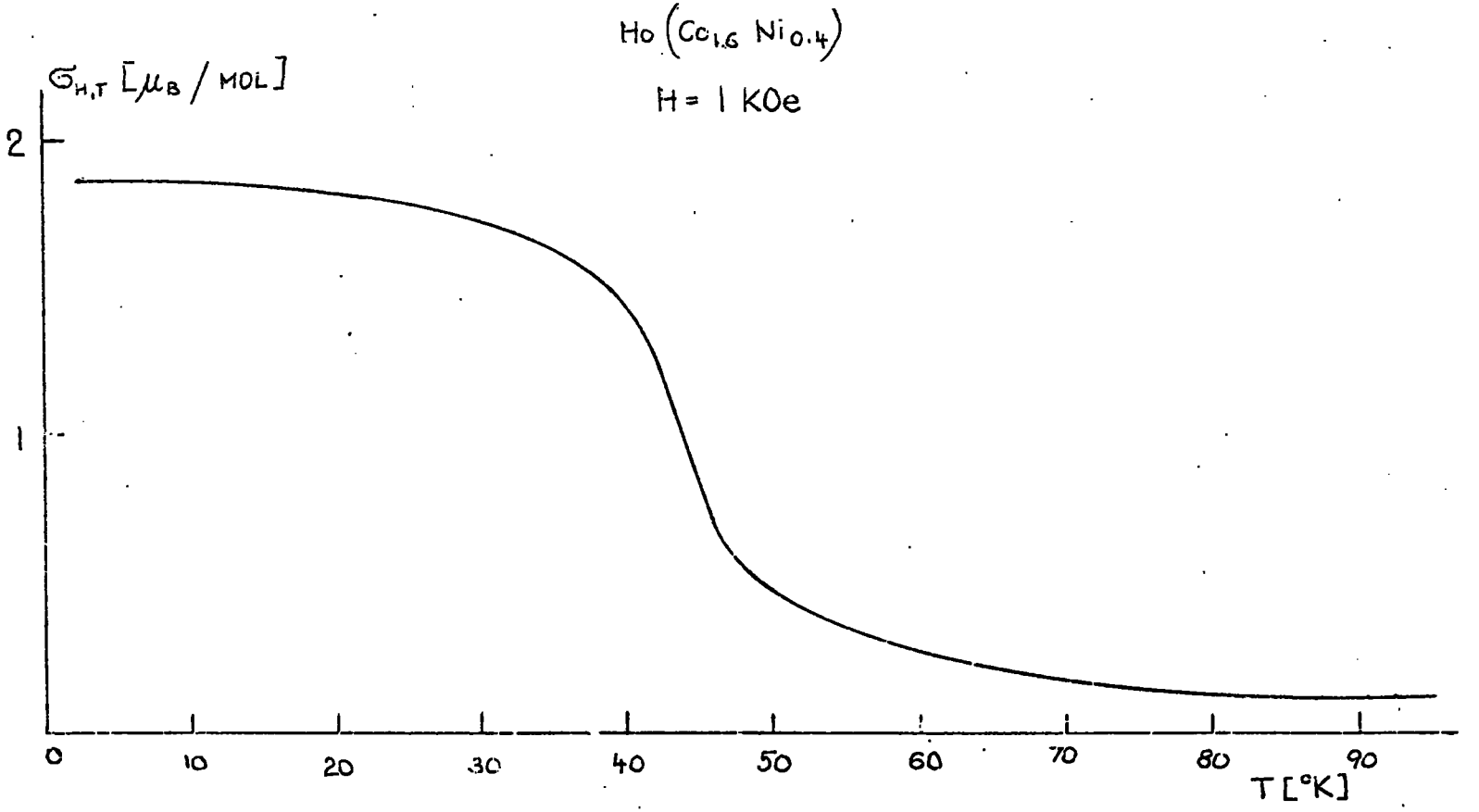

Figure 3.23 σ/T curve for Ho $(Co_{1.2}\ Ni_{0.8})$

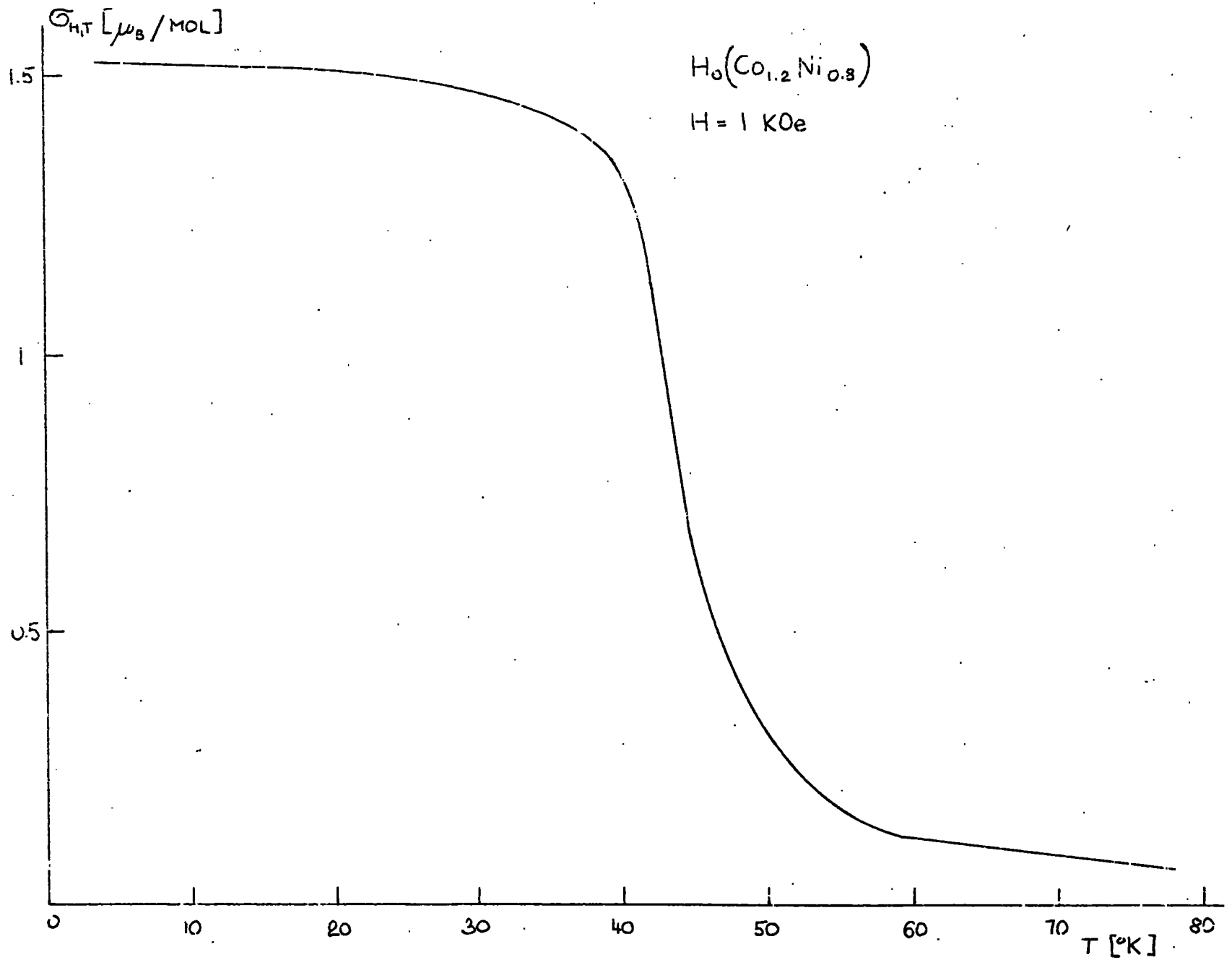

Figure 3.24 σ/T curve for Ho ($Co_{0.8}$ $Ni_{1.2}$)

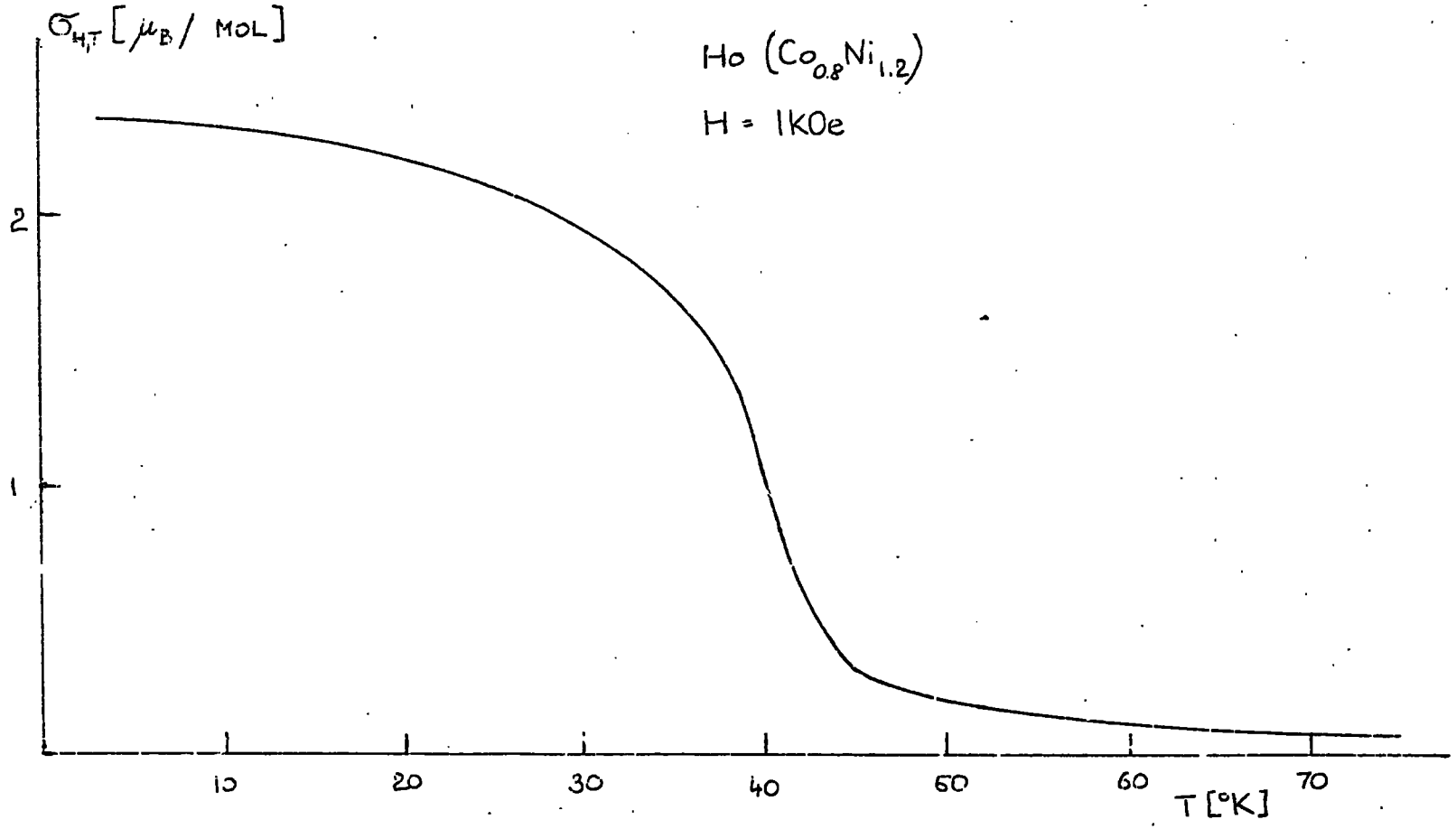

Figure 3.25 σ/T curve for Er $(Co_{1.6}\ Fe_{0.4})$

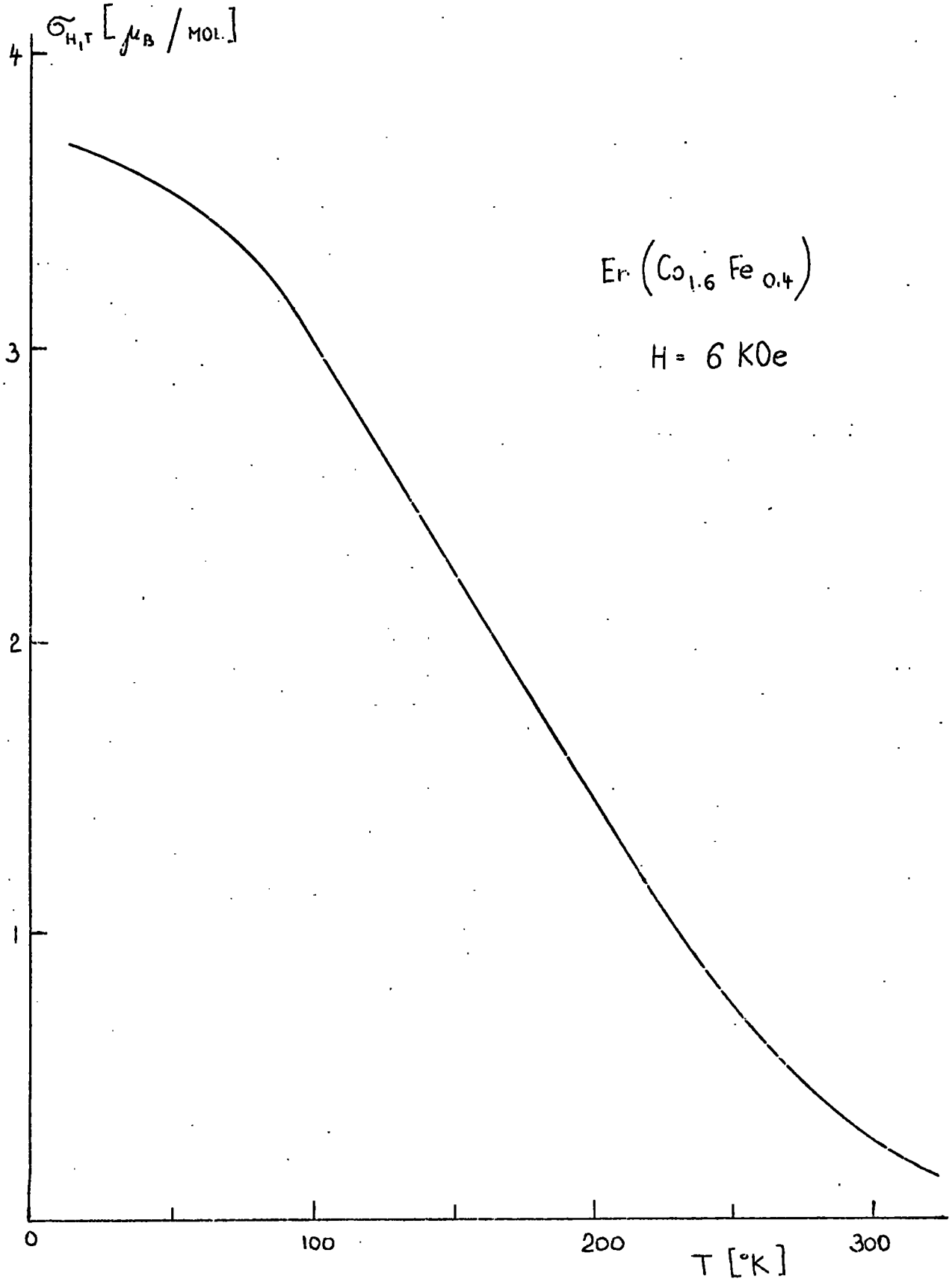

Figure 3.26 σ/T curve for Er $(Co_{1.666}\ Ni_{0.334})$

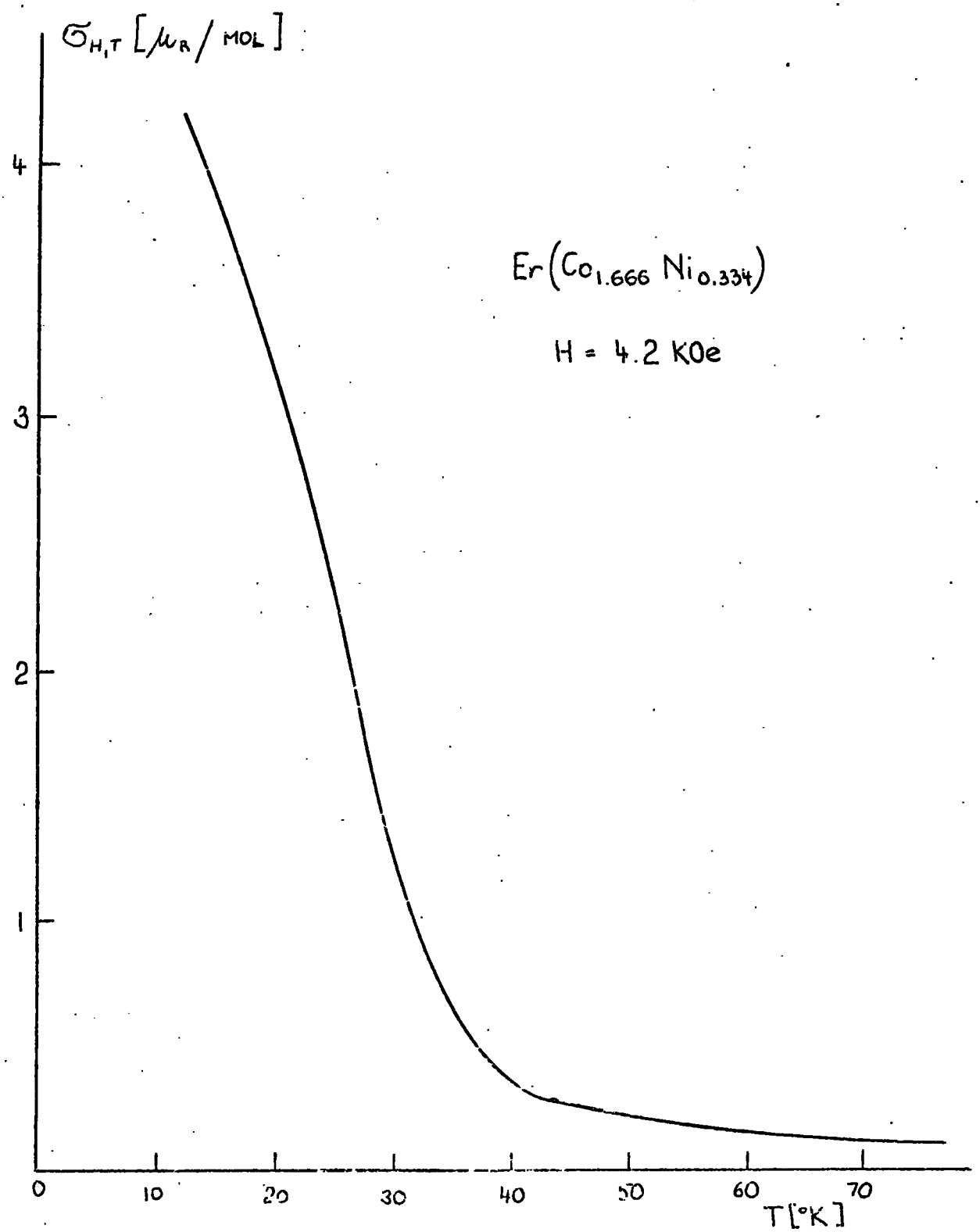

Figure 3.27 σ/T curve for Er $(Co_{1.332}\ Ni_{0.668})$

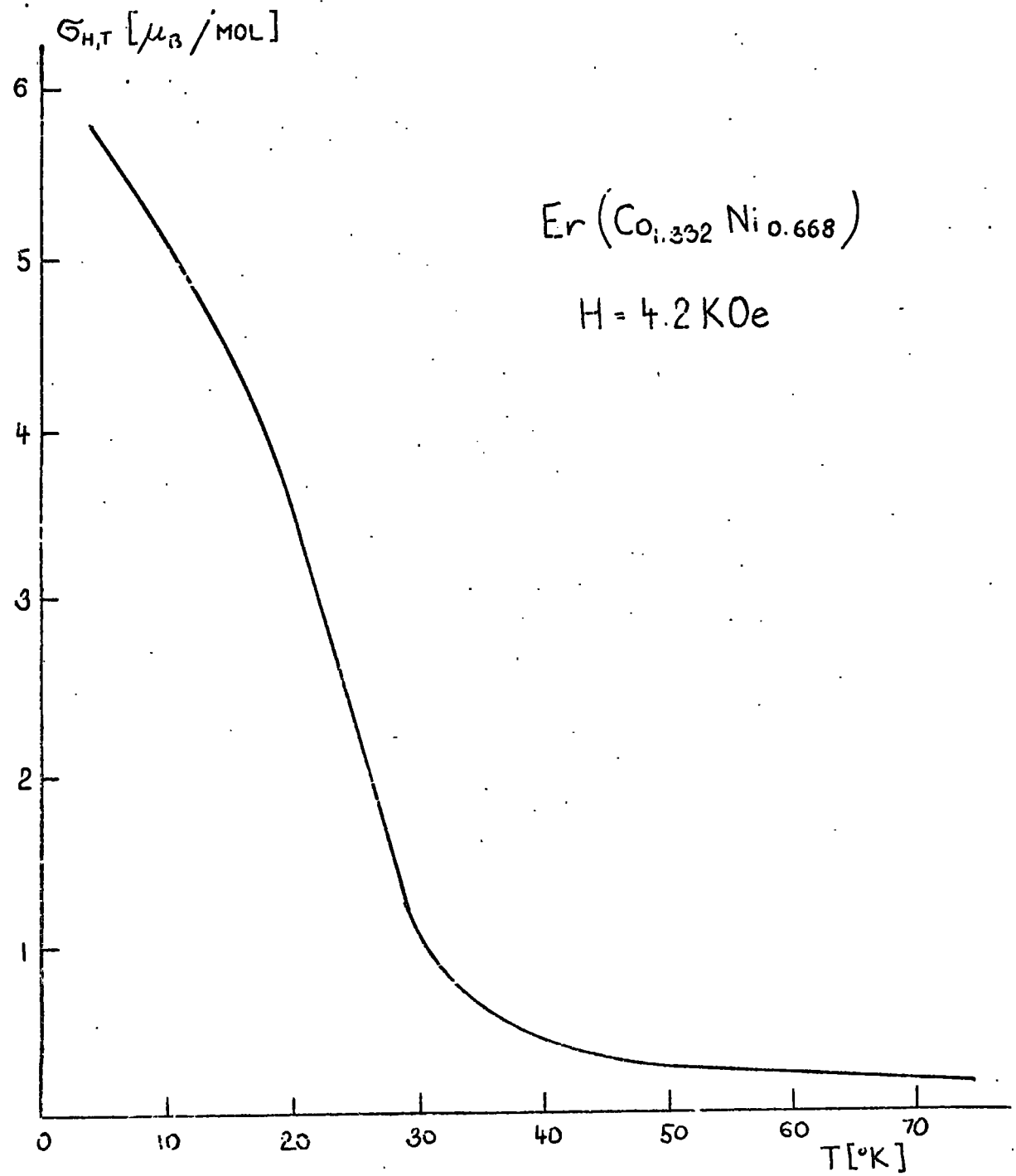

Figure 3.28 σ/T curve for Er ($Co_{1.0}$ $Ni_{1.0}$)

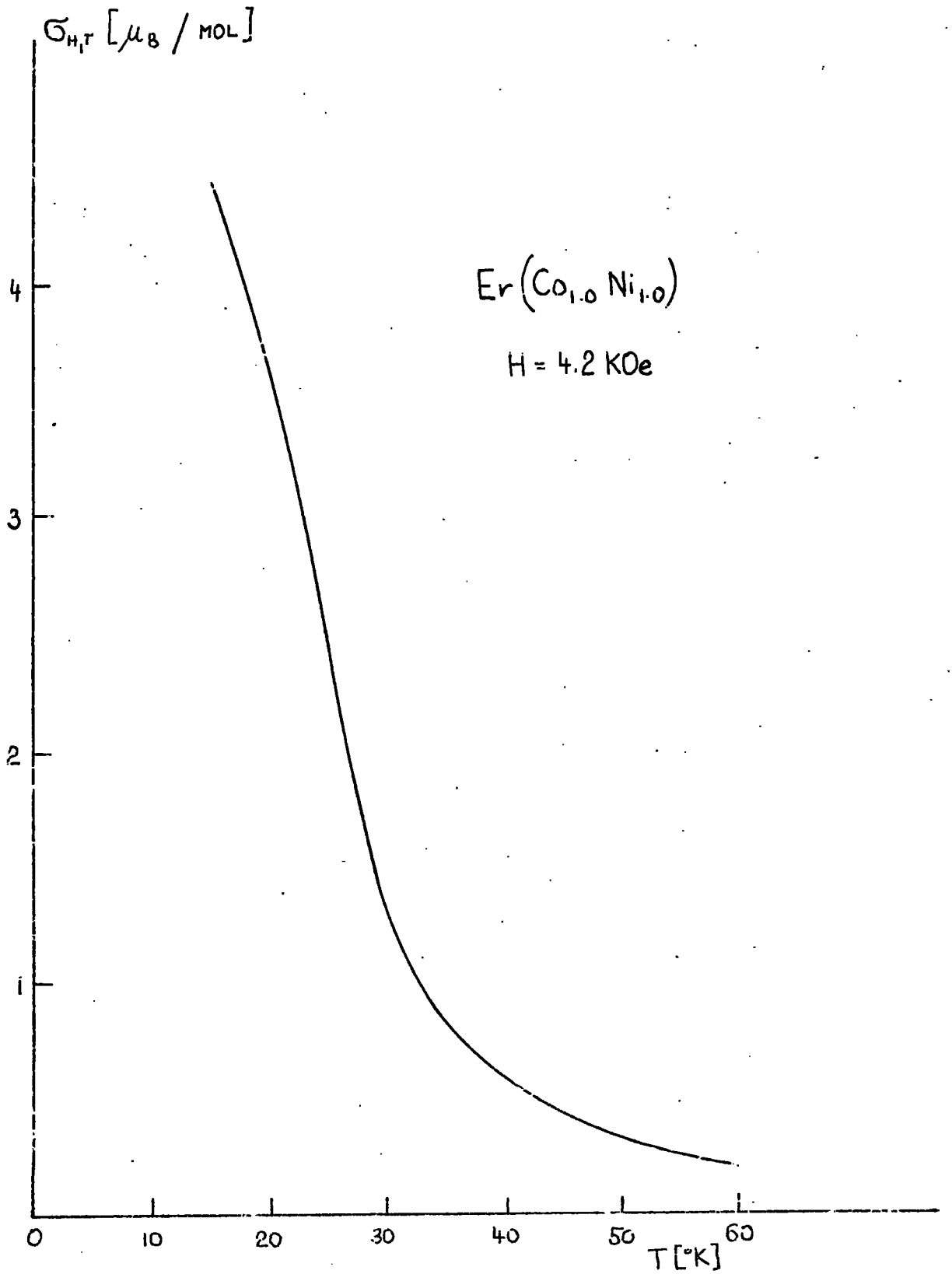

Figure 3.29 σ/T curve for Er $(Co_{0.668}\ Ni_{1.332})$

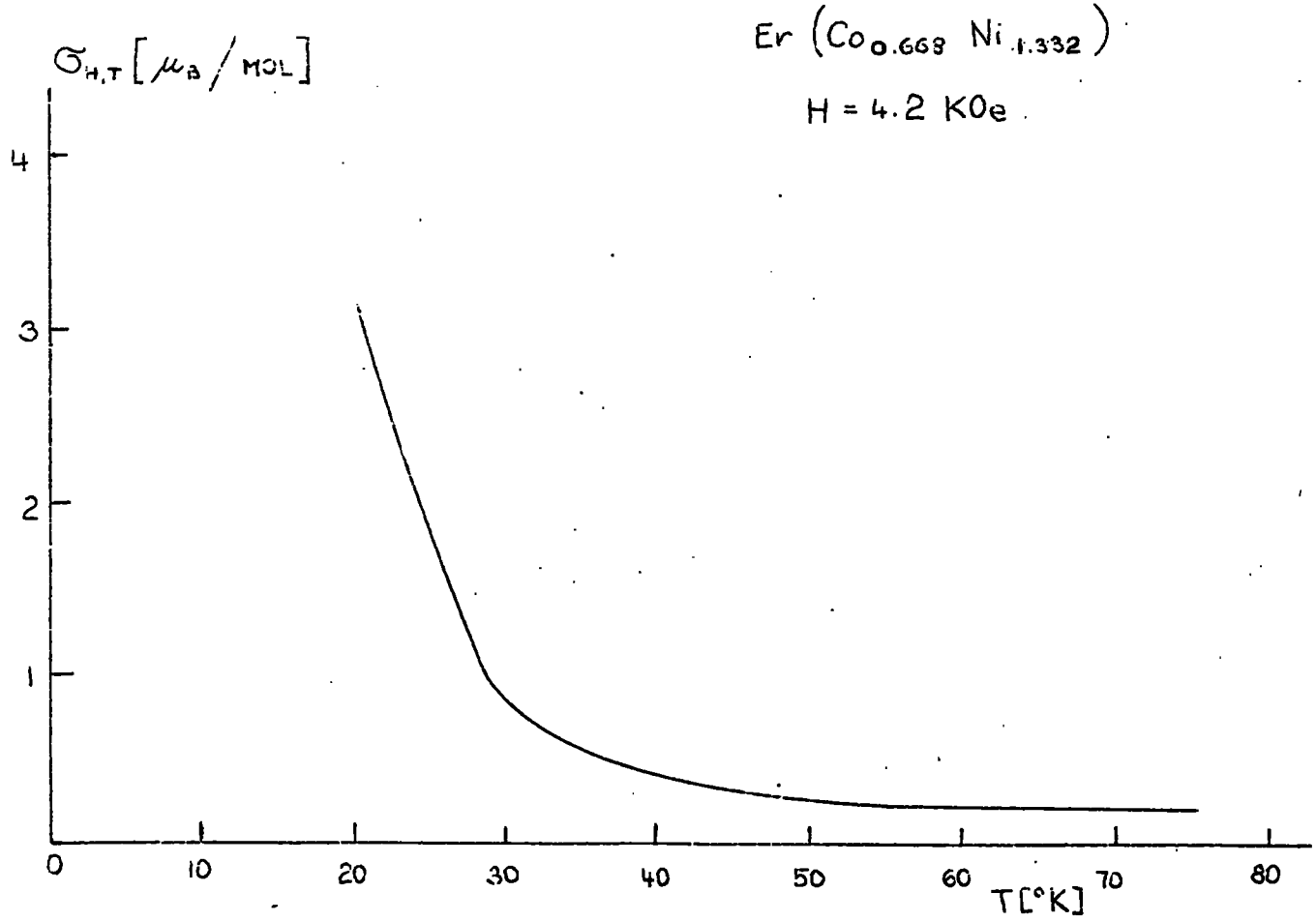

Figure 3.30 σ/T curve for Er $(Co_{0.334}\ Ni_{1.666})$

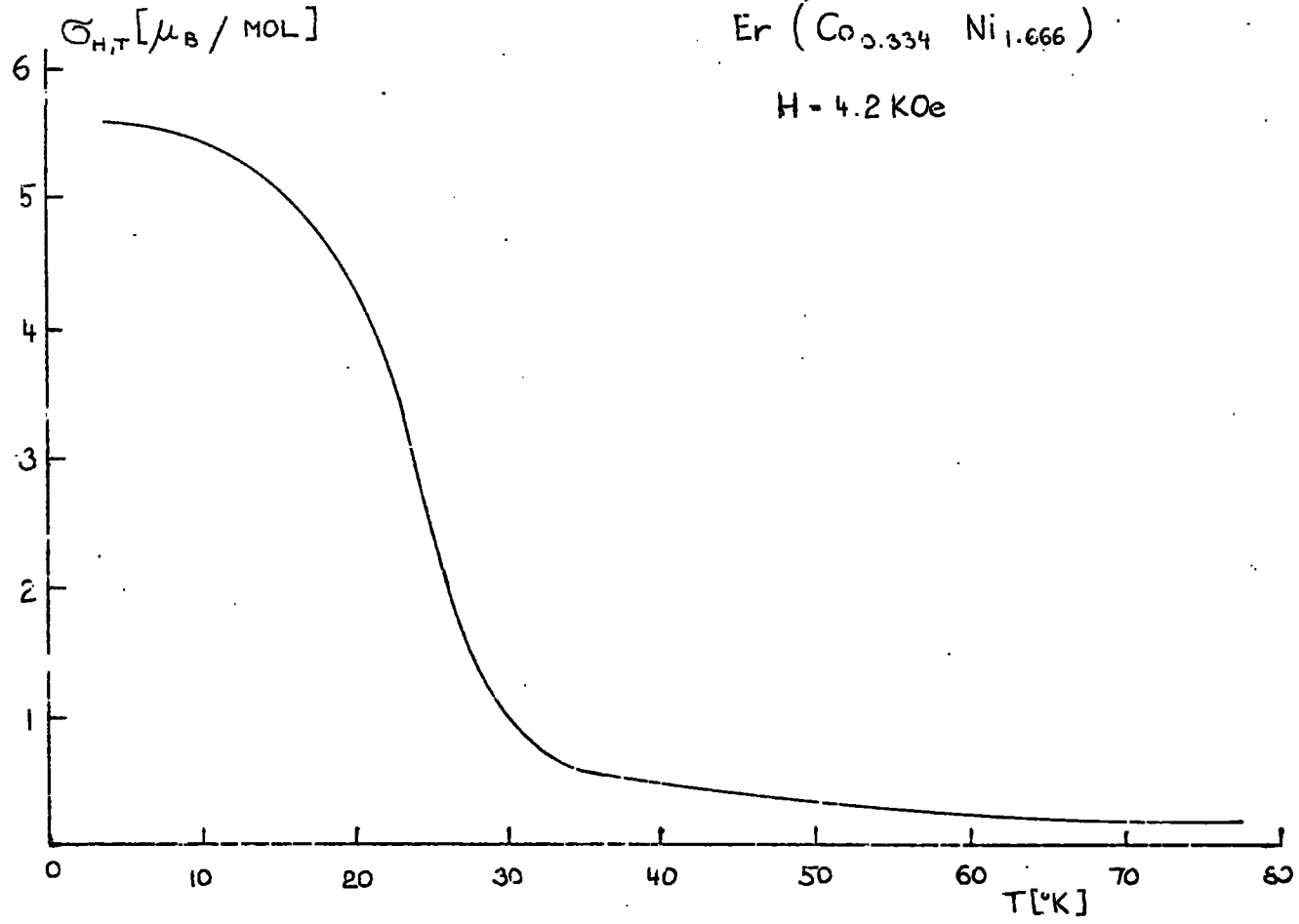

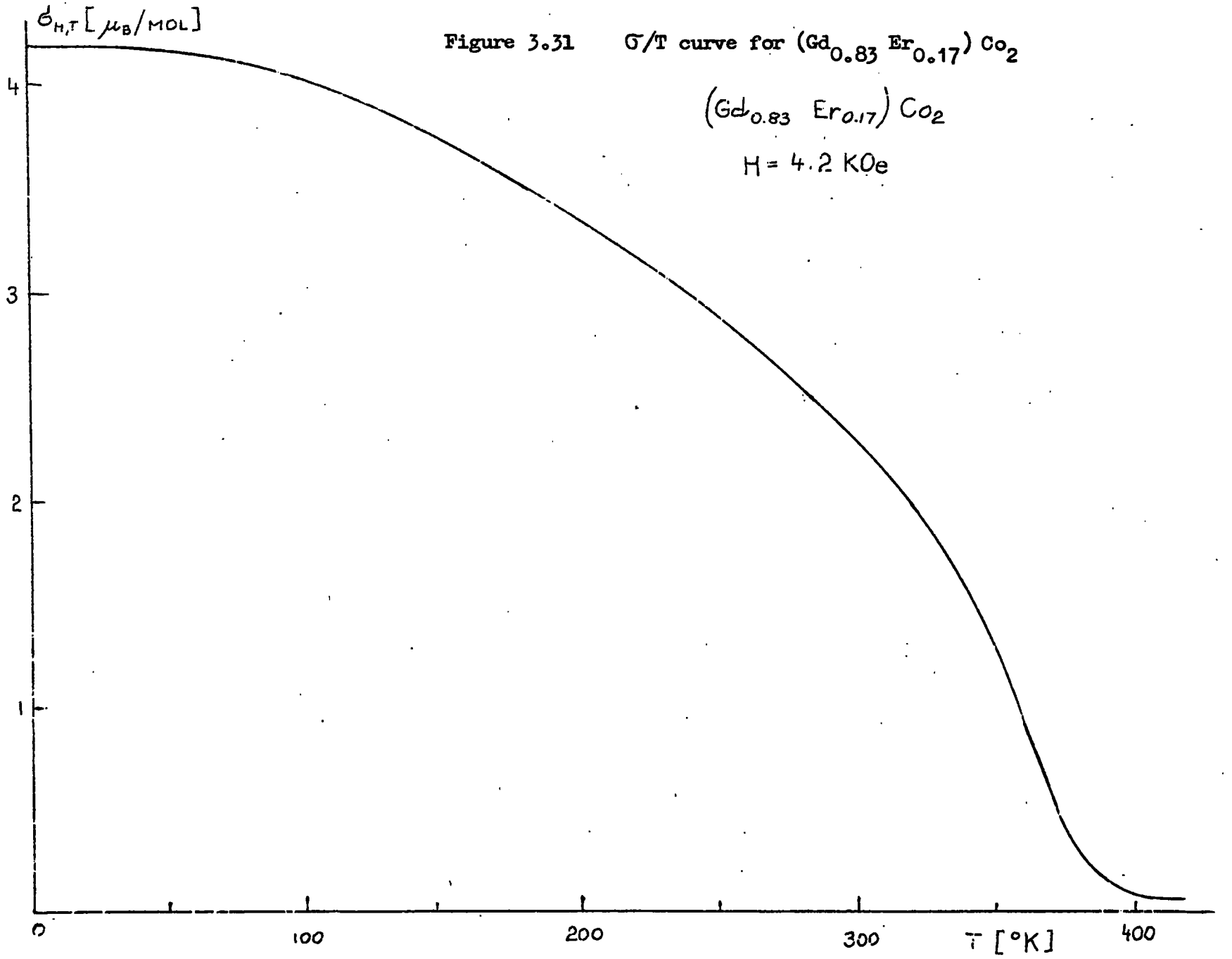

Figure 3.31 σ/T curve for $(Gd_{0.83}\ Er_{0.17})\ Co_2$

Figure 3.32 σ/T curve for $(Gd_{0.67}\ Er_{0.33})\ Co_2$

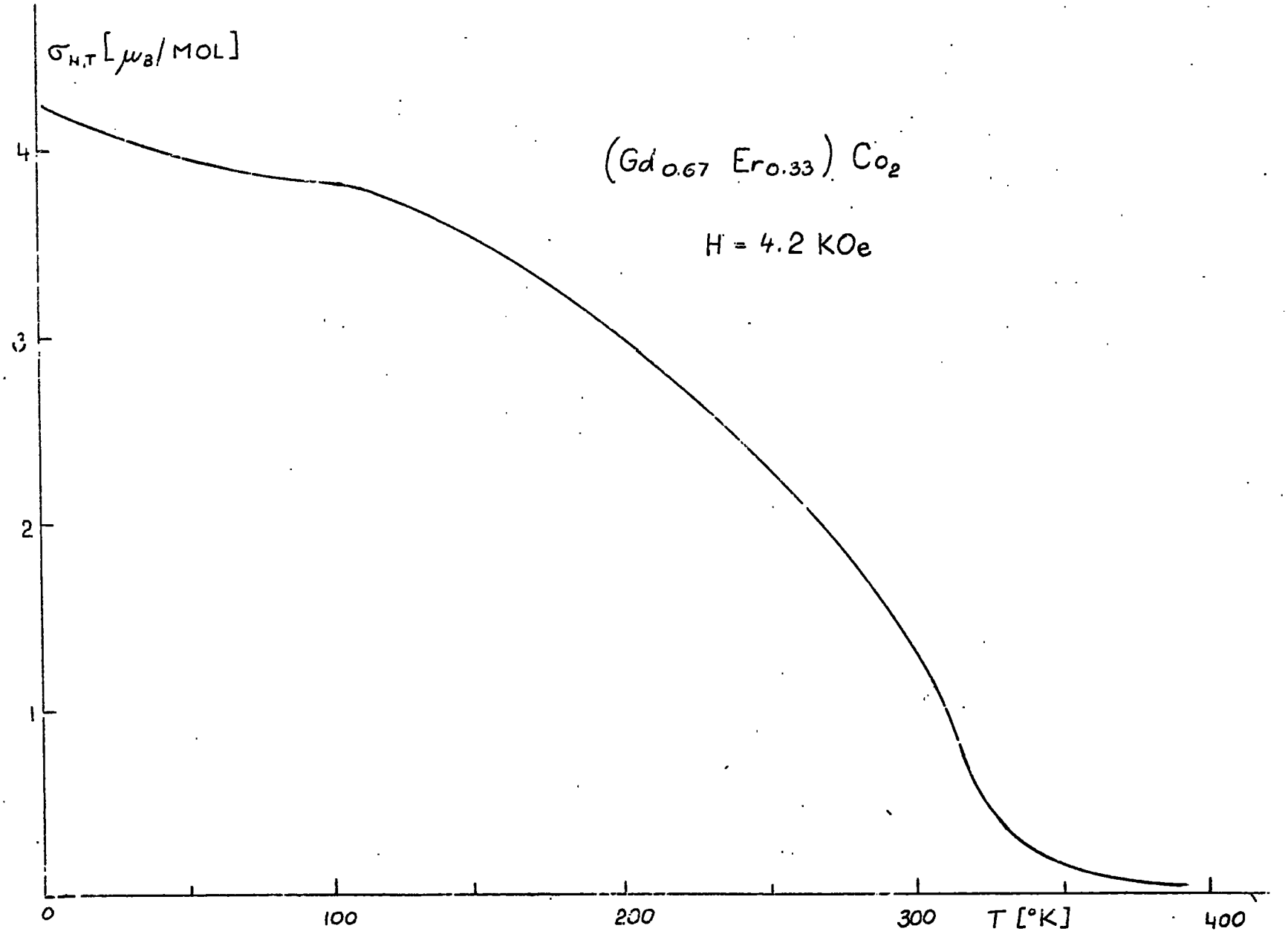

Figure 3.33 σ/T curve for $(Gd_{0.5}\ Er_{0.5})\ Co_2$

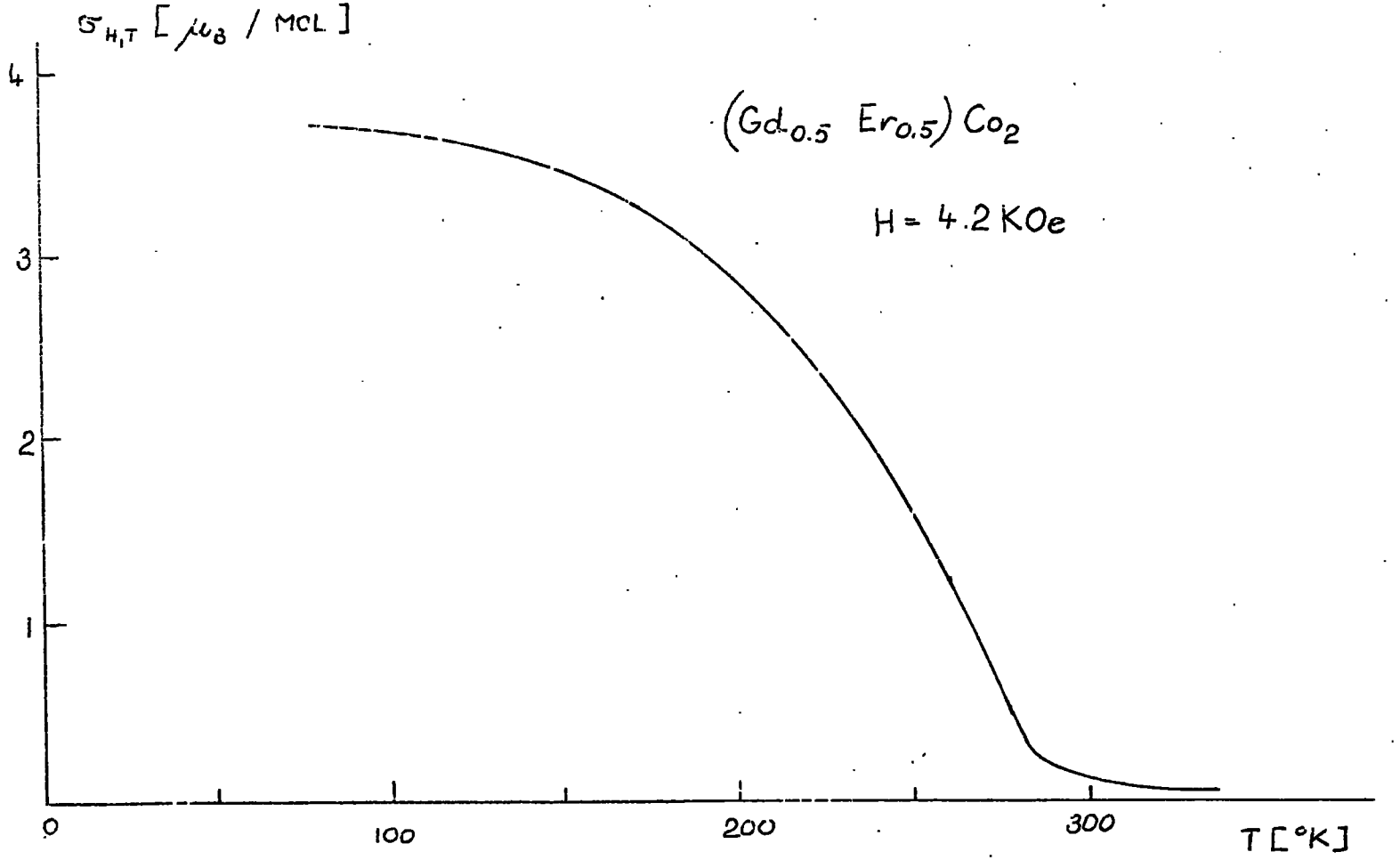

Figure 3.34 σ/T curve for $(Gd_{0.33}\ Er_{0.67})\ Co_2$

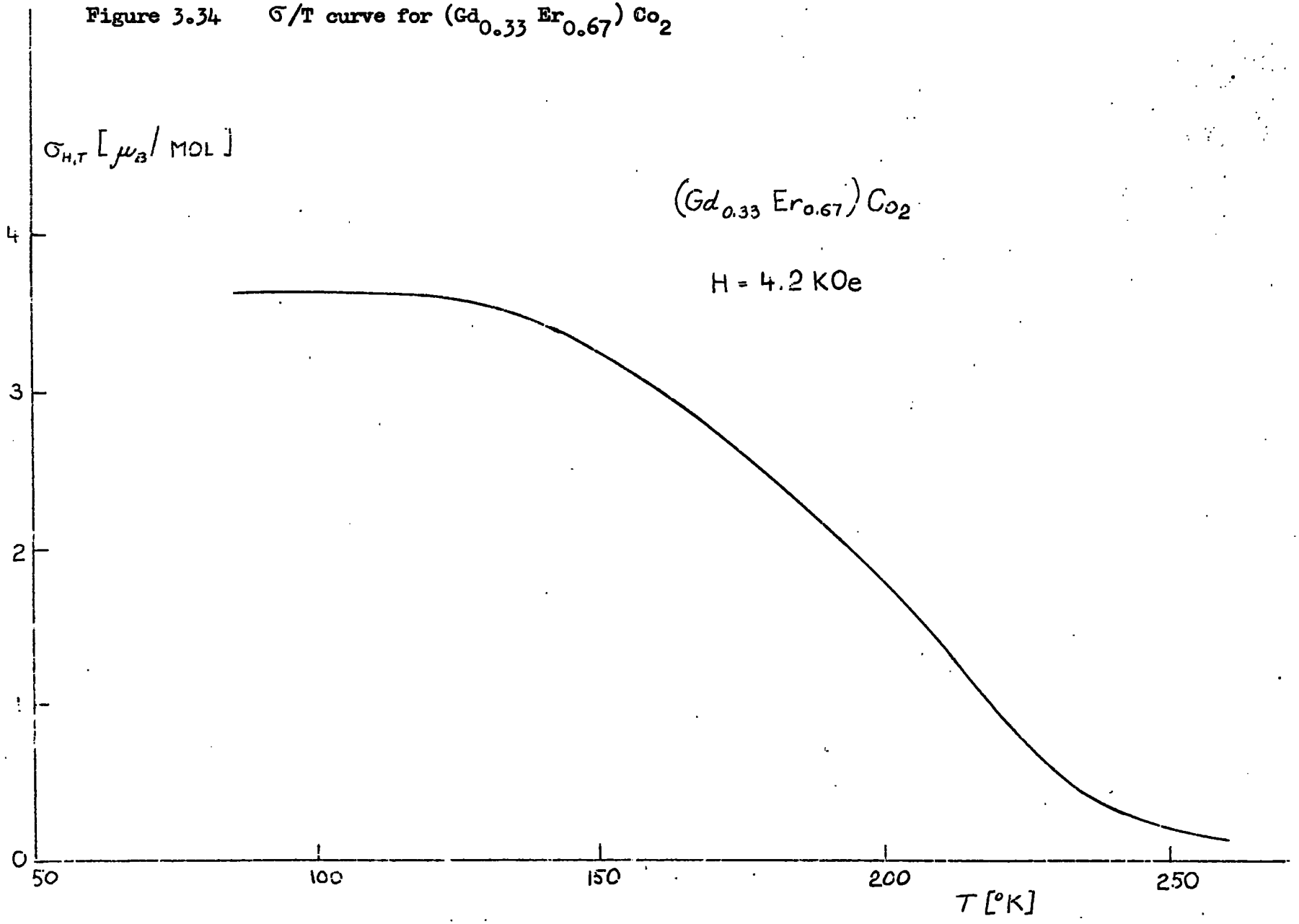

Figure 3.35 σ/T curve for $(Gd_{0.17}\ Er_{0.83})\ Co_2$

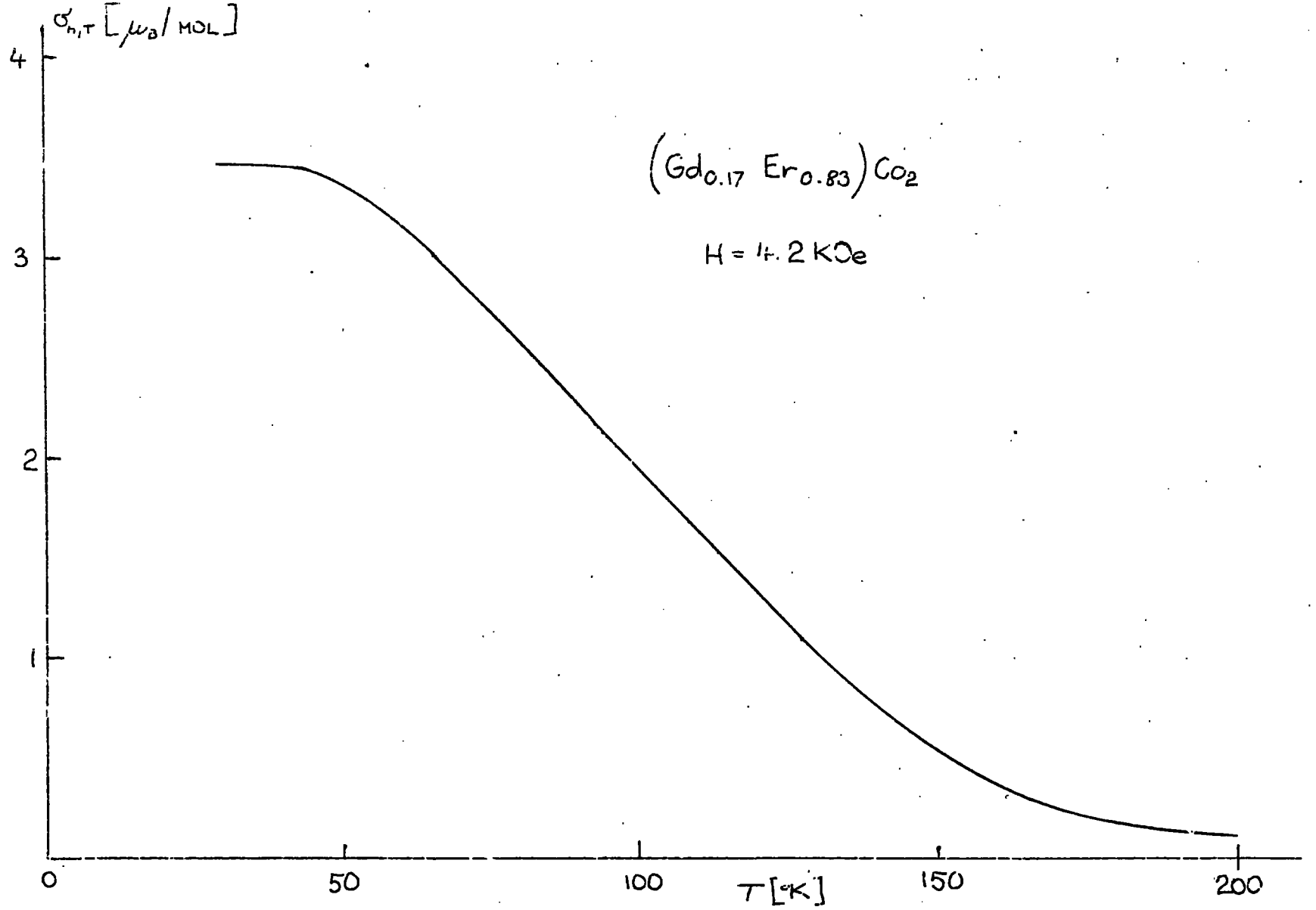

CHAPTER IV

Discussion

4.1 Structures and Lattice Parameters.

All the compounds examined in this work were found to be crystallized in the C15 phase. No other phase has been identified, although the X-Ray pattern contained a few other lines which could not be indexed. This is in agreement with measurements on other series (Ref. 1.45) of this type. The X-Ray diffraction pattern of Gd Co_2 by Harris et. al. (Ref. 3.2) exhibited strong diffraction lines in addition to these characteristic of the C15 structure and metallographic examination revealed that Gd Co_2 was in a two phase condition after homogenising for one week at 500°C. The extra diffraction lines could be indexed to a rhombohedral, $R\bar{3}m$ structure, indicating that the second phase is probably Gd Co_3 (Ref. 4.1, 2, 3).

The difficulty in obtaining a sample of Gd Co_2 in the single phase condition is consistent with this phase being formed by a peritectic type reaction. Buschow and Van der Goot (Ref. 4.1) reported that long homogenisation treatments (8 weeks at 600°C) were required to obtain Gd Co_2 as a single phase compound.

This gives us evidence that in pseudo-binary compounds in general there may exist small amounts of at least one other phase than C15, and since these will have different

magnetic properties from the host lattice some anomalies may occur in the observed magnetic behaviour.

In the series Ho $(Co, Ni)_2$ and Er $(Co, Ni)_2$ the lattice spacings plotted against composition (Fig. 3.2, 3) show only small positive deviations from Vegards Law. The valency states of the rare earth metals, and the interactions between them and cobalt and nickel are therefore similar.

For the Gd $(Fe, Co)_2$, Ho $(Fe, Co)_2$ and Er $(Fe, Co)_2$ (Ref. 1.42) systems, however, large positive deviations are shown. This behaviour suggests a difference between the interactions of rare earth metals with cobalt and nickel on the one hand and with iron on the other.

Mansey et. al. (Ref. 1.42) assumed that if there is a linear variation of the Curie temperature (T_c) for Er $(Fe, Co)_2$ with concentration then the alloys up to 50 mol% Er Co_2 will have Curie temperatures above room temperature, and this will contribute to the large positive deviations of the lattice spacings from ideality to an expansion of the lattice on ordering.

Our results (Fig. 3.9) showed that alloys of up to nearly 80 mol% Er Co_2 have Curie temperature above room temperature and similarly for Ho $(Fe, Co)_2$ (Fig. 3.7) where the Curie point becomes equal to 300°K at 85 mol%.

The explanation above does not, however, account

for the maximum in the lattice spacing - composition curve observed at about 8 mol% Er Co_2, 10 mol% Ho Co_2 and 15 mol% Gd Co_2.

However, it could be related to the variation of T_c, since in the series Gd $(Fe, Co)_2$ a maximum occurs at about 20 mol% Gd Co_2.

The system (Gd, Er) Co_2 has been examined in order to determine whether the proposal that the room temperature lattice spacings of Gd Co_2 and related compounds are affected by their magnetic state at this temperature (Ref. 3.1, 1.26) is correct and whether the deviations from Vegard's Law arise at least partly from a zero field magnetostriction for those specimens whose Curie point is above room temperature.

The room temperature (23°C) lattice spacings of some $(Gd_{1-x}\ Er_x)\ Co_2$ alloys are plotted against x in Fig. 4.1a together with the lattice spacings of some $(Gd_{1-y}\ Y_y)\ Co_2$ alloys obtained by Christopher et. al. (Ref. 1.45).

The variation of the Curie temperature across the series is shown in Fig. 4.1b and given in detail in Table 3.10, and it is apparent that samples for which $0 < x < 0.45$ are magnetically ordered at the temperature of lattice spacing measurement.

The Curie temperatures of the $Gd_{1-y}\ Y_y\ Co_2$ alloy series investigated by Taylor et. al. (Ref. 1.38) are also given on this figure and again the ordering temperatures pass

Figure 4.1. Lattice spacings and variation of the Curie temperature of $Gd_{1-y}\ Y_y\ Co_2$ (O) and $Gd_{1-x}\ Er_x\ Co_2$ (Δ) alloys.

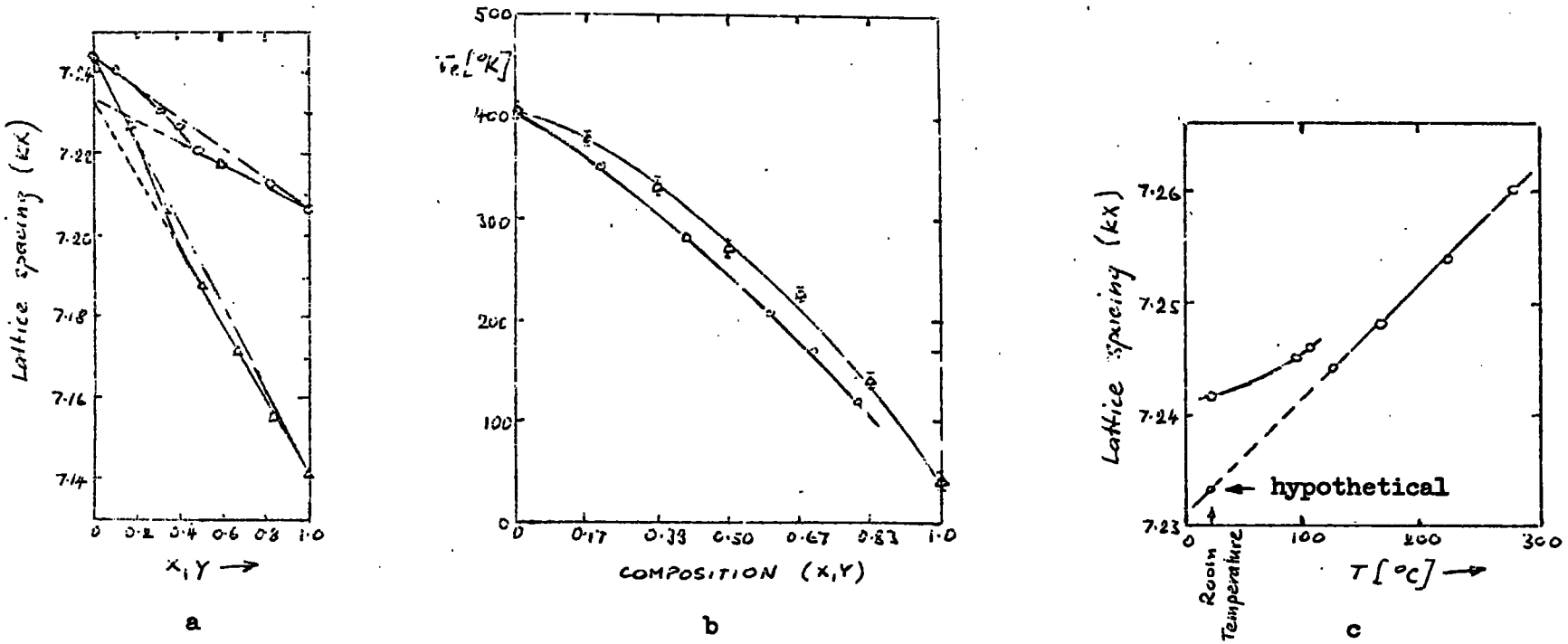

through room temperature at about the middle of the concentration range ($y \sim 0.4$). It is evident from Figure 4.1a that there is a pronounced change in slope of the lattice spacings of both alloy systems with decreasing $Gd\,Co_2$ concentration. This occurs at about $x = 0.45$ and $y = 0.45$, i.e. close to where the Curie temperature becomes equal to the temperature of the X-Ray measurements (i.e. room temperature).

Thus at the low $Gd\,Co_2$ concentration side of these critical concentrations the lattice spacings of both series of alloys correspond to the non-ferromagnetic state, and extrapolation of the linear variation of the lattice parameter with concentration in the range to the pure $Gd\,Co_2$ gives a value of 7.234 ± 0.001 kX in each case, for the lattice spacing of a hypothetical, non-ferromagnetic form of this terminal compound.

The high-temperature lattice spacings of $Gd\,Co_2$ have been determined by Mansey (Ref. 3.1), and if the variation of the lattice spacings with temperature above the Curie point is extrapolated to room temperature then a lattice spacing of 7.2333 ± 0.0005 kX is obtained for the non-ferromagnetic form of $Gd\,Co_2$ (Fig. 4.1c). Within the experimental accuracy, this value is identical with that obtained from the lattice spacings of the two alloy series discussed above and shown in Fig. 4.1a. This can be taken as further evidence that the

lattice spacing anomalies observed in these systems are due to a transition from the ferromagnetic to the non-ferromagnetic state with decreasing $Gd\ Co_2$ concentration at room temperature.

4.2 Magnetic Properties

4.2.1 $Gd\ (Fe, Co)_2$ series.

The data for the intermediate compositions show a continuous change in going from $Gd\ Fe_2$ to $Gd\ Co_2$. The observed variation of Curie temperature with composition (Fig. 3.5) is somewhat surprising, having a maximum value of T_c at about 20 mol% $Gd\ Co_2$. This effect must arise from the details of the coupling mechanism in these compounds and may be related to the changes in lattice parameter (Fig. 3.1).

The peak observed in the magnetization of $Gd\ (Co_{0.8}\ Fe_{1.2})$ at about 135°K (Fig. 3.14) and at about 130°K in $Gd\ (Co_{1.2}\ Fe_{0.8})$ (Fig. 3.13) may be due to a large decrease in the magneto-crystalline anisotropy. The measurements at higher fields would provide useful information about this behaviour. The decrease in magnetization which appeared in all intermediate compositions for which a magnetization maxima was observed is probably also related to a variation of the magneto crystalline anisotropy energy with temperature.

If we compare the variation of Curie temperature with composition in going from Fe→Co→Ni compounds with the curve showing the magnetization - composition behaviour, there is no

obvious relationship between the composition dependence of these two parameters. The Curie temperature drops close to the pure Gd Co_2 composition, but the change of magnetization in this region is very small.

A transition metal moment collapse in the Gd $(Co_{1-x}, Ni_x)_2$ series has been described by Taylor (Ref. 1.44), as mentioned earlier. On the basis of an itinerant electron model he showed that in terms of a rigid band, the moment behaviours shown for these compounds appear to imply that the Fermi level intersects both sub-bands in Gd Co_2. This is not unreasonable, as the exchange interaction strength appears to be relatively small, as indicated by the Curie temperatures. With the addition of nickel to the system one would expect that the moment would initially increase, due to the addition of electrons to the 3d - band, until the band is full. The Curie temperatures indicate a decrease in the spin up - spin down sub-band separation with increasing nickel content, and this will oppose the moment change due to the earlier process.

Once the spin-up sub-band is full, of course, both processes will contribute to a decrease in the observed transition metal moment. The nature of this decrease will then depend critically on the density of states curve in the vicinity of the Fermi level. Since this Fermi level must be close to the top of the band for these compositions, this can readily result in

a moment collapse of the type observed.

Taylor also compared this behaviour with the Y $(Fe, Co)_2$ observations, where the collapse was observed at much lower additional electron concentration (Fig. 4.2).

He suggested that if we assume that the spin-up - spin down sub-band separation arises both from the rare-earth-transition metal interaction (taken to be the predominant mechanism) and from the transition metal - transition metal interaction, then for a given band shape the magnitude of the observed transition metal moment in any system will depend on the rare-earth partner. Further, the detailed form of the variation of this moment with addition of electrons into the 3d band will also depend on the rare-earth atom involved.

Since the lanthanide contribution to the splitting can be expected to vary as the sublattice spin one might expect that in going from yttrium to gadolinium compounds the added electrons per atom value at which the moment falls to zero will increase.

4.2.2 Ho $(Fe, Co)_2$ and Ho $(Co, Ni)_2$ series.

In previous series the derivation of the transition metal moments was not difficult since gadolinium is essentially free from crystal field effects and consequently its moment can be taken as being constant and known, over the whole series.

In this series the moment of Ho Ni_2 ($8.4 \mu_B$ /molecule)

can be taken as due only to the holmium ions, since the nickel ions are known to carry zero moment (Ref. 1.25). Neutron diffraction studies of Ho Co_2 (Ref. 1.33), however, suggest a value for $\mu_{Ho} = 9.5\mu_B$. The results in the Ho (Co, Ni) region of Figure 3.6 however suggest that a transition metal contribution to the total moment only appears at about 10% nickel, and extrapolation of the results obtained for > 10% nickel, to pure Ho Co_2 would lead to a holmium moment of $9.2\mu_B$. This is in reasonable agreement with the neutron observations and will be taken as the holmium moment in what follows. Extrapolation then leads to $\mu_{Ho} = 10.0\mu_B$. The holmium moment in Ho Fe_2, is assumed to be $10.0\mu_B$ in agreement with the free ion value.

Subtraction of the observed molecular moments from the μ_{Ho} variation across the series then leaves the contribution from the transition metal ions. These are shown in Fig. 3.6, and as may be seen again show a sudden decrease with an increase in the number of added 3d - electrons. It is interesting that at the Ho Co_2 composition the cobalt moment is appreciably less than $1\mu_B$. The Curie temperatures also decrease rapidly in the vicinity of the moment collapse.

These results indicate that the considerations about the gadolinium series may also be applied to this series.

The spin-up sub-band is filled at about 60 mol%

Ho Co_2, and is followed by a decrease in the observed transition metal moment. As indicated by the variation of the Curie temperatures, there is also a decrease in the spin up - spin down sub-band separation with increasing cobalt content. The magnetization-temperature (σ/T) curves for the whole series were well behaved and showed no anomalies of the type observed in gadolinium series.

The Curie temperature results do not show a maximum of the type observed for Gd $(Fe, Co)_2$ which could be related to the maximum of the lattice parameter curve for Ho $(Fe, Co)_2$. Instead, the Curie temperature remains constant up to 20 mol% Ho Co_2.

4.2.3 Erbium compounds.

Using the method adopted in the holmium compounds, the Erbium moments in this series appear to be $9\mu_B$, $7.2\mu_B$ and $6.8\mu_B$ respectively for Er Fe_2, Er Co_2 and Er Ni_2 respectively.

This value is appreciably lower than that reported elsewhere for the cobalt compound (Ref. 1.33) and the implications of this are discussed later.

Subtraction of the observed moments again leads to the transition metal moment values shown in Figure 3.8, where the sudden increase in moment is again evident.

It appears from this that μ_{Co} in Er Co_2 is

approximately 0.1 μ_B, very severely less than that assumed previously and observed in neutron diffraction studies (Ref. 1.33). However, if the cobalt moment is to have the reported value of 1.0 μ_B in Er Co_2, the erbium moment itself must change rapidly between the cobalt and nickel compounds and little, if at all, between cobalt and iron compounds.

This is in marked contrast to the lattice parameter variation across the series and it would be difficult to reconcile the moment changes with crystal field effects. The transition metal moments derived assuming a linear erbium moment change from 6.8 to 8.9 μ_B are also shown in Figure 3.8. Under these conditions there appear to be two concentration regions for which the transition metal moment shows a rapid decrease.

The almost constant Curie temperatures in the Er $(Co, Ni)_2$ region would tend to support the earlier treatment, with the transition ions only developing a moment for $x < 0.9$ in Er $(Fe_{1-x}Co_x)_2$.

4.2.4 Dy $(Co, Ni)_2$ series.

This series has been observed to have time dependent magnetizations at 4.2°K and the evaluation of saturation magnetization values is difficult. The reasons for this are not yet understood but it is possible that it has its origin in the magnetocrystalline anisotropy. The approximate observed magnetic moments (Table 3.9) seem to have values comparable to the crystal field reduced Dy Ni_2 moment and consequently in the compositions

studied (Ref. 1.33) the transition metal is again carrying a very small moment.

The Curie temperatures (Table 3.9) are slightly above the straight line connecting Curie temperatures of Dy Co_2 and Dy Ni_2. Further measurements are necessary before any explanation of these measurements is possible.

From these series we can not determine unambiguously the magnetic moment of the individual transition metals. However, we can investigate transition metal moments as a whole and compare their variation in series using various rare earth partners. The results of the previous sections show that if we plot the variation of the transition metal ionic moment as a function of the number of electrons added to the 3d - band (Fig. 4.2, 3), the value at which the moment falls to zero is different for different rare earths.

Actually the value at which the moment collapses, increases in going from yttrium to gadolinium compounds. The collapse may not be complete in the erbium series and a residual moment may remain after the initial collapse.

Figure 4.2 Rare earth moment is taken as linear variation of rare earth from AFe_2 to ANi_2.

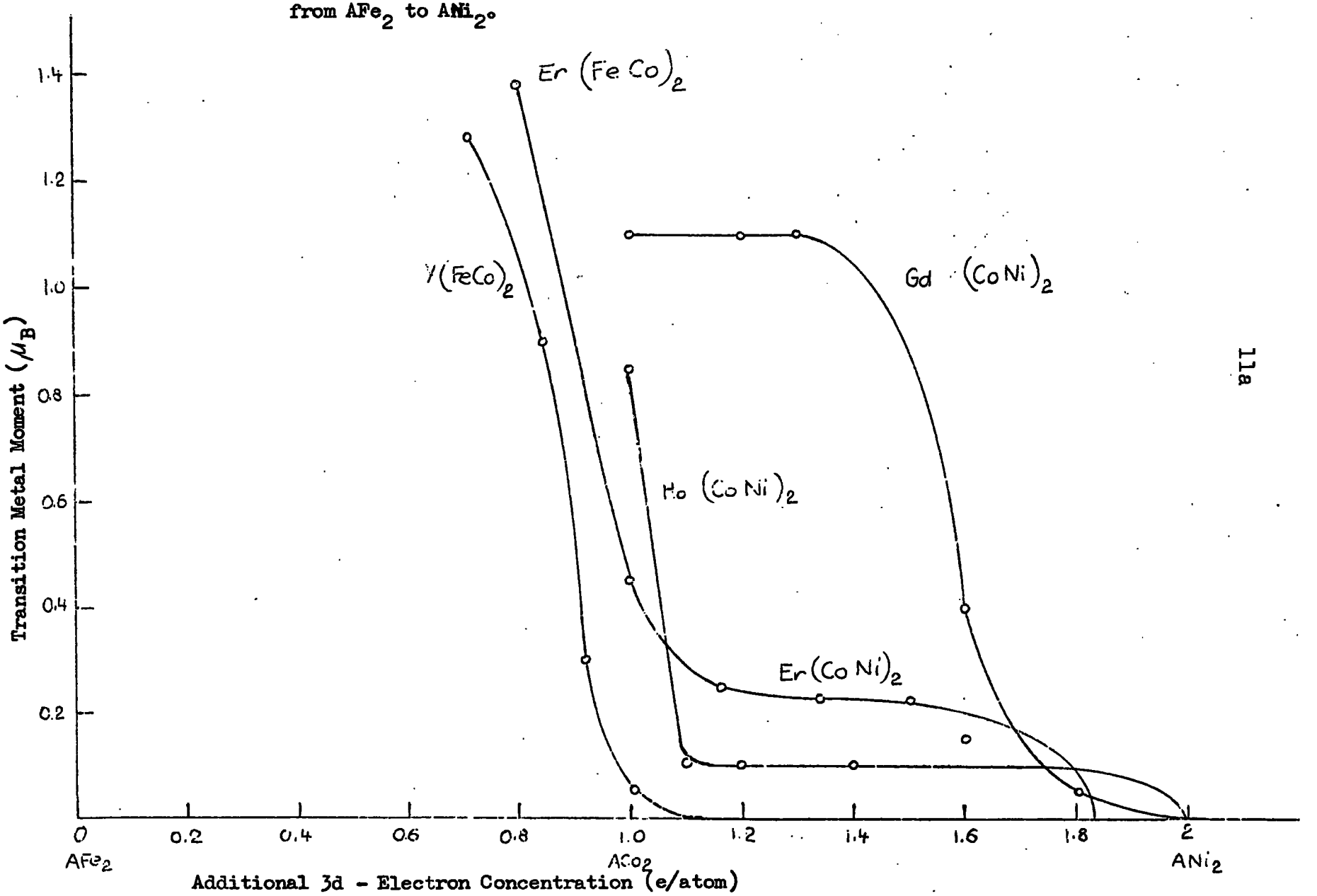

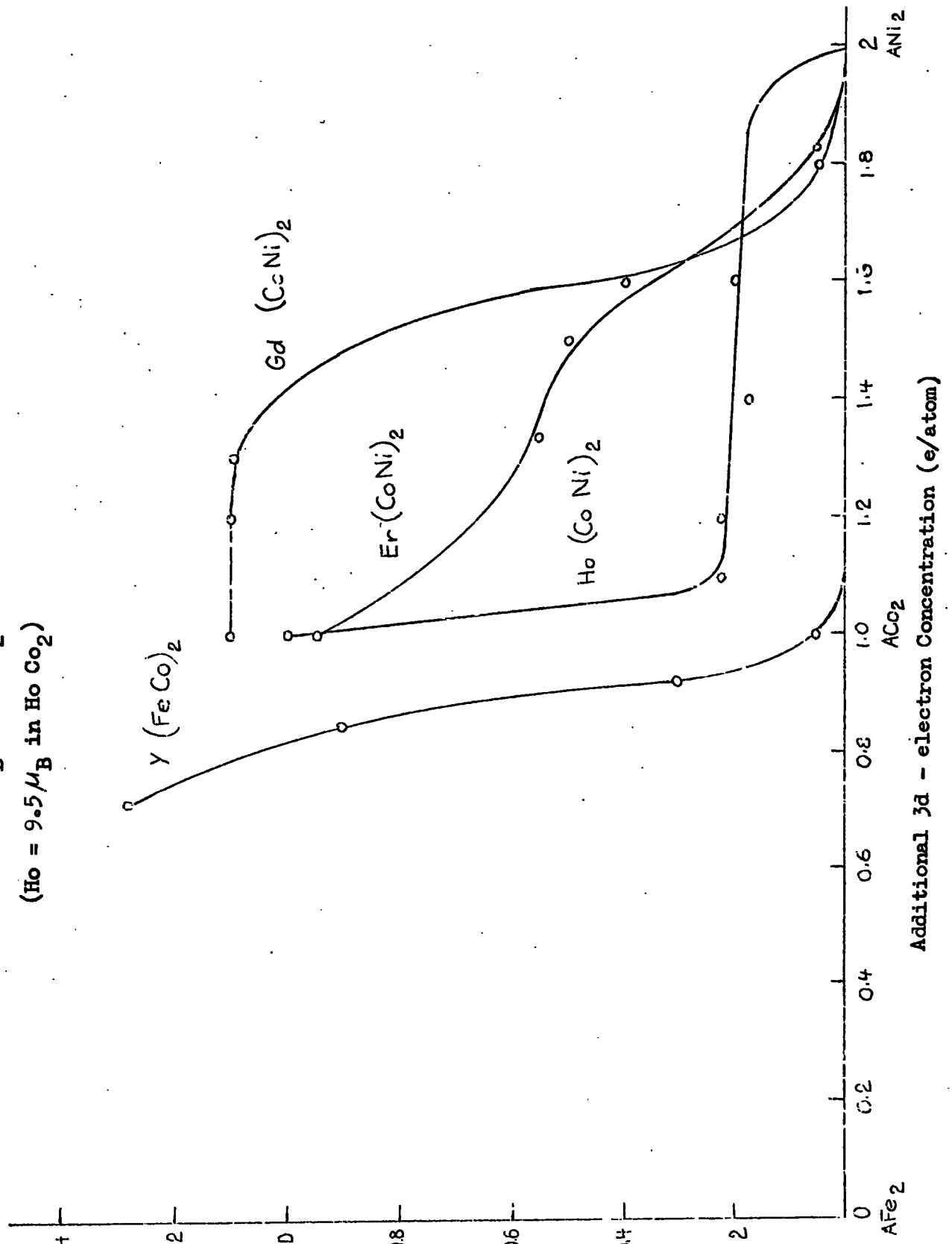

Figure 4.3 Rare earth moment is taken from neutron diffraction results (Er = 8.9 μ_B in Er Co_2)
(Ho = 9.5 μ_B in Ho Co_2)

CHAPTER V

Summary

The pseudo-binary series of the intermetallic compounds AB_2 presented in this work almost complete the investigation of some properties of this type of compound. ('A' represent only heavy rare earth metals). The transition metal moment collapse has been confirmed, and has an obvious relation to the Curie temperature variation and hence to the exchange interaction, although it seems likely that the latter will depend on the moment values themselves.

As has been stated in the previous section there is a relation between the value at which the moment collapse occurs and rare earth element involved. The exact form of this relation has not yet been found, but it is evident that the value of additional 3d - electrons at which the moment is almost zero increases going from yttrium to gadolinium compounds.

An estimate of the values of the magnetic moments of holmium and erbium in Ho Co_2 and Er Co_2 compounds are smaller than the previously reported results which were obtained from neutron deffraction measurements. The anomalous temperature - magnetization behaviour of some compounds was related to a variation of the magnetocrystalline anisotropy energy with temperature.

The room temperature lattice spacing anomaly observed

in (Gd, Er) Co_2 series is due to a transition from the ferromagnetic to the non-ferromagnetic state with decreasing Gd concentration.

ACKNOWLEDGEMENTS

I would like to tender my sincere thanks to my supervisor, Dr. K.N.R. Taylor, for his willingness always to help, and to give advice and encouragement.

I am greatly indebted to Professor G.D.Rochester, the Head of the Physics Department, to Dr. K.N.R.Taylor and to Dr. A.J.Banister, who made it possible for me to come to Durham and carry out this work.

My thanks are due also to my fellow research students and to the laboratory technicians for their willing help.

REFERENCES

1.1 Weis, P., Radium 4, 661, (1907)

1.2 Herring, C., in "Magnetism", Vol. IV (1966)

1.3 Argyres, P., and Kittel, C., Acta Met. 1, 241, (1953)

1.4 Mott, N.F., and Stevens, K.W.H., Phil. Mag. 2, 1364, (1957)
Ericson, M., and Jacrot, B., Compt. Rend. 246, 1018, (1958)
J. Phys. Rad. 20, 178 (1959); Phys. Chem. Solids 13, 235, (1960)
Lowde, R.D., Proc. Roy. Soc. A235, 305, (1956)

1.5 Friedel, J., Leman, G., and Olszewski, S., J. Appl. Phys. 32, 325S, (1961)

1.6 Zener, C., Phys. Rev. 81, 440, (1951), 83, 299, (1951)

1.7 Yoshida, K., Progr. Theoret. Phys. (Kyoto) 16, 45, 58, (1956)

1.8 Anderson, P.W., Phys. Rev., 124, 41, (1961)

1.9 Liu, S.H., Phys. Rev., 163, 472, (1967)

1.10 Koehler, W.C., Kjeller Reports KR - 132, 156, (1969)

1.11 Elliott, R.J., The Phys. Rev. 124, 346, (1961)

1.12 Cooper, B.R., in Solid State Physics Vol. 21, P. 392.

1.13 Evenson, W.E., and Liu, S.H., Phys. Rev. 178, 783 (1969)

1.14 Rudermann, M.A., and Kittel, C., Phys. Rev. 96, 99, (1954)

1.15 Yoshida, K., Phys. Rev. 106, 893, (1957)

1.16 Kasuya, T., Progr. Theoret. Phys. (Kyoto) 16, 45, (1956)

1.17 de Gennes, P.G., J. Phys. Rad., 23, J10, (1962)

1.18 Kasuya, T., in Magnetism Vol. II. b. Chap. 3, (1966)

1.19 Elliot, R.J., in Magnetism Vol. II. a, Chap. 7.

1.20 Dimmock, J.O., and Freeman, A.J., Phys. Letters 13, 750, (1964)
Freeman, A.J., Dimmock, J.O., and Watson, R.E., Phys. Rev. Letters 16, 94, (1966)
Keeton, S.C., and Loucks, T.L., Phys. Rev. 168, 672, (1968)
Williams, R.W., and Mackintosh, A.R., Phys. Rev. 168, 679 (1968)
Loucks, T.L., Phys. Rev. 144, 504, (1966)

1.21 Watson, R.E., Koide, S., Peter, M., and Freeman A.J., Phys. Rev. 139(A), 167, (1965)

1.22 Anderson, P.W., and Clogston, A.M., Bull. Am. Phys. Soc., 2, 124, (1961)

1.23 Lemaire, R., Cobalt 32, 132, (1966)

1.24 Cromer, D.T., and Larson, A., Acta Cryst., 12, 855 (1959)

1.25 Felcher, G.P., Corliss, L.M., and Hastings, J.M., J.Appl. Phys. 36, 1001, (1965)

1.26 Piercy, A.R., Ph. D. Thesis, University of Durham (1968)

1.27 Laves, F., and Witte, H., Mettallur. 15, 840, (1936)

1.28 Elliot, C.P., and Rostoker, W., Trans. A.S.M., 50, 617, (1958)

1.29 Slick, et. al. J. Chem. Phys. 43, 2788, (1965) and Wallace, W.E., and Craig, R.S., in Phase Stability in Metals and Alloy P.S. Rudman (Ed.) McGraw-Hill (1967)

1.30 Skrabek and Wallace, J. Appl. Phys. 34, 1356, (1963)

1.31 Bleaney, B., Proc. Roy. Soc. A276, 28, (1963) and in "Rare Earth Research", Vol. 2, k.s. Varres, ed., Gordon and Breach (1964) P.499

1.32 Ross, J.W., Crangle, J., Phys. Rev. 133, A509 (1964)

1.33 Farrell, J., and Wallace, W.E., Inorg. Chem. 5, 105, (1966)

1.34 Crangle, J., and Ross, J.W., Proc. Intern. Conf. Magnetism, Nottingham, 240, (1964)

1.35 Moon, R.M., Koehler, W.C., and Farrell, J., J. Appl. Phys. 36, 978 (1965)

1.36 Wallace and Skrabek, "Rare Earth Research" Vol. 2, P.431, (1964)

1.37 Schweizer, J., Phys. Lettr. 24A, 739, (1967)

1.38 Taylor, Ellis and Darby, Phys. Lettr. 20, 327, (1966)

1.39 Lemaire and Schweizer, Phys. Lettr. 21, 366, (1966)

1.40 Piercy, A.R., and Taylor, K.N.R., J. Appl. Phys., 39, 1096-7, (1968)

1.41 Oesterreicher, H., and Wallace, W.E., J. Less-Common Metals 13, 91, (1967)

1.42 Mansey, R.C., et. al., J. Less-Comm. Met. 14, 337, (1968)

1.43 Piercy, A.R., and Taylor, K.N.R., J. Phys. C1, 1112, (1968)

1.44 Taylor, K.N.R., Phys. Lettr. 29A, 372, (1969)

1.45 Christopher, J.T., Piercy, A.R., and Taylor, K.N.R., J. Less-Comm. Met., 17, 59, (1969)

2.1 Ellis, H.D., Ph. D. Thesis, University of Durham (1967)

2.2 Foner, Rev. Sci. Inst. 30, 7, 548 (1959)

2.3 Hutchinson, F., Ph. D. Thesis, University of Durham (1958)

2.4 Weis, P., and Forrer, R., Ann. Phys. (Paris) 12, 297, (1929)

2.5 Zijlstra, H., Experimental Methods in Magnetism Part 2, North-Holland Publishing Co., (1967)

2.6 'Reference Tables for Copper v. Constantan Thermocouples' British Standard No. 1828, (1961)

2.7 Morrish, A.H., 'The Physical Principles of Magnetism', Wiley P.265 (1965)

3.1 Mansey, Raymor and Harris, J. Less-Comm. Met. 14, 329 (1968)

3.2 Harris et. al., J. Less.Comm. Met. 19, 437 (1969)

3.3 Harris et. al. J. Less-Comm. Met. 9, 270 (1965)

4.1 Buschow, K.H.J., and Van Der Goot, A.S., J. Less. Comm. Met. 17, 249, (1969)

4.2 Ostertog, W., Trans. AIME, 239, 690, (1967)

4.3 Bertant, E.F., Lemaire, R., and Schweizer, J., Bull. Soc. Franc. Mineral. Crist. 88, 580, (1965)